

**University of Thessaly
School of Health Science
Department of Medicine**

Section of General Science
Laboratory of Medical Physics
Director: Professor C. Kappas
Academic year 2007-2008

**IN VIVO DOSIMETRY TO RADIOTHERAPY AND RADIOLOGY
PATIENTS FOR ERROR DETERMINATION**

By

ABDELMONEIM AM SULIEMAN
M.Sc, Medical Radiation Physics

Thesis submitted for the degree of Doctor of Philosophy in Medical Physics
In the Laboratory of Medical Physics

**Department of Medicine
School of Health Science
University of Thessaly**

**Larissa
March 2008**

The advisory committee

Professor Constandinos Kappas (Supervisor)

Professor Ioannis Fezoulidis

Assistant Professor Kiki Theodorou

The examination Committee

Professor Constandinos Kappas (Supervisor)

Professor Ioannis Fezoulidis

Professor John Kalef-Ezra

Professor Constandinos Gourgoulgiannis

Assistant Professor Kiki Theodorou

Assistant Professor Spiros Potamianos

Assistant Professor Marianna Vlychou

TABLE OF CONTENTS

ABSTRACT (Greek).....	viii
ABSTRACT	x
PUBLICATIONS	xii
DEDICATION	xiii
ACKNOWLEDGMENTS	xiv
CHAPTER 1: INTRODUCTION	
1.1 Ionizing radiation in medicine.....	1
1.1.1 Radiotherapy.....	1
1.1.1.1 Teletherapy.....	2
1.1.1.2 Brachytherapy.....	3
1.1.2 Radiology.....	3
1.1.2.1 Diagnostic radiology.....	3
1.1.2.2 Interventional radiology	3
1.1.2.3 Physical basic of radiology	4
1.2 Radiation risk.....	4
1.3 Occupational exposure	4
1.4 Radiation dose optimisation.....	5
1.5 Diagnostic reference level.....	6
1.6 Quality assurance in medicine	6
1.6.1 Quality assurance in radiotherapy.....	6
1.6.1.1 Quality audit and continuous quality improvement.....	7
1.6.1.2 Quality audit tools.....	7
1.6.2 Quality assurance in diagnostic radiology	8
1.7 Radiation dosimetry in medicine.....	8
1.7.1 Radiation dosimetry in radiotherapy.....	8
1.7.2 Radiation dosimetry in Radiology.....	9
1.8 In vivo dosimetry in medicine.....	9
2. Thesis aims and outline.....	12
CHAPTER 2: BACKGROUND	
2.1 Radiation classification.....	15
2.2 Radiation measurements.....	15
2.2.1 Interactions of radiation with matter.....	16

2.2.1.1 Direct ionizing radiation.....	16
2.2.2.2 Indirect ionizing radiation.....	17
2.3 Biological effect of ionizing radiation	17
2.3.1 Mechanisms of radiation damages.....	18
2.3.1.1 Cancer/heritable effects	19
2.3.1.2 Tissue reactions (Deterministic Effects).....	20
2.3.2 Radiation risk assessment.....	23
2.4 In vivo dosimetry in radiation medicine.....	24
2.4.1 In vivo dosimetry in high energy beams.....	24
2.4.2 In vivo dosimetry in low energy beams.....	25
2.5 Radiation dose measurements and units.....	26
2.5.1 Entrance surface dose.....	26
2.5.2 Organ dose.....	27
2.5.3 Equivalent and effective dose.....	27
2.6 Dosimetry Tools.....	29
2.6.1 Ionization chamber.....	29
2.6.2 Dose area product	30
2.6.3 Radiographic film.....	30
2.6.4 MOSFETS.....	31
2.6.5 Diamond detectors.....	31
2.6.6 Optical fibre dosimeter.....	32
2.6.7 Optically stimulated luminescence.....	32
2.7 Medical linear accelerator.....	32
2.7.1 Linear accelerator system.....	32
2.7.2 Electron versus X-ray Beam Therapy Systems.....	34
2.8 Diagnostic X ray Unit.....	35
 CHAPTER 3: THERMOLUMINESCENCE DOSIMETRY	
3.1 Historical background.....	41
3.2 Theory of Thermoluminescence.....	41
3.2.1 Thermoluminescence effect.....	41
3.2.2 Method of Manufacture TLD-100.....	43
3.3 Application TLD.....	44
3.4 TLD initialization.....	45
3.4.1 Sensitivity	45
3.4.2 Individual calibration factor.....	45
3.4.3 Pre irradiation annealing	46

3.4.4 Post irradiation annealing	46
3.4.5 TLD reading cycle.....	46
3.4.6 TLD reader.....	47
3.4.7 TLD dose response	48
3.4.8 TLD calibration.....	49
3.4.8.1 Background signal.....	49
3.4.9 Energy response	50
3.4.10 TLD Fading	50
3.4.11 TLD accuracy.....	51
CHAPTER 4: MATERIALS AND METHODS	
4.1 TLD materials.....	53
4.2 TLD calibration.....	54
4.2.1 TLD calibration for high energy beams.....	54
4.2.2 TLD calibration for low energy beams.....	54
4.4 TLD Oven.....	56
4.5 TLD reader.....	56
4.6 TLD handling accessories.....	57
4.7. Linear accelerators.....	57
4.8 X ray machines.....	58
4.9 Method of dose calculation.....	58
4.9.1 Entrance surface dose.....	59
4.9.2 Equivalent dose	60
4.9.3 Effective dose	60
4.9.4 Occupational exposure.....	61
4.9.4.1. Assessment of effective Dose from individual monitoring data	61
4.10 Patient dose assessment.....	63
4.10.1 NRPB software (NRPB-SR262)	63
4.10.2 CHILDOSE -SR279	63
4.11 Cancer risk estimation.....	64
Chapter 5 IN VIVO DOSIMETRY DURING HIGH ENERGY BEAMS	
5.1 Build up region	65
5.2 TLD and build up capsule.....	67
5.2.1 Capsule design	68
5.2.2 Testing build up cap.....	70
5.3 TLD calibration for entrance dose measurements.....	70
5.3.1 TLD calibration in build up capsule.....	71
5.3.2 Build up calibration for entrance dose measurements.....	72

5.3.2.1 Determination of geometrical correction factors...	72
5.3.2.2. Determination of physical correction factors.....	73
5.4 Thyroid dose measurements.....	74
5.5 Skin dose measurements.....	75
5.6. TLD and build up caps results and discussion.....	75
5.6.1 Perturbation behind the detector.....	76
5.6.2 Calculated correction factors (Copper capsule).....	75
5.6.3 Effect of high Z number in TLD signal	79
5.7 In vivo dose measurements.....	80
5.7.1 Patient Setup.....	80
5.7.2 Action of threshold in literature.....	81
5.8 In vivo dosimetry results and discussion.....	82
5.8.1 Head and neck	83
5.8.2 Breast.....	84
5.8.2.1 Thyroid and skin dose	86
5.8.3. Abdomen.....	88
5.8.4. Pelvis.....	90
5.8.5. Thyroid surface dose and cancer risks	91
5.8.6. Skin dose.....	93
5.9 General discussion and Conclusion.....	94
Chapter 6. IN VIVO DOSIMETRY IN LOW ENERGY BEAM	
6.1 In vivo dosimetry in radiology.....	97
6.1.1 Specific radiological procedures.....	97
6.1.1.1 Micturating Cystourethrography	98
6.1.1.1.1 Investigation procedure.....	98
6.1.1.1.2 Patient dosimetry.....	99
6.1.1.1.3 Co-patient dosimetry.....	100
6.1.1.2 Hysterosalpingography	101
6.1.1.2.1 Investigation procedure.....	101
6.1.1.2.2 Patient dose measurement.....	101
6.1.1.2.3 Staff dose measurement.....	102
6.1.1.2.4 Endoscopic Retrograde cholangiopancreatography	103
6.1.1.2.4.1 ERCP technique.....	103
6.1.1.2.4.2 Patient dose measurement.....	103
6.1.1.3.4 Examiner dose measurement	105
6.2 Results and discussion	107
6.2.1 Micturating Cystourethrography.....	107

6.2.2 Hysterosalpingography.....	110
6.2.3 Endoscopic Retrograde Cholangiopancreatography.....	117
6.3 Conclusion.....	126
6.4 GENERAL CONCLUSION	127
6.5 FUTURE WORK.....	128
7. REFERENCES.....	129
8. ANNEXES.....	141

ABSTRACT (Greek): ΠΕΡΙΛΗΨΗ

Σε αυτήν την διατριβή δοσίμετρα θερμοφωταύγεια (TLD) χρησιμοποιήθηκαν για την δοσιμέτρηση, στη διαγνωστική ακτινολογία και την ακτινοθεραπεία. Μελετήθηκαν από την άποψη της μείωσης του ακτινικού κινδύνου και της βελτιστοποίησης οι δόσεις ακτινοβολίας δόσεων σε ασθενείς και προσωπικό.

Η εργασία έχει δύο κύρια μέρη: 1) in vivo δοσιμετρία στις υψηλές ενέργειες φωτονίων που χρησιμοποιούνται στην ακτινοθεραπεία και 2) in vivo δοσιμετρία στις χαμηλές ενέργειες φωτονίων (ακτίνες x) που χρησιμοποιούνται στην ακτινολογία. Το πρώτο μέρος, σκοπεύει να αξιολογήσει τη δυνατότητα χρησιμοποίησης διαφορετικών υλικών (χαλκός, αργίλιο, ανοξείδωτος χάλυβας και Plexiglas) με βάση την αρχή της υπεργραμμικότητας, όπως επίσης να αξιολογήσει την ακρίβεια, στην μέτρηση της δόσης εισόδου κατά τη διάρκεια του εγκεφάλου και λαιμού, της κοιλίας και στην ακτινοθεραπεία της περιοχής της πυέλου. Οι περιφερειακές δόσεις (σε δέρμα και θυροειδής) μετρήθηκαν κατά τη διάρκεια της θεραπείας του μαστού. TLDs-100 χρησιμοποιήθηκαν μέσα σε διαφορετικά καλύμματα χαλκού για ενέργειες φωτονίων 6 και 15 MV σε δύο γραμμικούς επιταχυντές.

Η διαταραχή μπορεί να φθάσει σε μέχρι 20% του μεγίστου, το οποίο δρά ως περιορισμός για τις μετρήσεις δόσεων εισόδου. Η μέση δόση εισόδου του θυροειδή ήταν 3,7% της θεραπευτικής δόσης ανά συνεδρία και ενώ η μέση δόση εισόδου στους μαστούς υπολογίστηκε να είναι για να είναι 42% του μεγίστου, και για τα δύο πεδία ακτινοβολίας (εσωτερικό και εξωτερικό). Τα αποτελέσματα είναι συγκρίσιμα με εκείνα που υπάρχουν στην βιβλιογραφία. Ο κίνδυνος μοιραίου περιστατικού λόγω του καρκίνου θυροειδή ανά συνεδρία είναι 3×10^{-3} . Το μεγαλύτερο εύρος των μετρούμενων και των υπολογισμένων δόσεων βρίσκεται για τους ασθενείς με καρκίνο του μαστού.

Το δεύτερο μέρος σχετικά με την ακτινολογία. Οι δόσεις ακτινοβολίας μετρήθηκαν για τις συχνές εξετάσεις και θεωρήθηκαν ως τεχνικές χρυσών προτύπων για μερικές ευαίσθητες ομάδες πληθυσμού. Οι διαδικασίες περιλαμβάνουν Την ανιούσα κυστεογραφία (MCU), την σαλπγγογραφία (HSG) και το ενδοσκοπική οπισθοδρομική χολανγγειογραφία (ERCP).

TLDs-100 και TLDs-200 χρησιμοποιήθηκαν για να μετρήσουν τις δόσεις των ασθενών αλλά και του προσωπικού αντίστοιχα, λόγω των πολύτιμων χαρακτηριστικών τους. Τα TLDs συσκευάστηκαν σε έναν λεπτό φάκελο φτιαγμένο από διαφανές πλαστικό φύλλο.

Οι εξεταστές εκτελούσαν τις εξετάσεις βάση ενός πρωτόκολλου που σχεδιάστηκε για να ελαχιστοποιήσει τη δόση των ασθενών και των εξεταστών. Συνολικά 242 ασθενείς δοσιμετρήθηκαν. Η μέση τιμή της δόσης εισόδου (ESD) ήταν 1,13, 3,60 και 68,75 mGy αντίστοιχα για τις εξετάσεις MCU, HSG και ERCP, αντίστοιχα. Γενικά, ο κίνδυνος καρκίνου κυμαινόταν μεταξύ 10^{-6} και 10^{-7} . Ιδιαίτερες μεταβολές παρατηρήθηκαν μεταξύ των ασθενών από την άποψη της δόσης ακτινοβολίας, και του χρόνου ακτινοσκόπησης. Αυτές οι μεταβολές οφείλονται στις διαφορετικές ενδείξεις, τα χαρακτηριστικά των εξεταζόμενων και τα παθολογικά συμπεράσματα.

Τα στοιχεία που αναλύθηκαν σε αυτήν την εργασία παρουσίασαν ότι οι δόσεις μας είναι χαμηλότερες κατά περίπου 50% ως 300% έναντι των χαμηλότερων μέσων τιμών που παρουσιάστηκαν στη βιβλιογραφία.

Σαν γενικό συμπέρασμα, η εργασία αυτής της διατριβής παρήγαγε τα ακόλουθα αποτελέσματα:

- Πρωτόκολλα βαθμολόγησης των TLDs στις υψηλές και χαμηλές ενέργειες φωτονίων
- Πρωτόκολλα για την in vivo επαλήθευση των δόσεων στους ασθενείς που υποβάλλονται σε ακτινοθεραπεία

- Πρωτόκολλα για τον προσδιορισμό διαγνωστικών επιπέδων αναφοράς δόσεων (DRLs) που εφαρμόζονται στην κλινική πρακτική στις εξετάσεις της ακτινολογίας.

Το πρωτόκολλο επαλήθευσης δόσεων με την χρήση των TLDs είναι μέρος της διαδικασίας του ποιοτικού ελέγχου του τμήματος ακτινοθεραπείας του πανεπιστημιακού νοσοκομείου της Λάρισας.

ABSTRACT

The concept of dosimetry covers the determination of absorbed dose to a medium both by measurement and by calculation. Different instruments are used for absorbed dose measurements, all based on the detection of some of the physical and chemical changes caused by radiation. Radiation dosimetry was originally developed as a tool to quantify biological effects for use in setting dose limits for radiation protection and to determine accurately the irradiation needed to treat tumors or to prevent from deterministic effects and radiation risks. Clinical radiation dosimetry involves the absolute dose calibration and quality assurance of radiation beams. In addition, the aims of clinical radiation dosimetry are to evaluate current clinical practice and to provide verification and improvements where these are required. This approach optimizes the benefits of a procedure or treatment (e.g. diagnostic integrity, tumor control), whilst minimizing the detriment (e.g. risk of inducing cancer, side effects).

In this thesis Thermoluminescence Dosimeters (TLD) used in diagnostic, interventional radiology and radiotherapy were studied in terms of dose measurement, optimisation and radiation risk reduction for patients and staff. These dosimeters act as a quality assurance tool in radiology, and in radiotherapy they are used to measure entrance, exit, peripheral and intra-cavity dose during treatment. The presented work has two main parts: in vivo dosimetry in high energy photon beams used in radiotherapy treatments and in vivo dosimetry in low energy photon beams used in interventional radiology.

The first part, intends to evaluate the feasibility of different Buildup caps materials (Copper, Aluminum, Stainless steel and Plexiglas) on the onset of supralinearity of the entire dosimeters, and also evaluates the accuracy obtained from high z materials build up caps, measuring the entrance during head and neck, abdomen and pelvic radiotherapy. In addition to that, peripheral doses (skin and thyroid) were measured during breast treatment. Natural lithium fluoride doped with magnesium and titanium (LiF: Mg, Ti (TLD-100)) was used with different copper build up caps for 6 MV and 15 MV photon beams from two linear accelerators. In the thyroid case cancer risk is higher following radiation at a young age, and decreases with increasing age for patients during a radiotherapy course for breast, head and neck stomach and prostate.

The perturbation value can reach up to 20% of the D_{max} , which acts as a limitation for entrance dose measurements. An average thyroid skin dose of 3.7% of the prescribed dose was measured per treatment session while the mean skin dose breast treatment session is estimated to be 42% of d_{max} , for both internal and external fields. These results are comparable in those of the in vivo of reported in literature. The risk of fatality due to thyroid cancer per treatment course is 3×10^{-3} .

Previous results from this author and previous results in literature indicate that the thyroid receives a significant dose during breast radiotherapy. Therefore, the routine evaluation of thyroid function is important in patients, who have been treated with radiotherapy, and whose treatment portals have included a large part of the thyroid gland. A suitable protection of thyroid gland is important to be provided especially for the patient receiving radical radiotherapy when young.

The largest spread in ratios of measured and calculated entrance doses can be found for breast cancer patients, which are irradiated by a pair of tangential fields with wedge filters, applied to compensate for the curving of the breast. Satisfying results have been obtained for the, head and neck abdomen and pelvis. Errors increase for high-energy beams.

High Z Build up caps can be used to accurately determine and test doses given to patients as part of a regular quality assurance (QA) programme in in vivo dosimetry.

The second part concerning medical radiology, deals with considerable radiation exposure to patients and staff. While optimisation of the radiation dose is recommended, few studies have been published. In addition to this, international organizations recommend a diagnostic reference level for different radiological and interventional procedures.

Radiation doses were measured for frequent procedures and considered as gold standard techniques for some sensitive groups. These procedures include Micturating cystourethrography (MCU), Hysterosalpingography (HSG) and Endoscopic retrograde cholangiopancreatography (ERCP) are performed on infants and children, women in childbearing age and in the general population, respectively.

TLD-100 and calcium fluoride doped with dysprosium ($\text{CaF}_2:\text{Dy}$ (TLD-200)) were used to measure patients and staff doses, respectively for their valuable characteristics. TLDs were packed on a thin envelope made of transparent plastic foil. Each envelope contained 4 TLDs. three envelopes in minimum were used to measure the entrance surface dose (ESD).

The examiners were performing the investigations with a protocol that is designed to minimize patient and examiner dose. A total of 242 patients were investigated. The mean ESD were 1.13, 3.60 and 68.75 mGy for MCU, HSG and ERCP, respectively. Generally, the risk of cancer is ranges between 10^{-6} and 10^{-7} . Considerable variations were observed among patient populations in terms of radiation dose, and fluoroscopic time. These variations are due to the different indications, patient characteristics and pathological findings.

The results of this study provide valuable data for dose optimisation and establishing reference dose levels for the mentioned examinations by a direct method using TLDs. However, additional measurements are necessary to improve the technique and the statistical information by including patient from different hospitals in order to establish national reference levels. Fluoroscopic captured image technique accompanied by reduced number of images has the lowest radiation dose without extremely compromising the capability diagnostic findings. However, dose reduction does affect image quality. Thus, it is important not just to reduce doses but also to optimise each imaging technique, maximizing its efficiency and determining the right balance between dose and image quality.

The radiation risks associated with staff and co-patient are low. Although the radiation dose to examiners is very low, no radiation dose can be considered safe and in addition it is accumulated when a high workload coexists.

The data analysed in this work showed our doses to be lower by approximately 50% to 300% compared to the lower mean values presented in the literature.

As a general conclusion, the work of this thesis produced the following results:

- Calibration protocols for TLDs in high and low energies photon beams
- Protocols for in vivo dose verification to patients treated with radiotherapy
- Protocols for the determination of Diagnostic Dose Reference Levels (DRLs) that are applied in clinical practice in the interventional radiology procedures studied.

The TLD dose verification protocol is now part of the QA procedure at the Radiotherapy Department of the University Hospital of Larissa.

PUBLICATIONS

Publications to Peer Review Scientific Journals:

1. Radiation dose measurement and risk estimation for paediatric patients undergoing micturating cystourethrography. **A Sulieman**, K Theodorou, M Vlychou, T, Topaltzikis, D Kanavou , I Fezoulidis , C Kappas. The British Journal of Radiology. (2007) 80, 731-737.
2. Radiation dose optimisation and risk estimation to patients and staff during hysterosalpingography. **A. Sulieman**, K. Theodorou, M. Vlychou, T. Topaltzikis, C. Roundas, I. Fezoulidis and C. Kappas. Radiation Protection Dosimetry (published online on June 20, 2007).
3. Radiation exposure to examiners and patients during therapeutic ERCP: Dose optimisation and risk estimation. **A Sulieman**, G Paroutoglou, A Kapsoritakis, A Kapatzenakis, S Potamianos, E Makrigiannis, M Vlychou, I Fezoulidis, C Kappas, K. Theodorou. Journal of Clinical Radiology (Accepted).

Publications to be submitted:

1. Build-up caps to be used in vivo thermoluminescent dosimetry. **A. Sulieman**, K. Theodorou, C. Kappas, J. Kalef-Ezra. (to be submitted).
2. Entrance and peripheral dose measurements during radiotherapy. **A Sulieman**, K Theodorou and C. Kappas.(to be submitted).

Conference presentations:

1. Radiation dose optimisation during micturating cystourethrography using digital fluorographic images. Constantin Kappas, Ioannis Fezoulidis, Theofilos Topaltzikis, Mariana Vlychou, **Abdelmoneim Sulieman**, Kiki Theodorou. Oral presentation at the in the World Congress in Medical Physics and Biomedical Engineering. 28 August to 1 September 2006, Seoul, Korea.
2. Radiation dose measurements and risk estimation to patients and radiologists during hysterosalpingography. **Abdelmoneim Sulieman**, Theofilos Topaltzikis, Mariana Vlychou, Christos Roundas, Ioannis Fezoulidis, Constantin Kappas, Kiki Theodorou. Poster presentation at the World Congress in Medical Physics and Biomedical Engineering. 28 August to 1 September 2006, Seoul, Korea.
3. Reduction of radiation doses and related risks to patients during Endoscopic Retrograde Cholangiopancreatography. **Abdelmoneim Sulieman**, Georgeios Paroutoglou, Andreas Kapsoritakis, Anargeyros Kapatzenakis, Spiros Potamianos, Marianna Vlychou, Ioannis Fezoulidis, Constandinos Kappas, Kiki Theodorou. Poster presentation. International Conference on Medical Physics. Dubai, 14-16/4/08.

DEDICATION

To my beloved parents

ACKNOWLEDGMENTS

I am deeply grateful to my supervisor, Professor/ Constandinos Kappas, for the invaluable guidance and encouragement throughout the thesis project. I know the knowledge I gained working with him will serve me well throughout my career. I am especially grateful to assistant Professor, Kiki Theodorou, for her great support and guidance and fruitful discussions. Without her help, this work could not have been accomplished.

I also would like to thank Professor John Kalef-Ezra for the training on the TLD process and his unlimited support and valuable advice and comments on the work. His support gave me the confidence to perform thesis work.. Special thanks to Ass. Professor G. Plataniotis, Dr A Kapetanakis, Dr G Paroutoglou, Ass. Professor M. Vlychou, Professor S. Potamianos and to the staff of the Gastroenterology, radiotherapy and radiology departments.

I would like to express my sincere appreciation to the members of my thesis advisory committee: Ass. Professor M. Vlychou and Professor I. Fezoulidis for their support and advice.

I am deeply grateful to the Medical Physics Department staff members: Medical Physicist: Panaiotis Mavroidis (PhD), and George Komisopoulos (MSc) for their help and assistance in the calibration process of the TLDs.

Special thanks go to Dr. I. Tsougos , D. Kanavou and I. Grout for their valuable support.

Thanks to my colleagues in the Medical Physics Department, T.Topaltzikis, E. Kousi, H.Omer,M. Tsiakalos for their support.

I am deeply grateful to the staff of the radiotherapy department, especially Dr M Theofanopoulou, Dr K Sortiriazou and all the technologists.

Special thanks to Abeer Hamad for her unlimited encouragement, and to my family, Suzan Ahmed Yousif, parents, sisters brothers, special Mohamed and Abderlahim for their unlimited help.

Finally I am deeply grateful to the Greek Scholarship foundation (IKY) for their financial support.

1. INTRODUCTION

1.1 Ionizing radiation in medicine

Radiation has been used in medicine, since the discovery of x-rays in 1895 and radioactivity in 1896 by Roentgen and Becquerel respectively [1]. In 1898, Marie and Pierre Curie announced their discovery of polonium and radium. A benefit from the use of radiation was established very early on, but equally some of the potential dangers of radiation became apparent in the practitioners who overexposed to high doses [2]. The use of radiation in medicine has improved health care, but has resulted in medical radiation exposures becoming a significant component of the total radiation exposure of populations.

Radiation is widely used in medicine; the population exposure from medical x-rays contributes approximately 14% of the average annual population dose. More than 95% of human exposure to man-made ionizing radiation results from diagnostic and interventional radiology [3]. Fig.1.1 The medical uses of radiation are classified into two main fields, radiation therapy and radiology.

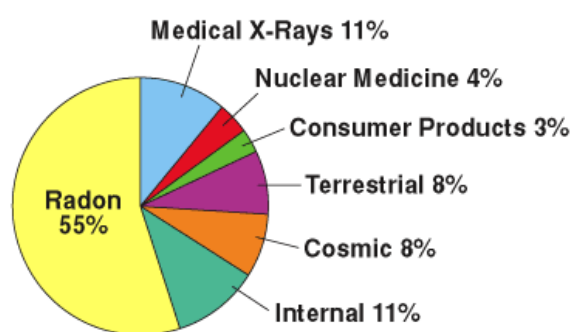


Figure.1.1: Sources of radiation exposure.

1.1.1 Radiotherapy

Radiotherapy is the use of ionizing radiation (photons high-energy beams of particles) to treat malignant tumors or some benign diseases such as the treatment of trigeminal neuralgia. The use of radiotherapy in non-malignant conditions is limited due to the risk of radiation-induced cancers cells [1-4]. The efficacy of the radiotherapy, which is applied in 50% of all cancer patients, is based on the radiosensitivity of the malignant cells and the ability of the healthy tissue to recover from the effects of radiation.

Radiotherapy has advanced rapidly during the last decades due to the technical advancements in the therapeutic equipment, which allows the delivery of a high dose to a tumor without causing unacceptable side effects to the patient. Organ motion has made the task of eradicating a tumor difficult, resulting in inhomogeneity of the dose distribution leading to an under-dosage of Planning Target Volume (PTV) and over-dosage of some organ at risk (OAR) [3,4,6].

There are two main risks to patients associated with radiation treatment, failure to control the initial disease, which when malignant can be lethal, and risk to normal tissue from irradiation. Radiotherapy may be used as the primary therapy or combined with surgery, chemotherapy, hormone therapy or a mixture of the three [3,5].

The radiation damage to the DNA of the cells in the area being treated, affects their ability to divide and grow. Cancerous cells are unable to repair this damage as quickly, so their growth is curtailed and the tumor shrinks. Although some normal cells are affected by radiation, most normal cells appear to recover more fully from the effects of radiation than do cancer cells.

There are principal differences between different types of radiation used in radiation therapy because the radiation quality of the low energy photons from an x-ray tube (200 kV in Fig. 2), deliver a maximum dose close to the surface of

the patient and are mainly used to treat skin carcinomas and other superficial diseases. For photons from a linear accelerator, or other high energy therapy accelerator, the decrease with depth is much slower (6 MV in Fig. 2). Thus, this radiation quality can be used to reach deep sited tumours. These photons also show a useful skin sparing effect. Electrons show a relatively steep slope in the depth dose when they reach their maximum range. This makes it possible to spare organs behind the treatment volume when electrons are used. At larger depths a dose of only a few percent is received from bremsstrahlung photons

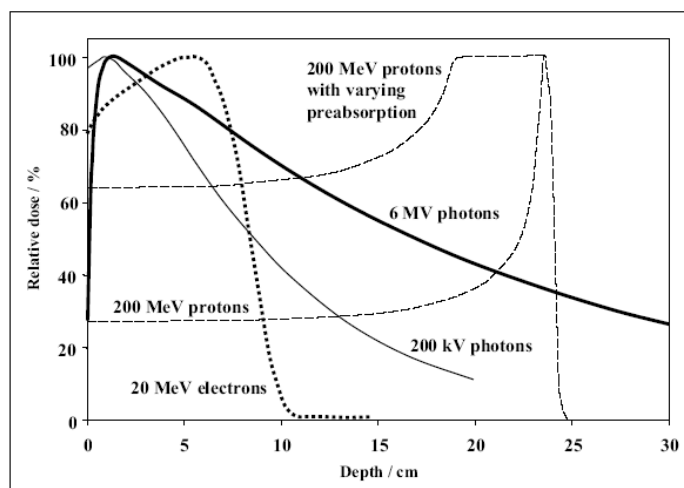


Figure.1. 2: Depth dose curves for some important types of radiation used for radiation therapy

In general, there are two modes of delivery of the radiation are teletherapy and brachytherapy:

1.1.1.1 Teletherapy:

Teletherapy (External radiation therapy) means a source of radiation coming from a distance. It is also called percutaneous radiotherapy. About 60% of cancer patients referred for radiotherapy are treated with Teletherapy equipment. Teletherapy mainly applies high-energy photons or electrons from a medical linear accelerator or Cobalt-60 machines. Over 90% of total radiation treatments are conducted by teletherapy or Brachytherapy, with radiopharmaceuticals being used in only 7% of treatments [4]. In general, teletherapy is divided into two types: Conventional and conformal teletherapy.

The term “conventional radiotherapy” refers to techniques that do not involve segmental modulation of beam intensity. Intensity Modulated Radiation Therapy and Tomotherapy are examples of delivery systems that are not conventional radiotherapy.

The treatment is planned or simulated for on a specially calibrated conventional diagnostic x-ray machine (or sometimes by eye), and to the usually well-established arrangements of the radiation beams to achieve a desired plan. In vivo dosimetry may be performed in conventional treatments, depending on the institution's practices.

Conformal radiotherapy refers to a method of treatment delivery that incorporates rigid immobilization and 3 dimensional computer planning and treatment systems to produce a high dose area of radiation that conforms to the shape of the target and highly conformal dose-distributions with steep-dose gradients [7]. Increased sophistication of 3D multimodality medical imaging has led to an ability to visualize tumours, not only anatomically, but also with functional and molecular image displays. These developments in technology can be combined together to provide modern radiotherapy delivery with the most exciting potential for increased tumour cure and decreased long-term morbidity.

Enhanced conformation allows for greater doses of radiation to reach the target volume while delivering less radiation to surrounding normal tissues [7]. As opposed to conventional radiation therapy, many fields and beam angles are used.

The dose delivery is modulated by multi-leaf collimator (MLC) within each field. Figure 1 illustrates these differences: the dose distribution is conforming closely to the tumor.

A dosimetry check of the dose calculation in a solid water phantom is usually performed before the treatment. Additionally, in vivo dosimetry is strongly recommended [8].

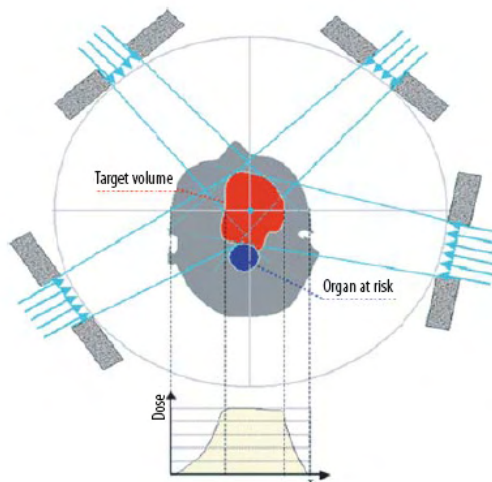


Figure 1.3: Basic idea of conformal radiotherapy

1.1.1.2. Brachytherapy

Brachytherapy: Brachy means 'short time' in Greek language. When the radiation source that emits γ ray (sealed radionuclides as tube, seeds, needles) is placed close to or within the tumor the treatment is called brachytherapy [3-5]. It is often used in combination with external beam radiotherapy and helps to preserve structure and function of the surrounding healthy tissue. There are three definite sub-specifications of brachytherapy: (i) Plesiocurietherapy (the radionuclide is placed on the surface of the skin (mould or plaque)), (ii) Intracavitary brachytherapy (inside the natural body cavity) and (iii) Interstitial brachytherapy (the radionuclide is implanted (needled) in to the substance of the tumor).

1.1.2. Radiology

Radiology is the use of ionizing radiation for medical diagnosis. It also uses techniques that do not involve radiation, such as magnetic resonance imaging (MRI) and ultrasound (US). Radiology is classified into two subfields. Besides radiology, diagnostic x-rays are also found in such clinics as cardiology, urology, orthopedics, gastroenterology, and dental [1, 2].

1.1.2.1. Diagnostic radiology

Diagnostic radiology is a discipline, which uses of ionizing radiation for medical diagnosis, especially the use of x-rays in medical radiography or fluoroscopy. It is concern with the use of various imaging modalities to aid in the diagnosis of disease.

1.1.2.2 Interventional radiology

Is the use of the imaging modalities to guide minimally invasive surgical procedures. It is performed by a physician skillful in radiologic techniques and experienced in the clinical problems. The procedures may be predominantly therapeutic or primarily diagnostic [1,2].

1.1.2.3 Physical Basic of Radiology.

Radiology works on the principle that when x-rays pass through human tissues the resultant physical processes (e.g. attenuation) provides contrast between different tissue types thus producing an image of human anatomy for the diagnosis of disease. Kilovoltage x-rays are used in various imaging modalities including: Conventional X ray, CT (Computed Tomography) scans which produce cross sectional images from a narrow fan x-ray beam, fluoroscopy, where the x-ray tube is left on or pulsed rapidly to produce real-time images, or mammography, where a high contrast image of the breast is produced by an x-ray beam with an effective energy less than 20keV and using K-edge filtration [13,14].

In contrast to the diagnostic benefit of ionizing radiation, exposure to any quantity of radiation carries with it some degree of risk of cancer induction [15,16]. The direct or indirect effects of ionizing radiation can cause cell modification, in particular DNA damage that may affect cell function or cause cell death. As a result, the benefit of each diagnostic procedure involving ionizing radiation must be weighed up against the potential risks involved. Consequently, clinical practice should be constantly reviewed to improve the benefit of the procedure (e.g. image quality) whilst minimizing radiation exposure.

During diagnostic procedures there are two contributions to exposure to the general population from medical x-rays that must be considered. First, occupational exposure to radiation workers must be minimized whilst optimizing medical procedures [14]. Second, it is necessary to avoid medical exposures that are clinically unjustified, repeated and/or unoptimised [15]. In particular, different population sub-groups are more sensitive to radiation than others and must be observed more closely. For example, paediatric patients are more sensitive than adults, since radiosensitivity is related to the growth rate of the tissue irradiated. In addition, due to their long remaining life expectancy, every neonate has a greater time period for a cancer to develop.

1.2. Radiation Risk

Radiation risks of diagnostic radiology patients are either tissue reaction (deterministic) or cancer/heritable (stochastic) in nature. Tissue reactions, such as tissue injury or cataract production, occur when a number of cells are involved and a threshold dose is reached. Above the threshold, the severity of the injury is proportional to the dose. Cancer/heritable radiation injuries, such as genetic effects and carcinogenesis, are caused by injury to a single cell and typically a threshold dose is not required. The probability of the injury is proportional to the dose, but the severity of the injury is independent of the dose. If one assumes a linear relation without a threshold for such effects, then any amount of radiation, including low-dose plain film procedures, may potentially have an effect [16, 18].

1.3. Occupational exposure

Radiologists and radiological technologists are among the earliest occupational groups exposed to radiation. In 1902, only 7 years after the discovery of x-rays, excessive occurrences of skin cancer, which was the first solid cancer linked to radiation, were noted among radiologists. In early 1950, excess mortality from leukemia among radiologists began to

receive attention, and this, together with the rising concern about the effect of chronic radiation exposure from nuclear weapons tests, led to two landmark cohort studies of radiologists

Today, a large number of professional and technical personnel in medicine are occupationally exposed to radiation whilst undertaking various radiological procedures, i.e., diagnostic, therapeutic, interventional and nuclear medicine. The latest United Nations Scientific Committee on Effects of Atomic Radiation (UNSCEAR) report estimates that, worldwide, there are 2.3 million medical radiation workers—half of the entire workers exposed to man-made sources of radiation. Health risks from radiation exposure in such a large occupational segment of the population are clearly of special concern. During the decades after the discovery of x-rays in 1895, radiologists were exposed to such high doses that dermatitis and other radiation-induced injuries were common. The first dose limit was introduced in 1902, which was about 0.1 Gy per day (30 Gy per year!); this was not based on biological data but rather on the lowest observable amount, i.e. fogging of a photographic plate [1,10,19].

1. 4. Radiation dose optimisation

Optimisation of exposure to ionizing radiation is important to both patient and examiner to reduce them where possible. Over the years, reductions in patient dose have been achieved through advances in technology and changes in clinical practice. In UK, National Radiological Protection Board (NRPB) [13] mentioned that there was an average of 30% reduction in mean doses for common types of X-ray examination since the survey in the mid 1980s, and that less than 10% of hospitals were exceeding the original national reference doses.

However, whilst some dose reduction measures have a positive effect on image quality, others degrade contrast or increase noise. Thus, it is important not just to reduce doses but also to optimize each imaging technique, maximizing its efficiency and determining the right balance between dose and image quality.

European Union directive 97/43/Euratom [20] stipulates that: “All doses due to medical exposure for radiological purposes except radiotherapeutic procedures... shall be kept as low as reasonably achievable consistent with obtaining the required diagnostic information...” Member states are required to pay special attention to exposures involving high doses to the patient, such as those considered in this study. The Ionising Radiation (Medical Exposure) Regulations (IRMER) 2000 [1], which extend the obligations to cover therapeutic as well as diagnostic exposures state that, “The operator shall select equipment and methods to ensure that for each medical exposure the dose of ionizing radiation to the individual undergoing the exposure is as low as reasonably practicable and consistent with the intended diagnostic or therapeutic purpose.” Since medical exposure has been justified, due to the potential benefit to the patient, there are no prescribed dose limits, but practitioners should apply the principle of optimization to ensure that patient dose is as low as reasonably achievable in order to avoid the stochastic effects and decrease the probability of non-stochastic effects while obtaining necessary diagnostic information [3, 4]. Optimization could be achieved by selection of modern equipment, technique, well-trained personnel and well-defined diagnostic reference level (DRL) consistent with the intended of diagnostic purpose [19, 20].

There are a number of different methods for reducing radiation dose, and these affect image quality in different ways. The challenge is to make the most effective use of the imaging equipment, so that the requisite clinical information can be obtained using the lowest practicable dose.

1.5. Diagnostic reference levels

The concept of ‘reference doses’ for common X-ray examinations was introduced in the UK in 1990 in a joint document by the Royal College of Radiologists (RCR) and the NRPB entitled Patient Dose Reduction in Diagnostic Radiology [21]. DRL is defined as the dose level in Medical –radio diagnostic or in case of pharmaceutical the level of activity, for a typical examination of group of size patients or standard patients for broadly type of equipments. DRL is applied only for diagnostic procedures in diagnostic radiology or nuclear medicine, and does not apply to radiation therapy [18].

The purpose of the reference dose was to provide a trigger to the first step in the optimization of patient doses and identify those practices in most urgent need of investigation and corrective action.

ICRP [18] recommended that values should be selected by professional medical bodies, reviewed at intervals representing a compromise between the necessary stability and the long-term changes in observed dose distributions, and be specific to a country or region. Interestingly, the ICRP also recommended that DRLs need to be established only for common types of diagnostic examination and broad types of equipment. They are not intended to be used in a precise manner and a multiplicity of levels would reduce their usefulness.

Wide variations in individual patient doses are to be expected and it is only sensible to compare the mean dose values (or perhaps the median, which is less influenced by extreme outliers) on representative groups of patients to monitor local trends with time, equipment or technique. Mean or median values, used as dose audit standards to monitor local trends, are not the same as third quartile values used to indicate abnormally high doses on a national or regional scale.

1.6. Quality Assurance (QA) in Medicine

1.6.1. QA in Radiotherapy

According to the definition of International Standards Organization (ISO), quality assurance (QA) means all the planned or systematic actions necessary to provide adequate confidence that a product or service will satisfy given requirements for quality [22]. Specifically in radiation oncology, the quality can be defined as the totality of features or characteristics of the radiation oncology service that bear on its ability to satisfy the stated or implied goal of effective patient care [16].

Presently, however, it is generally appreciated that the concept of quality in radiotherapy is broader than a restricted definition of technical maintenance and quality control of equipment and treatment delivery, and instead that it should encompass a comprehensive approach to all activities in the radiotherapy department; thus, it has clinical, physical, and administrative components. The clinical requirements for accuracy are based on evidence from dose-response curves

An assessment of clinical requirements in radiotherapy shows that a high accuracy is necessary to produce the desired result of tumour control rates that are as high as possible, consistent with maintaining complication rates within acceptable levels [22]. Quality assurance procedures in radiotherapy can be characterized as follows:

- Quality assurance reduces uncertainties and errors in dosimetry, treatment planning, equipment performance, treatment delivery, etc., thereby improving dosimetric and geometric accuracy and the precision of dose delivery. This improves radiotherapy results (treatment outcomes), raising tumour control rates as well as reducing complication and recurrence rates.

- Quality assurance not only reduces the likelihood of accidents and errors occurring, it also increases the probability that they will be recognized and rectified sooner if they do occur, thereby reducing their consequences for patient treatment. This is the case not only for larger incidents but also for the higher probability minor incidents.
- Quality assurance allows a reliable inter-comparison of results among different radiotherapy centres, ensuring a more uniform and accurate dosimetry and treatment delivery. This is necessary for clinical trials and also for sharing clinical radiotherapy experience and transferring it between centres.
- Improved technology and more complex treatments in modern radiotherapy can only be fully exploited if a high level of accuracy and consistency is achieved.

Radiation therapy with external radiation beams the absorbed dose at the specification point in a patient should be known with an overall uncertainty of 3.5% (1sd) [4, 5]

Geometric uncertainty relative to target volumes or organs at risk also leads to dose problems, either under dosage to the required volume (decreasing the TCP) or over dosage to nearby structures (increasing the NTCP). Consideration of these effects has led to recommendations on spatial uncertainty of between 5 and 10 mm (at the 95% confidence level).

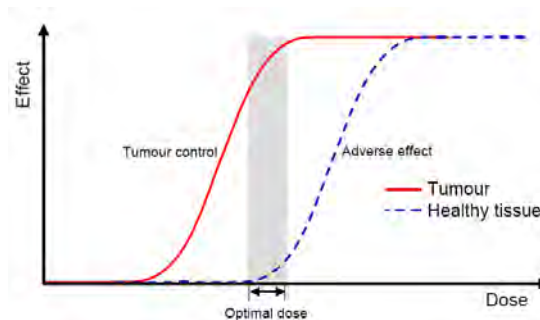


Fig.4 Tumor control probability (TCP) and the probability of normal tissue complication (NTCP) as a function of radiation dose, in a hypothetical case.

The ICRU recommendations [23] indicate that the error should not exceed 3-5%; and the recommended accuracy on dose delivery is generally 5–7% on the 95% confidence level, depending on the factors intended to be included [23]. On spatial accuracy, figures of 5–10 mm (95% confidence level) are usually given depending on the factors intended to be included. These are general requirements for routine clinical practice. In some specific applications, such as stereotactic radiotherapy, IMRT, or radiotherapy with ion beams, better accuracy might be demanded which consequently has an impact on increased QA efforts.

1.6.1.1 Quality audit and continuous quality improvement

Quality audit is a systematic and independent examination to determine whether or not quality activities and results comply with planned arrangements, and whether or not the arrangements are implemented effectively and are suitable to achieve the stated objectives. Any result of non-compliance found during the process of quality audit then must be feed back into quality manual [1, 16, 17, 22]. The important that the quality manual is be kept flexible in such a way that it allows the possibilities of changes and improvements based on regular audits and assessments.

1.6.1.2 Quality audit tools

- Postal audit with mailed dosimeters (usually TLD): these are generally organized by secondary standard dosimetry laboratory (SSDL) or agencies, such as the IAEA, Radiological Physics Center (RPC) in the U.S., ESTRO quality assurance laboratory (EQUAL), national societies, national quality networks, etc. They can be applied at various levels in the clinical dosimetry chain and can include procedural audit by using a questionnaire.

- ii. Quality audit visits can audit practical aspects in detail, limited only by time. They can audit procedural aspects by questioning staff and by inspection of procedures and records.
- iii. Finally, possible aims of a quality audit visit are to check: infrastructure, documentation, measurements of beam calibration geometry, measurements on other equipment, such as simulator, CT scanner, etc.

1.6.2 Quality assurance in Diagnostic radiology

QA means the planned and systematic actions that provide adequate confidence that a diagnostic x-ray facility will produce consistently high quality images with minimum exposure of the patients and healing arts personnel. The determination of what constitutes high quality will be made by the facility producing the images. QA actions include both “quality control” techniques and “quality administration” procedures.

QA in diagnostic radiology has been systemically started in imaging departments since 1930s [24].

“Quality control techniques” are those techniques used in the monitoring (or testing) and maintenance of the components of an x-ray system. The quality control techniques thus are concerned directly with the equipment.

“Quality administration procedures” are those management actions intended to guarantee that monitoring techniques are properly performed and evaluated and that necessary corrective measures are taken in response to monitoring results. These procedures provide the organizational framework for the quality assurance program.

1.7. Radiation dosimetry in medicine

The concept of dosimetry covers the determination of absorbed dose to a medium both by measurement and by calculation [14]. Different instruments are used for absorbed dose measurements, all based on the detection of some of the physical and chemical changes caused by radiation.

Radiation dosimetry was originally developed as a tool to quantify biological effects for use in setting dose limits for radiation protection and to determine accurately the irradiation needed to treat tumours or to prevent from deterministic effects and radiation risks.

Clinical radiation dosimetry involves the absolute dose calibration and quality assurance of radiation beams. In addition, the aims of clinical radiation dosimetry are to evaluate current clinical practice and to provide verification and improvements where these are required. This approach optimizes the benefits of a procedure or treatment (e.g. diagnostic integrity, tumour control), whilst minimizing the detriment (e.g. risk of inducing cancer, side effects).

1.7.1 Radiation dosimetry in radiation therapy

The aim of dosimetry in radiotherapy is to determine the absorbed dose to the irradiated tissues with sufficient accuracy. Difficulties arise due to nuclear reactions in which a broad variety of heavy ionizing particles and radioactive nuclei are created.

Dosimetry has a vital role in dose distribution optimisation. It is important to verify the accurate delivery of a large amount of radiation to a defined tumor volume, which ensures minimal injury to normal or critical tissue. Deviations

from the intended dose distribution can affect treatment outcome, particularly for brachytherapy treatments where the dose gradient outside the target volume is steep [5, 18].

1.7.2 Radiation dosimetry in Radiology

In diagnostic and interventional radiology, the aim of dosimetry is to quantify the doses delivered to the patient and staff during medical procedures and estimate risks of the radiation exposure. Furthermore using our knowledge of techniques and equipment, the diagnostic or therapeutic value of the procedure can be further optimized whilst minimizing unnecessary exposure. This is particularly important for more radiosensitive patients (e.g. neonates) and sensitive organs (e.g. thyroid, gonads, and lens).

1.8. In vivo dosimetry in Medicine

For both diagnosis and treatment, dose measurement during the course of interventions on real patients (i.e. in vivo dosimetry) is the most direct method to assess clinical practice. Phantom measurements do not account for dose variations due to differences in patient composition and size/weight.

Several types of radiation detectors are available for this purpose. The three most widely used detectors in clinical radiation dosimetry are ionisation chambers, radiographic film and Thermoluminescence dosimeters (TLDs). Other detectors include radiochromic film, semiconductor diodes, diamond detectors, MOSFETs, scintillation detectors and gels.

The detector types most commonly employed for in vivo dosimetry are:

- a) Thermoluminescence dosimeters (TLDs)
- b) Semiconductor detectors
- c) 2D techniques (Radiographic films and Electronic Portal Imaging Devices (EPIDs))
- d) Ionization chambers and DAP meters
- e) Diamond detectors
- f) Chemical dosimeters
- g) Scintillation detectors (Optical fiber dosimetry)

Thermoluminescence dosimeters, semiconductor diodes and films are the tools most commonly used in in vivo dosimetry in radiotherapy to date. Some other detector types have also been tested for in vivo dosimetry purposes, but are not yet in routine clinical use. Other detectors, such as plastic scintillators, alanine and diamond detectors have also been studied for in vivo dosimetry purposes. Diamond detectors and plastic scintillators have the advantages of good stability, a high spatial resolution, nearly water equivalence, and linear response versus dose rate. They are much less energy and dose rate dependent than diodes, show less radiation damage and are not affected by temperature variations. Alanine detectors offer the possibility of measuring the integrated dose during the overall treatment series. However, these detectors require expensive and complicated reading equipment and have therefore mainly been used under laboratory conditions and not on a routine base in clinic. Metal oxide semiconductor field effect transistors (MOSFET) are also suitable for in vivo dosimetry purposes, because of minimal high-voltage and very small size.

In radiology, DAP meters and TLDs are more preferable than others detectors. Table 1.1, presents a brief overview of their characteristics, and their advantages and disadvantages. Properties and uses of the different detectors are also compared in Table 1.1

Table 1.1: The advantages and disadvantages of the most common radiation dosimeters, other than Thermoluminescence Dosimeters, used in medicine for phantom or in-vivo dosimetry [25-31].

Detector	Radiology application	Radiotherapy application	Advantages	Disadvantages
Ionisation Chamber	Calibration of output	Absolute dosimetry, Beam data acquisition & QA	High precision, gold standard	Cables, high voltages
Dose Area Product Meter (DAP)	Monitoring of DAP for patients	-	Online measurements	Doesn't directly measure Entrance surface dose
Semiconductor Diodes	In vivo dosimetry	Water tank, In vivo dosimetry	Small size, online measurements, arrays	Cables, energy, temperature, dose rate, and directional dependence
MOSEFET	In vivo dosimetry	Phantom measurements, In vivo dosimetry	Small size i.e high special resolution, online measurements resolution, online measurements directional dependence	Cables, destroyed by static, reproducibility, temperature and directional dependence
Gels & NMR Dosimetry	-	Phantom measurements, 3D dosimetry, Canter intercomparisons	3-D dose distribution, Tissue equivalent detector & phantom shaped into any form	Complicated readout using NMR(Nuclear magnetic resonance), Not reusable, detection limit of 0.05 Gy 'fading'
Radiographic Film	Image quality assessments	Phantom measurements, Qualitative dosimetry, dose distributions, dosimetry of dynamic treatments	High spatial resolution	Not reusable, require development, variability, energy and dose rate dependence
Radiochromic Film	-	Phantom measurements, Dose distribution (incl. high dose rate brachytherapy sources)	High spatial resolution, self developing, tissue equivalence	High dose(> 10Gy) dosimeter, stability, temperature dependence, not reusable
Diamond Detector	-	Dose distributions, dosimetry of small fields	High spatial resolution, online measurements, tissue equivalence	Cables, dose rate dependence, expensive
Scintillator	Entrance surface dose for interventional radiology	Potential for brachytherapy	High spatial resolution, online measurements, good stability, water equivalence, high efficiency	Cables, small temperature dependence, energy response at low energies expensive and complicated readings

2. Thesis aims and outlines

This PhD thesis is intended to measure radiation dose for both patients and staff during diagnostic and radiation therapy using TLDs. The thesis describes methods of radiation dose optimization during diagnostic and interventional radiology by measuring the entrance and peripheral doses to thyroid and skin for patients during breast, head and neck and prostate treatments. The use of build up caps constructed from materials with different atomic number enable us to measure high radiation energies with acceptable accuracy. The radiation risk for both patients and staff was also evaluated. The main objectives of the thesis are summarized as:

- (i) Evaluation of the radiation dose to patients and staff using TLDs during Hysterosalpingography (HSG), Micturating cystourethrography (MCU) and Endoscopic retrograde cholangiopancreatography (ERCP) procedures according to the protocol used by the Radiology Department of the University Hospital of Larissa (UHL), Greece.
- (ii) Estimation of the thyroid surface dose (TSD) and dose to radiosensitive organs located in an outside the irradiation field;
- (iii) Estimation of the risk due to the radiation dose.
- (iv) Comparison of the doses based on available data obtained by other researchers and reference levels recommended by international organizations.
- (v) Evaluation of the effects of different Buildup cap materials (Copper, Aluminum, stainless steel and Plexiglas) on the onset of supralinearity of the entire dosimeter and analysis of any perturbations arising through the use of various materials for 6 MV and 15 MV beams. The effect of different geometrical settings (source surface distance (SSD) and field size) was also studied so as to obtain a base line data set with continuing increase in the use of build up caps.
- (vi) Evaluation of the dose at entrance surfaces of the patient using LiF TLD accommodated in build up caps is performed to find the differences between the predicted and measured dose in different situation and geometry. From the results the correction factors could be derived which are then applied to estimate the actual dose at the point of interest.

The thesis was organized accordingly in the following chapters:

Chapter 1. Introduction, brief summary of the application of radiation dose in medicine, in vivo dosimetry and related radiation risks.

Chapter 2. Background, describes the radiation interactions, measurements and effects of direct relevance to this thesis with an explanation of the biological reasoning behind dosimetry applications.

Chapter 3. Describes the physical principles of TLDs and their manufacture, properties and limitations.

Chapter 4. Presents materials and calibration of TLDs in relation to beam parameters: the reproducibility, linearity, energy dependence, etc. It also provides an outline of equipment and methods used in this thesis.

Chapter 5. Deals with the results and discussion of the usage of metallic build up caps, with particular focus on its application to entrance dose measurements in high energy beams. This chapter also contains thyroid absorbed dose measurements and skin dose during head and neck, breast, abdomen and pelvis treatments.

Chapter 6. The results and discussion of applying TLDs to dosimetry in diagnostic and interventional radiology. Measurement of radiation doses delivered to patients and staff during medical imaging procedures MCU, HSG and ERCP, is now possible using fluoroscopic captured image technique, allowing further optimization of radiation dose.

2. BACKGROUND

2.1 Radiation classification:

Radiation can be defined as the propagation of energy through matter or space. The released energy can be in the form of energetic particles or electromagnetic waves. Radiation is often separated into two categories, ionizing radiation (IR) and non-ionizing (NIR), to denote the energy and danger of the radiation. The practical threshold for radiation risk is 10 eV since the energy of a hydrogen atom is 13.6 eV [32]. IR is divided into two major categories according to the interactions: charge particles and uncharged (Figure 2.1).

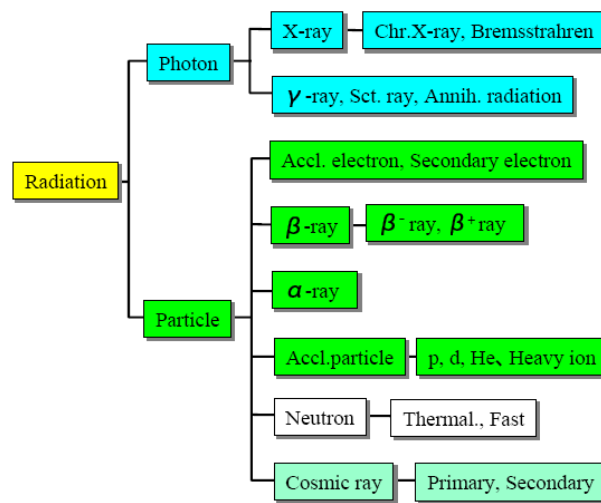


Figure 2.1: Electromagnetic spectrum and its classification according to the frequency

2.2. Radiation Measurement

Radiation dosimetry is a technique used for evaluating the intensity and characteristics of ionizing radiation by measuring the dose at a certain point as a result of this incident radiation. Dosimetry of medical ionizing radiation is important. It enables the amount of radiation delivered to patients to be measured. In addition to this, the amount of radiation involved in occupational exposures can be measured. In diagnostic procedures such as x-ray examinations, nuclear medicine, CT scans, Positron Emission Tomography (PET) etc, this measurement is both for the optimisation of image quality, and for radiation protection purposes. However, the need for accurate dosimetry is greatest in radiation therapy for cancer. In radiotherapy, a high dose of radiation is delivered to a tumour and the effectiveness of the treatment depends on delivering the dose with an accuracy of 5% or better [5,18]. It is believed that a decrease of 10%–15% in dose delivery will result in a decrease in the chance of cure by a factor of 2 or 3 while an increase in dose will similarly increase the chance of irreversible damage to healthy tissue [7].

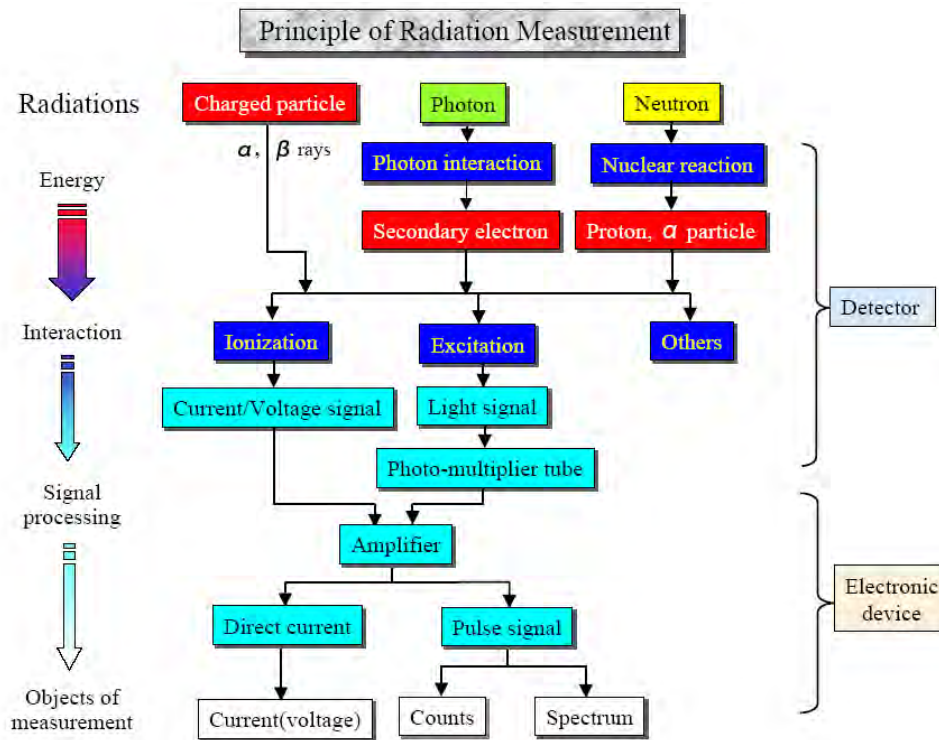


Figure.2.2: Principle of radiation measurements

2.2.1 Interaction of radiation with matter

Radiation can be classified into two general groups, ionizing and non-ionizing; therefore, it may be expected that interactions with matter fall into two groups. Charged particles directly ionize the media through which they pass, while uncharged particles and photons can cause ionization only indirectly or by secondary radiation (Figure 2.2).

2.2.1.1 Direct ionizing radiation

Directly Ionizing Radiation is composed of charged particles that produce ion pairs at small intervals along their path as a result of energy imparted to orbital electrons. Impulses are exerted at a distance through electrical forces between the charged particles and the orbital electrons. An electron is held in the atom by electrical forces, and energy is lost by the beta/alpha particle in overcoming these forces. The amount of energy lost by the charged particle depends upon its distance of approach to the electron and on its kinetic energy. The ejected electron may receive a significant amount of energy, enough to allow it to travel a long distance and to leave a trail of ion pairs. Because beta particles have the same mass as orbital electrons, they are easily deflected during collisions and thus beta particles follow a tortuous path as they pass through matter. Alpha particles interact in much the same manner, however because of their high electrical charge and relatively low velocity; they have a very high specific ionization [25, 32].

2.2.1.2 Indirect Ionizing Radiation

Indirectly ionizing particles are uncharged and they collide with electrons, atoms, or nuclei, resulting in the liberation of energetic charged particles (e.g., e^-). The charged particles that are thus liberated are directly ionizing, and it is through these that ionization in the medium occurs. The interaction occurs in a variety of alternative mechanisms, the three most important are photoelectric effect, Compton scattering and pair production. In the photoelectric effect, all of an x-/ γ -ray photon's energy is transferred to an atomic electron, which is ejected, from its parent atom. The photon in this case is completely absorbed. Compton scattering is an interaction between a photon and an essentially free electron whose binding energy is much less than the photon energy. Only part of the energy of the photon is transferred to an atomic electron and the photon is thereafter scattered with a reduced energy. Pair production occurs in the intense electric field close to a charged particle, usually a nucleus. An energetic ($E > 1.02$ MeV) γ -ray photon is converted into a positron-electron pair and the two particles share the available energy in excess of the 1.02 MeV required to produce the pair. The probability of each of these interactions depends upon the photon energy and the atomic number [25, 32] (Figure 2.3).

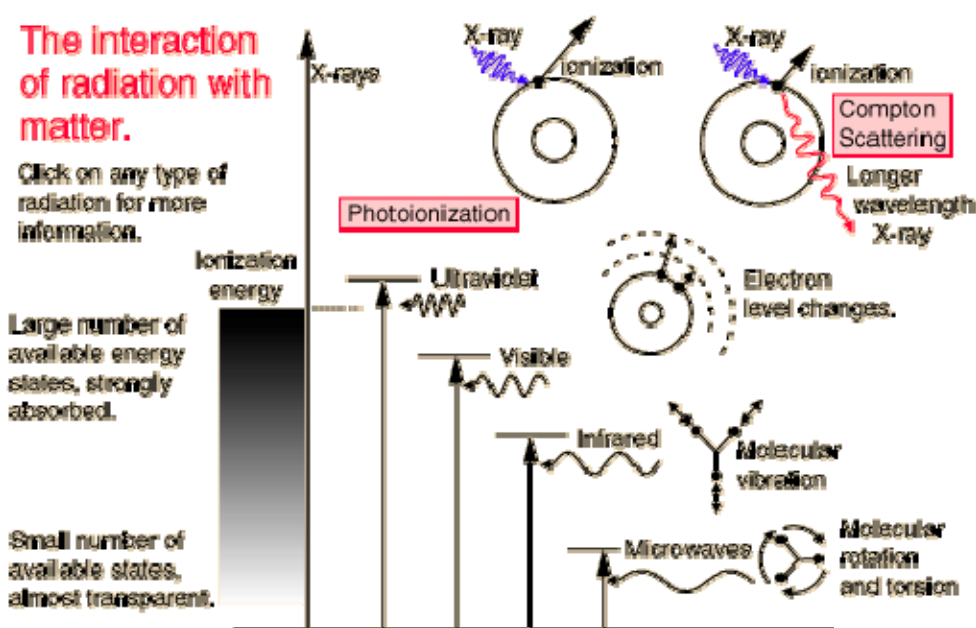


Figure 2.3 Interaction of radiation with matter

2.3 Biological effects of ionizing radiation

This section reviews the biological effects of radiation exposure and highlights the important role of dosimetry in medicine.

2.3.1 Mechanisms of radiation damages

Ionizing radiation affects humans by ionizing atoms and molecules encountered along its path through the body tissue. The x-ray is characterized by deep penetration into tissue with a relatively low spatial rate of energy loss [33]. Radiation provides the energy necessary to add or remove an electron to or from an atom or molecule. The affected atom or molecule might be part of a strand of DNA or it might be a free particle which when ionized can react with cellular material. While the body has repair mechanisms for many types of DNA damage, the mechanism may not be sufficient if many radiation lesions occur to the DNA close together in time and space [33].

The common types of DNA damage following exposure to ionizing radiation are single strand breaks and 'double strand breaks (Figure 2.4). Single strand breaks are produced by both low and high Linear Energy Transfer (LET) radiations and are repaired quickly and effectively. Double strand breaks are more lethal and repair is often incomplete and slow. High LET radiation is more effective at producing double strand breaks than the low LET radiation [33]. The potential mechanisms by which radiation produces carcinogenic changes in the cells include (i) mutations in a single gene or chromosome, (ii) changes in gene expression without mutations, and (iii) induction of oncogenic viruses, which in turn affect gene expression, leading to neoplasia [33]. Ionizing radiation is more effective at producing DNA-strand breaks than producing point mutations. Even though the single-strand breaks are rapidly repaired, the double-strand breaks can result in chromosomal rearrangements.

If not lethal to the cells, such aberrations can lead to cancer due to changes in gene expression or inactivation of tumor suppressor genes [33]. Carcinogenic effects of radiation on bone marrow, breast, thyroid, and lung have been observed in studies of atom bomb survivors and other irradiated human populations. These tissues are highly radiosensitive and therefore more prone to the effects of ionizing radiation.

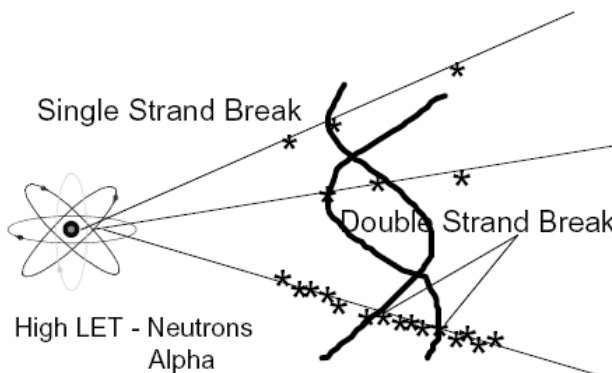


Figure.2.4: Types of DNA damages

The process of carcinogenesis is believed to be a 3-stage mechanism, involving initiation, promotion and progression [34]. The third stage is necessary before obviously malignant tumor cells are produced. It is assumed that a similar 3-stage mechanism exists for radiation carcinogenesis [35]. A synergistic interaction between the initiating effects of radiation and specific promoting agents has been reported in many different cell systems [36]. Radiation itself can enhance tumor promotion and tumor progression by the generation of free radicals, which in turn cause DNA damage [36].

There is a time course in cancer induction with a latency period between the exposure to radiation and the onset of observable cancers.

2.3.1.1 Cancer/heritable effects (stochastic)

Cancer effects are those for which the probability of an effect occurring is a function of dose without threshold and its severity is dose-independent [37]. Stochastic effects can be categorized as somatic (carcinogenic) effects and hereditary (genetic) effects, which may occur from injury to one or a small number of cells. Since a single cell may be enough to initiate the effect, there is a finite probability that the effect will occur however small the dose. Thus, stochastic effects are normally assumed to have no dose threshold below, which the effect cannot possibly occur.

Since stochastic effects may occur at any level of radiation exposure, the exposure should be kept as low as reasonably achievable [37]. Unnecessary exposures should be avoided, and necessary exposures should be optimized to provide the maximum benefit to the patient. Total doses should be limited to the minimum amount consistent with the medical benefit to the individual patient [38]. In the case of optimizing medical procedures for the best dose-benefit outcome, the main concern should be the amount and type of information derived from the examination and its diagnostic value. Neonates and children have a risk probability, for developing a radiation-induced cancer, hereditary effects or other serious disorders, four times more than that of all adults 50 years of age, due to greater cell proliferation rate, the radiation field which covers a relatively large area of the infant, their long life span expectancy, and also of the difficulty to shield radiosensitive organs [36, 37].

A modified somatic cell may still retain its reproductive capacity and may give rise to a clone of modified cells, which may eventually result in cancer.

A modified germ cell in the gonads, with the function of transmitting genetic information to the descendants of an exposed individual, may transmit incorrect hereditary information and may cause severe harm to some of those descendants (Figure 2.5).

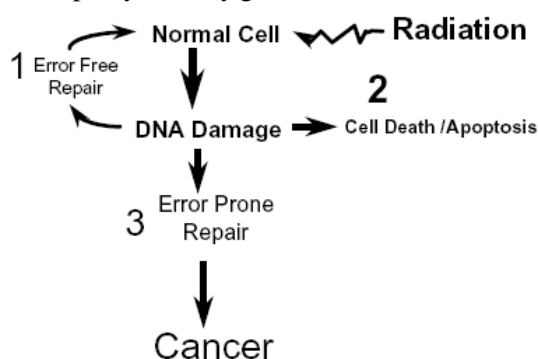


Fig.2.5: Cell and radiation damage

These somatic and hereditary effects, which may start from a single modified cell, are called stochastic effects [37]. Repair and defense mechanisms make cancer induction a very improbable outcome. Nevertheless, the probability of a cancer resulting from radiation exposure increases with increments of dose, and is assumed to have no low or high threshold (linear non-threshold model). If the damage occurs to a germ cell any resulting effects, of different types and severity, are expressed in the offspring of the exposed person [38, 39].

The probability of a fatal cancer was determined from studies of Japanese survivors of the atomic bombs. The estimates of severe hereditary effects are also based on genetic effects in animals. Stochastic effects are quantified using the probability of attributable fatal cancer, the weighted probability of attributed non-

fatal cancer, the weighted probability of severe hereditary effects and the length of life lost if the harm occurs [37].

Whole body irradiation or its equivalent as expressed by the effective dose equivalent or effective dose can be converted to a stochastic risk estimate using a total risk factor as determined by the ICRP [40] Table 2.1.

Table 2.1 Detriment adjusted nominal risk coefficients for cancer and hereditary effects (10^{-2} Sv^{-1})

Exposed	Cancer		Heritable effects		Total	
	ICRP2007	ICRP60	ICRP 2007	ICRP60	ICRP2007	ICRP 60
Population						
Whole	5.5	6.0	0.2	1.3	5.7	7.3
Adult	4.1	4.8	0.1	0.8	4.2	5.6

From the ICRP attempt to estimate absolute stochastic risks from whole-body irradiation, a risk coefficient of 5.5% cancers and genetic abnormalities per mSv of radiation dose was derived.

Caution is given to the current uncertainties associated with the extrapolation of radiation risks from high doses to those normally encountered in diagnostic radiology [5, 10].

Although knowledge of the patient effective dose associated with radiologic procedure is helpful, it is important to note that any resultant detriment will depend on the age of the exposed individual. As aforementioned the stochastic radiation risks of carcinogenesis and genetic effects are generally greater for children than for adults to at least a factor of two to three [37, 38]. These factors would need to be taken into account when converting any patient effective doses into a value of risk or detriment. As a result, direct comparisons of patient doses with those of adults need to be treated with circumspection.

2.3.1.2 Tissue reactions (Deterministic Effects)

Tissue reactions as a result of ionizing radiation include the types of injuries resulting from whole-body or local exposures to radiation that cause sufficient cell damage or cell killing to substantial numbers or proportions of cells, impairing the function of the irradiated tissues or organs [38]. Since a given number or proportion of cells must be affected, there is a threshold dose below which the number or proportion of cells affected is insufficient for the defined deterministic injury to occur [39]. The threshold dose depends on the level of injury or the sensitivity of the tissues or organs being irradiated. Any increase in dose above the threshold increases the level of injury, since fewer cells will survive at increased radiation dose. The effect will also increase with increased dose rate. Increased dose rate will accelerate cell damage without allowing enough time for more effective cell repair or repopulation [37].

The doses that result in the clinical appearance of deterministic effects are generally of the order of a few Gray to tens of Gray. The time at which the effect becomes noticeable may range from a few hours to some years after exposure, depending on the type of effect and the characteristics of the irradiated tissue.

The levels of radiation exposure and the irradiated tissues involved in diagnostic radiology are below the tissue reaction threshold but they may be reached in interventional radiology (Figure 2.6).

Deterministic effects will often have a more severe impact on children, since tissues are actively growing in comparison to adults [38]. Additional deterministic effects that have been observed from irradiation during childhood include effects on growth and development, hormonal deficiencies, organ dysfunctions and effects on intellectual and cognitive functions. From current data available [38], there is no evidence that the threshold of deterministic effects to the skin and eyes are any different for children or adults.

Radiological protection aims at avoiding deterministic effects (e.g. skin erythema, cataract formation and impaired fertility) by setting dose limits below their thresholds. Table 2.2 lists the estimated thresholds for deterministic effects in the adult gonads, lens and skin as stated in ICRP [18].



Figure.2.6: Appearance of radiation-induced skin injury approximately 18 to 21 months following multiple coronary angiography and angioplasty procedures – evidence of progressive tissue necrosis

Table 2.2: Projected threshold estimates of the acute absorbed doses for 1% incidences of morbidity and mortality involving adult human organs and tissues after whole body gamma ray exposures

Effect	Organ/tissue	Time to develop	Absorbed
		Effect	Dose (Gy)
Morbidity:			1% Incidence
Temporary sterility	Testes	3-9 weeks	~0.1
Permanent sterility	Testes	3 weeks	~6
Permanent sterility	Ovaries	< 1week	~3
Depression of blood-	Bone marrow	3-7 days	~0.5
Forming process			
Main phase of skin	Skin (large areas)	1-4 weeks	<3-6
Reddening			
Skin burns	Skin (large areas)	2-3 weeks	5-10
Temporary hair loss	Skin	2-3 weeks	~4
Cataract (visual	Eye	Several years	~1.5
Impairment)			
Mortality:			
Bone marrow			
syndrome:			
- Without medical care	Bone marrow	30-60 days	~1
- With good medical	Bone marrow	30-60 days	2-3
care			
Gastro-intestinal			
Syndrome:			
- Without medical care	Small intestine	6-9 days	~6
- With conventional	Small intestine	6-9 days	>6
Medical care			
Pneumonitis	Lung	1-7 months	6

2.3.2 Radiation risk Assessment

The most effective method of assessing the risks from exposure to radiation is by calculating the absorbed doses in individual tissues and subsequently determining the effective dose. The absorbed dose to a specific tissue has traditionally been difficult and time consuming to measure.

The organs to be considered in radiologic risk assessment were standardized by the ICRP [6] with the introduction of the effective dose equivalent (EDE). Calculations of the EDE require knowledge of the absorbed dose (total energy deposited per unit mass) to the entire tissues. These absorbed doses, or more specifically, dose equivalents, are then multiplied by tissue weighting factors (wt), which represent the fraction of total radiation risk (cancer mortality and severe genetic damage) attributed to irradiation of that tissue. The EDE is calculated as a summation of these weighted doses and thus represents a single radiation dose proportional to the total radiation risk of the exposure, regardless of whether the irradiation is uniformly or non-uniformly delivered.

This dosimetry concept was further expanded in 1990 with the introduction of the effective dose (E) in which tissue weighting factors were reassessed based on a more recent analysis of radiobiological effects [18]. While originally defined for radiation protection purposes, these quantities of EDE and E have been widely reported in the medical literature for both nuclear medicine procedures and for diagnostic radiology examinations. Their intended use in medicine is to provide physicians with a unified quantity for risk communication and a quantitative means for procedure optimization. As defined in ICRP Publications 26 and 60 [6,18], the tissue weighting factors are specific only to populations of adults and should not be applied in the estimation of radiation risk to individual patients [41](Poston 1993). For use in risk communication and/or procedure optimization, tissue weighting factors specific for children have been proposed by Almen and Mattsson [42].

The determination of organ doses in diagnostic radiology is typically a two-step process. First, an indicator dosimetry quantity is measured in the clinical setting. Examples include the ESD or the DAP. Second, these indicator quantities must be multiplied by an organ dose coefficient to obtain individual organ doses [43, 44]. These conversion factors are obtained either through experimental measurement within physical phantoms or through computer simulations within mathematical models of the patient.

One may also estimate radiation risk for diagnostic procedures by measuring the total energy imparted to the patient for a given diagnostic exam (the integral dose). Extensive studies of energy imparted in diagnostic radiology have been made [18].

2.4 In vivo dosimetry in radiation medicine

In vivo dosimetry is the final stage in a long series of quality assurance (QA) procedures in radiation medicine. As the term *in vivo* indicates, these measurements are generally performed during patient treatment or diagnostic examination, and the measuring instrument is either positioned inside the patient, on the patient's skin or as close as possible. The other quality assurance procedures are performed in phantoms (Fig.2.7), (i.e., in the absence of the patient) in order to check the behavior of the medical apparatus (linear accelerator, or diagnostic imaging unit) or the validity of a computer-designed treatment plan. Today, the use of in vivo dosimetry is increasing following the recommendation by many national and international organizations [1, 10, 18, 20]. New diagnostic and treatment techniques introduce new challenges and requirements, such as the need to provide real-time dosimetry devices with high spatial resolution, sensitivity and accuracy. In view of the topic of this thesis work, the discussion will be limited to two sub fields: external radiation therapy and diagnostic and interventional radiology.

ICRU [45] recommends that “all the procedures involved in the planning and execution of radiotherapy can contribute to a significant uncertainty in the absorbed dose delivered to patient, and an ultimate check of the actual treatment given can only be made by using in vivo dosimetry”

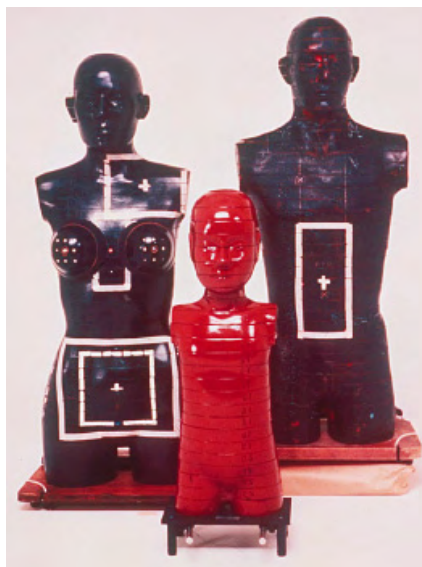


Figure 2.7. Anthropomorphic (Alderson-Rando) phantoms, adult male, adult female, and 6-year-old child.

2.4.1 In vivo dosimetry in high energy energies

The role of in vivo dosimetry in radiation therapy is:

1. To verify the calculations of the Treatment Planning System (TPS) at interfaces, i.e. close to the skin.
2. To evaluate the target dose in order to verify the treatment delivery process.

The former goal can be reached by using entrance and exit detectors, positioned on the patient's skin during treatment. In general, entrance dose measurements serve to check the output and performance of the treatment device, the accuracy of patient setup, and the calculation of the number of monitor units. Exit dose measurements serve, in addition, to check the relative dose calculation algorithm and to determine the influence of shape, size, and density variations of the patient on the dose calculation procedure [5,46] (Figure 2.7).

According to the European Society for Therapeutic Radiation Oncology (ESTRO), the latter condition can only be fulfilled when detectors are inserted in natural body cavities, because of all the potential errors associated with entrance and exit measurements [26]. In vivo checks can detect systematic errors as well as estimate the accuracy of the treatment delivery.

The frequency of in vivo measurements varies greatly among institutions. However, the common practice is to perform in vivo entrance measurements for each patient, or only for specific groups of patients. Nonetheless, in vivo dosimetry is performed in relatively few institutions because of time or financial constraints.

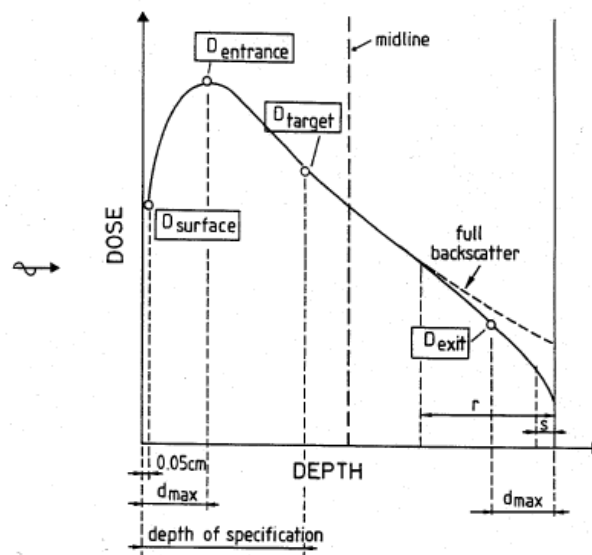


Figure. 2.8: Schematic representation of the characteristics of a single photon beam passing through a medium in a treatment situation showing different doses involved for in vivo and in vitro dose measurements in radiotherapy. Where D_{entrance} surface is the dose at ~ 0.05 cm below the skin surface, D_{target} is the target dose at depth of dose specification, D_{exit} surface is the dose at exit surface ~ 0.05 cm interior to the skin surface, ' s ' is the electron backscatter range and ' r ' is the photon backscatter range.

2.4.2 In vivo dosimetry in low energies

In vivo dosimetry of patient ESD during radiological procedures has been performed using ionisation chambers, TLDs and DAP or using mathematical model calculations based on the X-ray tube output.

[47]. The average organ dose cannot be measured directly, but can be derived from the entrance surface dose using Monte Carlo simulation Data.

The vast majority of these studies have used DAP more than other methods, because the patient position is less important so the measurements does not interfere with the examination of the patient and there is no need to disturb the patient with the measurements. The disadvantage of DAP in pediatric treatments is that the dose can be low while the absorbed dose is high when a small area is irradiated. The opposite can happen when a large area is irradiated [43,44].

TLDs are being widely used to estimate in vivo dose because of their small size, inexpensive, rugged, good spatial resolution and flexibility to position in various situation. Moreover they are capable of detecting systemic errors during execution of the treatment. Furthermore, TL dosimetry can be placed on different parts of the body and in cavities, which offers unique opportunity to measure the dose in complex situations. For these aforementioned reasons, TLDs are used in this study.

2.5 Radiation dose measurements and unites

Patient dose measurement in radiological procedures is an important and indispensable way of assessing the quality of procedures and the detriments of exposure to ionizing radiation. It is of particular application for interdepartmental comparison of the quality of procedures, of different protocols and of new techniques.

2.5.1 ESD

ESD, which is defined as: the absorbed dose to the entrance skin of the patient at the central point of irradiated area including back scatter radiation [43,44], is measured by different methods in literature. The direct method: with small detectors attached in the skin of the patient at the beam entrance, including, TLD, films, and more recently diodes or Metal-Oxide Semiconductor Field- Effect (MOSFET) detectors [46]. The indirect method: with a DAP meter which is attached to a light beam diaphragm. A DAP meter uses a transmission type air ionisation chamber, which measures the radiation dose, as a function of the field size, or by using mathematical model calculations based on the X-ray tube output [46,48], (Figure 2.8)

The ESD is estimated in order to assess the possibility of skin dose exceeding the threshold for deterministic effects [49]. The total values of imparted radiation dose from all fluoroscopic and radiographic exposures involved in the specific examination are measured.

ESD surface dose is the simplest and most frequent method used to measure patient dose from radiologic examinations because direct measurements on patients can be performed easily at the skin surface. ESD can be obtained from detectors attached to the skin surface during the examination. (i.e., TLDs, or ion chambers). ESD may also be converted to organ doses with Monte Carlo software, although such an approach may result in errors of more than 20% [43, 49].

Although simple to obtain, the surface dose is a poor indicator of the true significance of radiation exposure to the patient because it overlooks a number of important factors. For example, in a fluoroscopic exam the surface dose does not account for changes in the depth of the radiosensitive organs, changes in the exposed field size, changes in the position of the patient, changes in the beam qualities, overlaying exposure fields and partial exposure of organs [49]. More importantly, the surface dose does not account for the area of exposure or the penetrating ability of the x-ray beam as the energy of x-rays varies.

The above factors make surface dose a quantity of limited dosimetric value when estimating stochastic risks. However, the surface dose is the quantity of choice when trying to predict the occurrence of deterministic radiation effects of the skin during high dose interventional radiologic procedures. ESD depends on the followings: exposure parameters (Tube voltage, Total filtration, mAs and FFD), and patient's conditions (patient positioning, field size, and film screen system).

2.5.2. Organ dose

Organ dose, which is used to determine the risk to the patient undergoing radiological examination, can be measured in vivo with TLDs, DAP and air kerma free in air by applying a dose conversion factor [18,49] or in vitro by using a tissue equivalent phantom, which represents a patient

2.5.3 Equivalent and Effective Dose

The fundamental quantity in radiation dosimetry is the absorbed dose, D , or energy absorbed per unit mass, in units of Gray, Gy.

Equivalent dose extends the meaning of absorbed dose by taking into consideration the type and energy of radiation involved (Table 2.3). The absorbed dose is weighted by a radiation-weighting factor, which is selected to be representative of the relative biological effectiveness of that radiation in inducing stochastic effects at low doses. Radiation-weighting factors for different radiation types are given in Table 2.3 (ICRP, 1991) [18].

Table 2.3: Radiation weighting factors [6]

Type and energy range	Radiation weighting factor, W_R
Photons (all energies)	1
Neutrons (Factors dependent on energy)	5-20
Protons (>2 MeV)	5
Heavy nuclei	20

Effective dose takes into account the distribution of absorbed dose within the body via radiation and tissue weighting factors. The SI unit of effective dose is the Sievert (Sv). Effective dose provides the basis for

estimating the probability of stochastic effects of absorbed doses that are well below the thresholds for deterministic effects [18]. When the W_R is 1, such as with x-rays, the relationship between the probability of stochastic effects and absorbed dose depends on the organ or tissue irradiated. Tissue-weighting factors shown in Table 2.4 represent the relative contribution of that organ or tissue to the total detriment due to these effects resulting from a uniform irradiation of the whole body.

The tissue weighting factors, w_T , are gender averaged and are for dose assessment of workers as well as members of the public, including children.

Table 2. 4 Tissue weighting factors [6]

Tissue	W_T	$\sum w_T$
Bone-marrow, Colon, Lung, Stomach, Breast, Remainder Tissues* (Nominal w_T applied to the average dose to 14 tissues)	0.12	0.72
Gonads	0.08	0.08
Bladder, Oesophagus, Liver, Thyroid	0.04	0.16
Bone surface, Brain, Salivary glands, Skin	0.01	0.04

*Remainder Tissues (14 in total)

Adrenals, Extrathoracic (ET) region, Gall bladder, Heart, Kidneys, Lymphatic nodes, Muscle, Oral mucosa, Pancreas, Prostate, Small intestine, Spleen, Thymus, Uterus/cervix.

Evaluating the risk associated with a diagnostic radiological procedure has been acknowledged by the 2005 draft recommendations from the ICRP [50]. The ICRP 2005 states "That exposure is not limited by any regulatory process, but is controlled by the physician, who therefore should be aware of the risks and benefits of the procedures involved". The direct outcome of the ICRP recommendations is that a physician must then balance the risk versus benefit equation by maximizing the diagnostic information while maintaining the exposure to ionizing radiation as low as diagnostically achievable (ALARA). The physician and physicist that ignore ALARA have the potential of increasing patient dose unnecessarily.

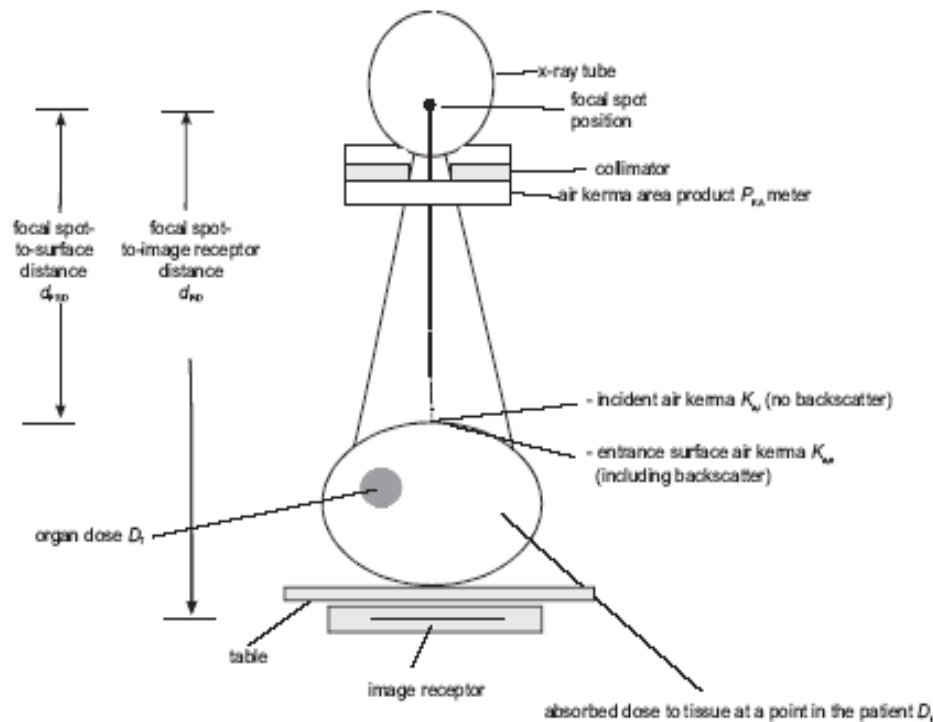


Figure 2.9. Simple exposure arrangement for radiography showing some of the dosimetric and geometric quantities recommended in the present Report for determination of patient dose.

2.6 DOSIMETRY TOOLS

This section briefly reviews the dosimetry tools (dosimeters other than TLD) in diagnostic radiology. The ideal diagnostic radiology dosimeter is one that provides an immediate response to the radiation field (real-time), is accurate, tissue-equivalent, inexpensive, easy to operate, exhibits no angular dependence and does not interfere with the diagnostic information in the image [48].

2.6.1 Ionisation Chambers

Ionisation chambers are the gold standard in medical dosimetry. They provide accurate absolute dose determination, and are therefore used to calculate absorbed dose to air, in free air, in diagnostic radiology. The latter measurements are done on the axis of the x-ray beam without the patient or phantom present then corrected to entrance surface dose using appropriate backscatter factors and the inverse square law [47,51]. Ionisation chambers are not used for most direct patient measurements because they are bulky, require connecting cables and high voltages, are difficult to attach close enough to the patient's skin to completely measure the backscattered radiation, severely restrict patient mobility, and cast interfering shadows on radiographs [51].

Ionisation chambers consist of two electrodes with a potential difference maintained between them. Ions are produced in the sensitive volume of the chamber by the radiation beam and are collected by the electrode. The resulting ionisation current in the chamber's external circuit is proportional in magnitude to the measured beam intensity [48, 51].

2.6.2 DAP meter

DAP meter overcomes the difficulties of conventional ionisation chambers for on-line patient dose measurements. DAP meters are commonly used to monitor doses delivered to patients in diagnostic radiology and interventional radiology. Even though it is a large area, parallel-plate ionisation chamber, it is not considered to be as accurate as those used in radiotherapy. DAP meters can be mounted on the diaphragm housing of an x-ray unit to intercept the entire cross-section of the x-ray beam and integrate the absorbed dose over the whole beam area, for any number of exposures. These ionisation chambers are usually transparent so that when fitted to an over-couch x-ray tube the light beam diaphragm device can still be used. DAP quantity (Gy.cm^2) is defined as the absorbed dose to air averaged over the area of the x-ray beam in a plane perpendicular to the beam axis, multiplied by the area of the beam in the same plane. Radiation backscattered from the patient is excluded. DAP can be measured at any point between the diaphragm housing of the x-ray tube and the patient since it is invariant with distance from the tube focus, as long as the point of measurement is not close enough to the patient to receive significant backscattered radiation [51]

DAP meters can provide a single measurement of the total amount of radiation used in even the most complex examinations involving radiography and fluoroscopy [51] Therefore, for calculation of dose, DAP meters do not require the precise recording of all exposure factors for each examination, or the long processing time of TLDs [52].

The vast majority of the studies in the literature have used DAP for both the individual radiographic views and fluoroscopic procedures [49, 52, 53], because the patient position is less important, so the measurement does not interfere with the examination of the patient and there is no need to disturb the patient with the measurements [53]. On the other hand, the disadvantage of DAP in children is that the dose can be low while the absorbed dose is high when small area is irradiated, and the opposite happens when large area is irradiated. The scattered radiation from the collimator affects the reading, without affecting the radiation dose [53].

2.6.3 Radiographic Film

For radiographic film, the degree of film blackening is related to the dose deposited and can be expressed in terms of optical density. The dose response curve is only linear within a certain range of optical densities and a calibration curve must be derived for quantitative dosimetry. Optical density can be quantitatively evaluated using an optical densitometer.

Radiographic film is available with different sensitivities. In diagnostic radiology, film speed is always quoted when referring to patient doses. Faster film requires less dose to develop the same optical density as a slower film and thus avoids unnecessary exposure of the patient in diagnostic radiology [48].

2.6.4 MOSFETs

MOSFETs, or Metal Oxide Semiconductor Field Effect Transistors, are relatively new detectors in medicine.

Advantages include:

- High spatial resolution (active area of $0.2 \times 0.2 \text{ mm}^2$ [31].
- Active depth of $1 \mu\text{m}$ (for skin dose assessment).
- Immediate dose read out.

Disadvantages include:

- Visible on diagnostic radiographs,
- Limited capacity for accumulation of absorbed dose,
- Poor reproducibility,
- Temperature and directional dependence, and
- Cables attached.

The operation of a MOSFET dosimeter is based on the ionizing radiation causing a build-up of charge on the silicon oxide gate. The charge build-up will affect the threshold voltage at the gate required to allow current flow from source to drain. The voltage variation caused by the irradiation is most commonly evaluated by maintaining a constant current between source and drain and measuring the required gate bias, which is proportional to the absorbed radiation [54]. In clinical practice a voltage of typically 3 to 6V is applied during irradiation allowing the MOSFET to measure up to about 50Gy [54].

Fading makes MOSFETs unsuitable for the long screening times involved in interventional radiology procedures [31]. MOSFETs have been used for surface dose measurements [55], in-vivo dosimetry in radiotherapy [56] and diagnostic radiology [31]. However, to date there are few reports on the clinical application of MOSFETs. They would find application when steep dose gradients are present, i.e. in brachytherapy dosimetry.

2.6.5 Diamond detectors

The use of synthetic diamonds as in vivo radiation detectors has been reported as early as 1987 [57]. Diamonds have been considered suitable for clinical purposes because of their small size and good tissue equivalence. They are also resistant to radiation damage. However, their use for in vivo dosimetry can be impaired by their dose-rate dependence and the need for pre-irradiation [58]. Diamond detectors exhibit high sensitivity and high resolution (with a sensitive volume of 1 mm^3), but their advantage over diodes is debated except in very small fields.

Diamond detectors also have less angular dependence than diodes in electron beams Bucciolini et al [59] compared diamond detectors to diodes and ionization chambers, and concluded that in spite of their

positive characteristics, diamonds did not offer a significant advantage over diodes in photon beams in conventional radiation therapy.

2.6.6 Optical fiber dosimetry

Plastic scintillator systems also offer excellent tissue equivalence, but their present design makes it difficult to subtract the noise signal produced in the light-guide (Cerenkov radiation and fluorescence) from the signal originating from the actual plastic scintillator chip [60]. Several approaches have been reported to improve the signal-to-noise ratio. One approach consists in adding a blank optical fiber for subtraction of the light-guide signal: this can compromise the size of the optical fiber and make the scintillator probe too bulky to be inserted in a patient. Another approach is the optimization of the coupling between the fiber and the scintillator, which, so far, has only had a limited success in reducing the influence of the noise signal from the light guide plastic scintillation dosimetry, may benefit from a renewed interest if this problem gets solved [60].

2.6.7 Optically stimulated luminescence

Optically stimulated luminescence is related to thermoluminescence, but uses light (e.g., from a laser) instead of heat as the stimulation source. Huston et al [61] described an OSL system for radiation therapy that uses two light guides (one for the laser light, the other for the signal) and copper-doped glass as the detector. This system demonstrated a very high sensitivity, dynamic range, and stability, no dose rate dependence, and little energy dependence. Though promising, this system has not been applied in internal in vivo dosimetry to date. Few results have been reported from this system, which seems to be designed for radioprotection dosimetry more than in vivo radiotherapy applications.

2.7 Medical Linear Accelerators

The Linear accelerator is the single most influential development in radiation oncology. The first medical linac (8 MV) was installed at Hammersmith Hospital in London 1952, with the first patient treated in August 1953 [62]. The development of mega-voltage radiation machines, that are capable to delivering adequate doses of radiation to tumors located in all areas of the body continues to improve treatments.

2.7.1 Linear accelerator system

An electron source arises from a hot filament or cathode in an evacuated tube. There is an accelerating voltage between the cathode and the target or anode. The accelerating voltages are fixed for a particular system and they normally range from about 4 MV to 35 MV. The system employs thick collimators to shape the beam. High-energy linacs ($E > 7$ MeV) have the potential to generate neutrons from interaction with heavy metals found in the target material, walls of the accelerator structure, wave-guide, filters, and collimators. While neutron activation of the air around the patient and of the patient is possible, it is very

little and only of minor concern. A maze is usually incorporated in the room design to prevent neutron scatter from reaching the control console. Because all medical linacs serve the same purpose, they tend to have similar components. Some of the major components in a linac are (Figure 2.9) the gantry, the stand, the control console, and the treatment couch. The two major structural components are the stand and the gantry. The stand is anchored firmly to the floor and the gantry rotates on bearings in the stand. The operational accelerator structure is housed in the gantry and rotates about a horizontal axis fixed by the stand. Other major components include: The klystron is the source of microwave power used to accelerate the electrons. This power is conveyed to the accelerator structure in the gantry by a wave-guide and there is a circulator inserted in the wave-guide, which isolates the klystron from any microwaves reflected back from the accelerator. The circulator diverts these reflected microwaves so they won't damage the klystron [25,46].

A cooling system is used to cool the various components that experience heat buildup and insures stable operating temperature sufficiently above room temperature to prevent condensation of moisture from the air.

The accelerator structure is the component where electron acceleration takes place. It consists of a copper tube with its interior divided by copper disks or diaphragms of varying aperture and spacing (Figure 2.9) and is kept under a high vacuum.

Electrons are injected into the accelerator structure with an initial energy of about 50 KeV by the electron gun (i.e., cathode) and are energized by the microwaves emitted by the klystron.

The high-energy electrons emerge from the window of the accelerator structure in the form of a pencil-thin beam about 3 mm in diameter. In low energy linacs ($E < 6$ MV) the electrons strike the tungsten target to produce x-rays. In high-energy linacs, the accelerator structure is so long that the electrons are sent through the field of a bending magnet in the treatment head which deflects the electrons in a loop (usually 90° or 270°) before they can strike the target and produce x-rays or be used for electron treatment. The treatment head also contains beam shaping and monitoring devices.

X-rays are produced when the electrons hit a tungsten target. The target is water cooled and thick enough to absorb most of the electrons. The average photon energy of the beam is about one-third of the maximum electron energy. Directly opposite the collimator and extending from the bottom of the gantry may be a beam stopper. This is a large absorber, which reduces room-shielding requirements because it absorbs the radiation beam that emerges from the patient.

Some linacs are also capable of producing electron beams for therapy. The electrons produced in an accelerator are usually monoenergetic, consequently their energy is designated in units of million electron volts (e.g., 10 MeV), whereas the x-ray beam is more heterogeneous and designated in units of megavolts (e.g., 18 MV) [25,46,63].

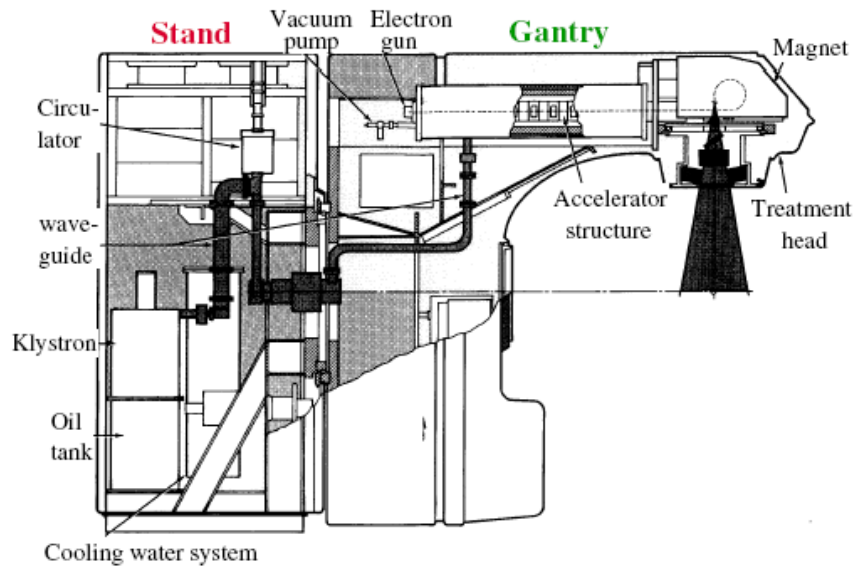


Figure 2.10: Medical Linear accelerator

2.7.2 Electron versus X-ray Beam Therapy Systems

Not all tumors are deep. Some are either on the surface or just beneath the surface. Shallow tumors are often treated with electrons generated from the linac. Figure 2.11 compares the treatment head arrangement for an electron beam versus an x-ray beam. As the electrons exit the accelerator structure, the beam is pencil thin. For electron therapy, instead of striking a tungsten target, the beam of electrons is made to strike an electron scattering foil in order to spread the beam as well as get a uniform electron density throughout the treatment field. This foil is most often a thin lead foil which scatters the electron beam without producing a significant number of bremsstrahlung x-rays.

Electrons are desirable for treating superficial tumors (< 5 cm deep). The types of tumors suitable for electron therapy are skin and lip cancers, chest wall irradiation in breast cancer, boost doses to lymph nodes, and head and neck cancers. Electron beam therapy is desirable because it produces a uniform dose in the target volume and minimizes dose to deeper tissues [25, 63].

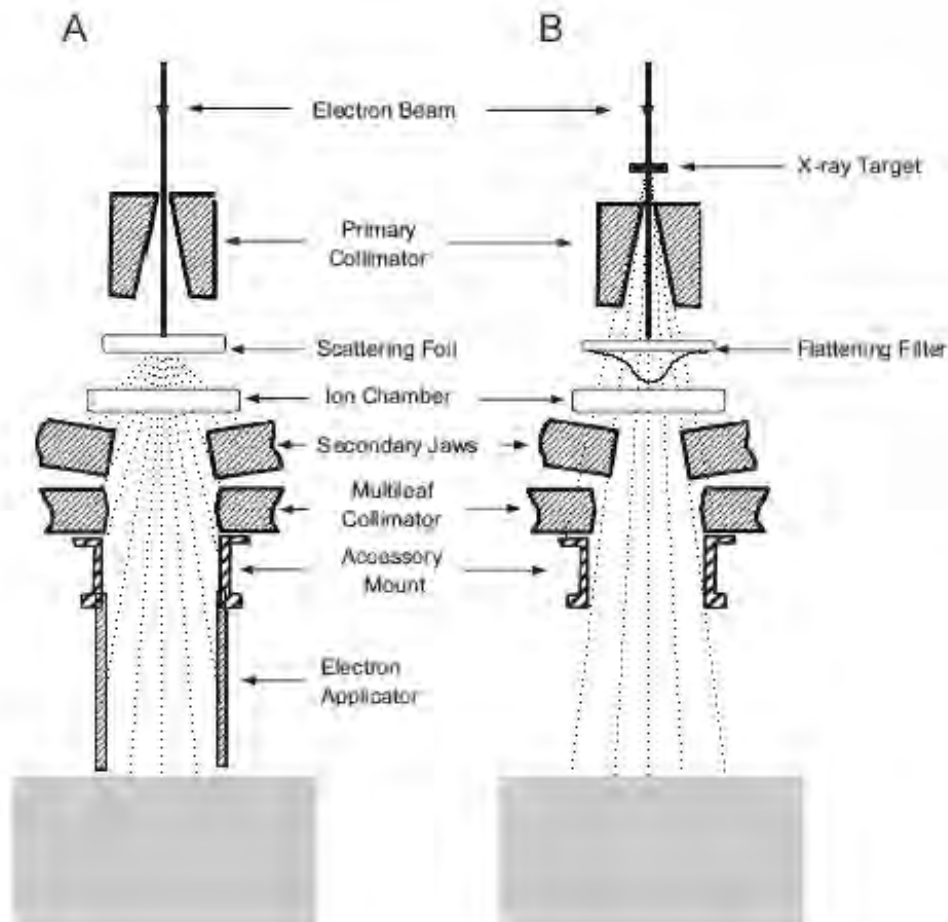


Figure 2.11: Schematic illustration of the cut-away view of the collimator of a linear accelerator in (A) electron beam and (B) photon beam modes

2.8 Diagnostic X-ray unit

The x-rays produced by diagnostic x-ray systems (e.g., medical, dental, veterinary, etc.) usually possess higher energy, and thus are more penetrating than those produced by analytical machines. To generate these higher energies, special tubes are required.

X-ray tubes (Figure 2.12) consist of a cathode and an anode. A low amperage cloud of electrons is generated at the cathode and the electrons are accelerated by a large voltage potential difference across the small gap toward the anode. In radiology, the cathode is usually referred to as the filament and the anode as the target. Except for dental x-ray tubes, which use stationary anodes, diagnostic x-ray units usually employ rotating anodes because they are usually three-phase systems. Older, single-phase systems produce x-ray pulses, which follow the sine wave of the electric current. A 3-phase system produces an x-ray pulse, which is nearly flat, and ripple free resulting in more efficient x-ray production and higher effective x-ray energy. Rotating anodes are suited for 3-phase systems because:

- These units usually have the capability of operating at very high voltages. The peak kilovoltage (kVp), or x-ray tube potential, determines the maximum energy of the x-rays. Modern tubes are usually capable of operating at maximum tube potentials of 150 kVp.
- The systems operate at very high tube currents. Some systems may be capable of operating at currents of 1000 mA. The rotating anode helps to remove the heat produced from absorbing the electrons in the anode.

The x-rays are produced by bremsstrahlung. The efficiency of x-ray production is defined by the equation:

$$f = 7 \times 10^{-4} Z^2 E \quad (2.1)$$

Where Z is the atomic number of the target and E the energy (in MeV) of the electrons (i.e., the tube potential).

Most diagnostic units use tungsten as the target. Thus, for a tube potential of 100 kVp and a tungsten target (i.e., $Z = 74$), the fraction of bremsstrahlung x-rays produced would be 0.00518 per electron. Most (> 99%) of the electron beam energy is dissipated as heat and does not produce x-rays. A rotating anode spreads the electron beam over a much larger surface as it rotates than does a stationary anode. This allows these systems to absorb even more heat energy and to operate at higher tube potentials and tube currents.

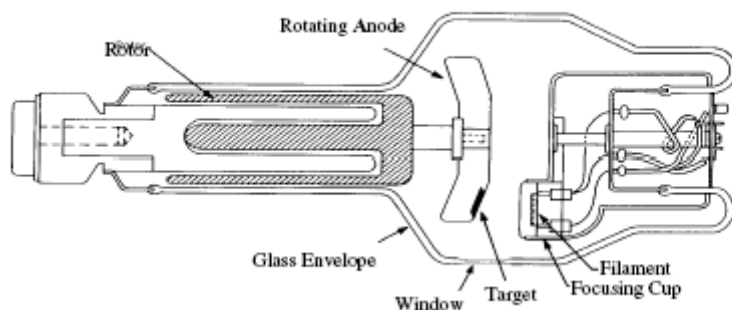


Figure 2.12: X ray tube

The x-rays produced fall into two classes of x-rays (Figure 2.12). The bremsstrahlung spectrum is essentially continuous. However, some of the bombarding electrons interact with and eject orbital electrons from the inner orbits of the target atoms producing characteristic x-rays (Figure 2.11). The characteristic x-rays have energies characteristic of the element in which they were released. At diagnostic energies (> 70 kVp), tungsten produces both K- and L-shell x-rays. The K characteristic x-rays have possible energies of 57.4, 66.7, 68.9, 69.4 keV with an effective energy of 69 keV. The L-shell characteristic x-rays are emitted with an effective energy of 12 keV.

The higher the energy of the electrons, the more penetrating the x-ray radiation produced. While x-rays with effective energies of 69 keV are good for imaging most body parts, they are too penetrating to easily

distinguish soft tissue anomalies. For that reason, mammography x-ray units usually operate at lower peak tube potentials (e.g., 20 - 35 kVp) and employ a molybdenum target. Molybdenum has an atomic number of 42 and has K characteristic x-rays of 17.5 and 19.6 KeV; energies very useful for soft tissue diagnosis. A tungsten target x-ray tube operated at the same tube potential would have characteristic x-rays about 12 KeV, too low for diagnosis (Figure 2.12).

The glass, diagnostic x-ray tube is enclosed in a protective (lead) tube housing (Figure 2.12), which is designed to shield personnel from unnecessary (leakage) radiation and reduce the risk of electric shock.

Some x-ray tubes have voltages as high as 150 kV. The protective housing incorporates specially designed high-voltage receptacles to protect against accidental electric shock. X-rays produced in the target are emitted isotropically, that is with nearly equal intensity in all directions. Those not directed toward the patient are useless. The tube housing contains lead to absorb most of the useless radiation and has a specially designed window or port to direct the x-ray beam toward the patient.

X-rays emitted from the x-ray tube are categorized into primary, scatter, and leakage radiations. The primary radiation is the radiation beam, which passes through the window and is allowed to expose the patient or material. When addressing patient safety, the concern is with primary radiation. Scatter radiation is that part of the primary radiation beam which has been deflected in direction by air, the patient, or other material in the beam. Leakage radiation is the radiation, which escapes through the x-ray tube housing. The sum of scatter and leakage radiation is called stray radiation. When addressing operator and worker safety we are concerned with stray radiation. This radiation must be shielded so exposures are kept ALARA.

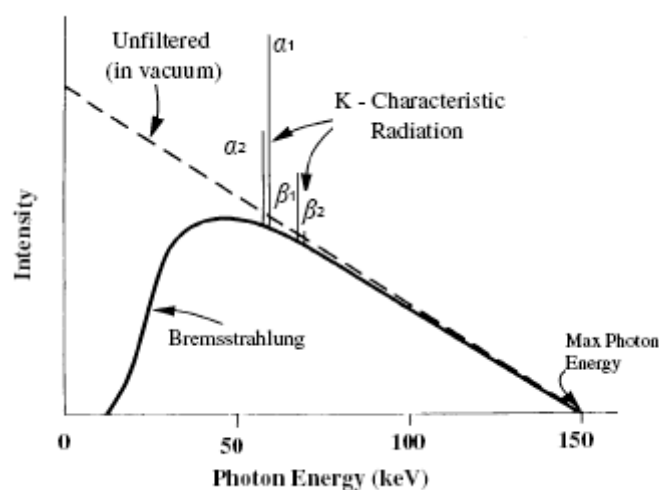


Figure 2.13. radiation spectrum in an X ray tube

Diagnostic x-ray units can be divided into several types of systems: radiographic (and dental), fluoroscopic, angiographic and cardiac, tomographic, mammographic and bone densitometry. Each has special uses and capabilities.

Radiographic units are by far the most common and include both fixed and portable x-ray units as well as dental units. The general concept of operation (Figure 2.13) is that a patient is placed at a certain distance from the tube (normally 40 - 48 inches, but chest radiographs are usually made at 72 inches and dental [bite wings] are normally made at 7 - 9 inches), in front of the image receptor (i.e., the x-ray film or digital image plate) where the x-ray image is produced. Most modern stationary radiographic systems have a radiation detector, called a phototimer or automatic exposure control, which automatically terminates the x-ray exposure when enough radiation has been given to produce a readable image on the film or other image receptor. Some exposures are made using manual techniques. In this mode the technician measures the thickness and density of the body part in question and, refers to a technique chart to determine the optimum technique factors (kVp, mA, sec) to obtain a quality film.

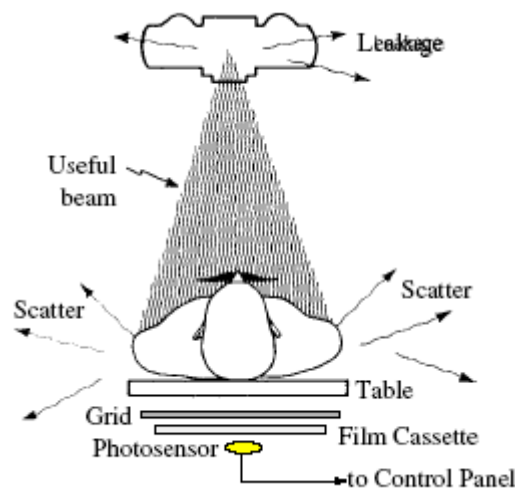


Figure 2.14: Patient exposures during a radiological examination

Fluoroscopic units are often used in the investigation of dynamic body functions and localization of devices (e.g., angiography and cardiology). Most fluoroscopic systems (Figure 2.14) consist of the x-ray tube, an image intensifier and a remote display. Until about 1960, most fluoroscopic units were direct view. In this system, the radiologist would dim the room lights and place a luminescent screen against the patient.

The x-ray image would form on the screen and the radiologist would directly view the image to make a diagnosis. All of these systems have been replaced by image-intensified units. The image intensifier is a special amplifying tube which is used to increase the image brightness by as much as 6000-times the brightness of a regular (non-intensified) fluoroscopic screen (Figure 2.14).

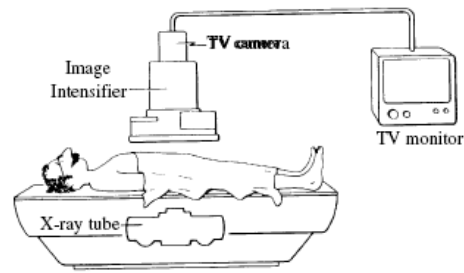


Figure 2.15: fluoroscopic X ray machine

This image can then be viewed under normal lighting conditions using either a series of mirrors (very rare) or by video pickup and projection or storage onto videotape. Radiographs (i.e., x-ray images), called spot films, may also be made to provide a hard copy of the area of interest to the radiologist. Often fluoroscopic exams use a dense contrast media such as iodine ($Z = 53$) or barium ($Z = 56$) to increase the density between the cavity of interest and the soft tissue ($Z = 6 - 10$) surrounding the cavity.

3. THERMOLUMINESCENCE DOSIMETRY

3.1 Historical background

Luminescence is the generation of light without heat due to the movement of electrons within a substance from more energetic states to less energetic states. There are many types of luminescence, including chemoluminescence, produced by certain chemical reactions, chiefly oxidations, at low temperatures; electro luminescence, produced by electric discharges, which may appear when silk or fur is stroked or when adhesive surfaces are separated; and triboluminescence, produced by rubbing or crushing crystals: bioluminescence is luminescence produced by living organisms such as glow worms, fireflies, and various fungi and bacteria found on rotting wood or decomposing flesh.

There are two categories of luminescence: Fluorescence is emission of light during or immediately after irradiation (less than 10^{-8} s). This is not a particularly useful reaction for TLD use. Phosphorescence is the emission of light after the irradiation period. The delay time can be from 10^{-8} s to weeks, months or years.

Thermoluminescence (TL) is defined as the latent luminescence induced by ionizing or ultraviolet radiations in some materials, which is released at temperature significantly above the irradiation temperature [64]. The phenomenon of the Thermoluminescence of minerals was known empirically as early as 1663. It was in this year that sir Robert Boyle described how, upon warming a diamond in contact with his body in the dark, he saw a glimmering light. Wiedemann and Schmidt are the first used the term ‘thermoluminescence’ in literature in 1895 for the observation of excess light emission over thermal background. They were also the first to synthesise $\text{CaSO}_4 \cdot \text{Mn}$, TL, which was used for detection of radiation from electrical discharge [65]. Marie Curie reported the ability of Calcium fluoride to produce TL after being exposed to a radium source [65]. Prizbram recorded the first glow curve in 1923. At the same year, Farrington Daniels reported the first successful application of thermoluminescence in radiation dosimetry in 1953 during atomic bomb testing and in vivo measurements in patients following therapeutic doses of Iodine-131 [66]. The topic became more interesting after the introduction of TLD-100 in 1963, which is the most popular in occupational and medical dosimetry. The wavelength of the emitted light is a characteristic of luminescent material [64-66].

3.2 Theory of thermoluminescence

3.2.1 Thermoluminescence Effect

Theoretical evaluation of the thermoluminescence behavior was first considered by Randall and Wilkins [67] in their expression for the probability of an electron escaping a trap. Electrons in some solids can exist in two energy states, a lower energy state called the valence band and a higher energy state called

the conduction band. The difference (energy region) between the two bands is called the band gap. Electrons in the conduction band or in the band gap have more energy than the valence band electrons. Normally in a solid, no electrons exist in energy states contained in the band gap. This is a "forbidden region."

The ionized electrons created by radiation passing through a TLD are trapped in molecular complexes created by the dopant atoms [65,67,68]. In order for the trapped electron to escape from its forbidden state it must gain energy from some outside source. After climbing out of the trap the electron can fall back to its ground state, a process that must be accompanied by the emission of a photon to remove the excess energy. The photon possesses an energy that is the difference between the electron energy when it is boosted out of the trap and the energy of its ground state, which is equivalent to a wavelength of primarily 410 to 415 nm in LiF: Mg, Ti [68,69]. If the material is heated at some later time, these metastable electrons return to their ground state, releasing the stored energy as visible light (0.4%)[66]. The probability per unit time p of the thermal release of an electron trapping is given by the Boltzman

$$\text{equation: } p = s \cdot e^{(-E/KT)} \quad (3.1)$$

With s is the frequency factor (sec^{-1}), depending in the number of hits of an electron in the trap, E is the thermal activation energy (eV), k the Boltzman constant and T the absolute temperature (K).

The wavelength of the emitted luminescence light is proportional to the energy difference ΔE between the traps and the luminescence centres.

$$\lambda = \frac{hc}{\Delta E} \quad (3.2)$$

h = Planck's constant, c = velocity of light

If we assume that no released electron is retrapped and if the temperature kept constant, the number of trapped electrons n decrease with time t according to the following expression:

$$\frac{dn}{dt} = -p \cdot n \quad (3.3)$$

The intensity I of the luminescence is time-dependent

$$I(t) \propto -\frac{dn}{dt} \quad (3.4)$$

Integrating Eq. (3) and using Eq. (1)

$$\int_{n_0}^n \frac{dn}{n} = -\int_{t_0}^t s \cdot e^{-\left(\frac{E}{kT}\right)} dt \quad (3.5)$$

Where n_0 is the number of trapped electrons at time $t_0=0$

$$\ln n - \ln n_0 = -s \cdot t \cdot e^{-\left(\frac{E}{kT}\right)} \quad (3.6)$$

And

$$n = n_0 . e^{-s.t.e - \left(\frac{E}{kT} \right)} \quad (3.7)$$

The typical shape of a glow curve (I vs. T) can be deduced by solving this differential equation. A simplifying assumption of only one kind of trap present (with the energy depth E) and of recombination of all released charge carriers leads to first-order kinetics

$$I(t) = -a.s.t.e - \left(\frac{E}{kT} \right) \quad (3.8)$$

The total amount of light emitted when the electrons return to their ground state is proportional to the number of electrons that were trapped, and this is proportional to the radiation dose absorbed by the material. Therefore, the amount of light emitted when thermo luminescent material is heated is proportional to the total radiation dose absorbed (Figure 3.1).

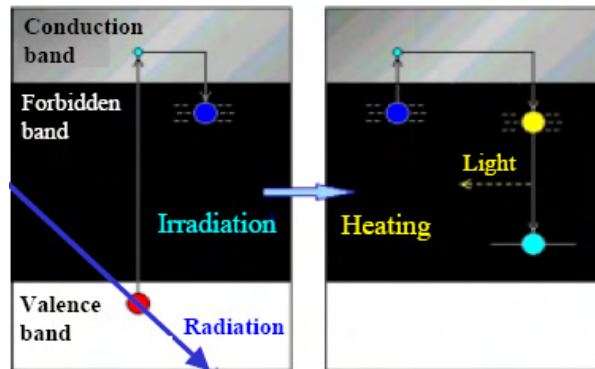


Figure 3.1: The scheme of luminescence, excitation and emission in solids.

3.2.2 Method of manufacturing TLD-100

TLD-100, in the form of powder and solid pellets, is recognized universally as the "golden standard" for applications in radiation protection dosimetry, monitoring of environmental radiation and medical dosimetry.

Harshaw lithium fluoride based dosimeters have been in use for many years. The material is available in powder, extrusions and pressed chip forms. The pressed chips are produced in a variety of shapes and in several thicknesses. The manufacturing techniques used to produce these materials have been refined to the point where very consistent performance is obtained from batch to batch. The current method of producing these materials consists of the following steps [70, 71]:

- (1) Purifying the raw material.
- (2) Growing doped LiF crystals.
- (3) Grinding the crystal to powder.
- (4) Blending different batches for sensitivity.
- (5) Pressing the powder to slug form.
- (6) Slicing the slug into discs.
- (7) Dicing the discs to the desired shape.

3.3 Application of TLDs

TLDs have three major uses: as personal dosimeters for people who work with or around radiation, environmental monitoring, and for verifying the radiation doses given to patients [65, 66]. Personal dosimeters must be sensitive to small amounts of radiation, accurately record a wide range of doses and different types of radiation, and be stable for wearing periods of one to three months (Figure 3.2).

Environmental dosimeters should be especially sensitive to pick up the very low radiation they are exposed to and be rugged and stable enough to withstand months of exposure time outdoors in varying temperatures and humidity.

In radiation therapy treatments for cancer the type and energy of the radiation is well known and a relatively large dose is delivered in a very short time. Also, medical TLDs must be very accurate. As little as a 5% difference in the dose delivered to a tumor can have adverse consequences in some treatments, so the measurement system must be at least this accurate [65, 67, 68]. In the medical field TLDs are also sometimes used to quantify the lower doses received by patients undergoing diagnostic X-ray, CT, or nuclear medicine procedures [66-69].

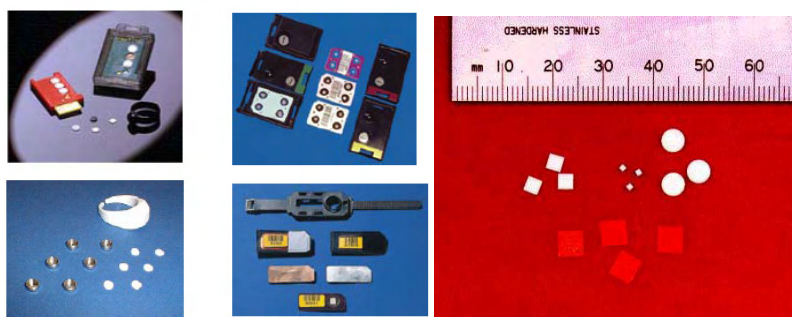


Figure 3.2 TLD materials

There are several driving factors in the choice of a thermoluminescent material for a dosimeter. One important material characteristic is how close to tissue equivalent the crystalline material behaves. Tissue

equivalent materials will absorb the same amount of dose for a given energy and type of radiation within a constant factor. Another important characteristic, to maximize in this case, is the amount of light output for a given dose. One more factor is the range of doses over which the material can produce an accurate dose. This brings in many considerations such as the average atomic number, the concentration of traps, the band gap energy of the crystal, and the various energy levels of the traps.

3.4 TLD Initialization

Before beginning irradiations, the stability and sensitivity of each TLD should be established in order to obtain the maximum accuracy of the detector [65-67]. The TLDs were first selected according to their appearance. Only clean TLDs of excellent shape (no scratches) and no change in color were chosen. For initialization, the TLDs were annealed several times to stabilize their sensitivity. After this preparation, the TLDs were examined again and those showing obvious defects (cracks or coloration) were rejected. The finally selected TLDs were annealed once again before irradiation.

Each TLD is annealed in an annealing oven according to the manufacturer recommendations [65]. At the end of the procedure, the dosimeters are read to check the background signal and to check batch homogeneity. If the background has remained low over these cycles, the initialization is terminated and dosimeters are ready for use. The background signal depends on the voltage applied to the Photo multiplier Tube (PMT), its thermal history and the room temperature. This "initialization" process is repeated three times to ensure constancy of the dosimeters [65]. It is imperative to always use the same procedure for heating and cooling because the glow curve of the material is strongly affected by the cooling [65].

3.4.1 Sensitivity

Sensitivity, defined as the TL output per unit mass and unit absorbed dose, is influenced by many factors (i.e., type of phosphor, the type and features of the reader, heat treatment, etc.). Typically, only the relative sensitivity is quantified. The sensitivity of $\text{CaF}_2:\text{Dy}$ relative to $\text{LiF}:\text{Mg, Ti}$ is approximately a factor of 100 up to 300 per unit mass. In general, there is a decrease in sensitivity for TLD phosphors after many reuses. For all TLD chips, a loss of sensitivity of less than 2% is expected during as many as 500 re-uses. In addition, all phosphors exhibit less than 0.8% degradation for every 100 re-uses, up to a total of 2000 reads [72].

3.4.2 Individual calibration factor

The amount of light given off by each individual TLD irradiated to the same dose will actually be a bit different because of several factors. To account for the differences, the light output of each TLD is normalized to the average light output of the entire batch.

Element correction factors (ECF) are calculated by subtracting the individual background from the TLD reading and then dividing that net individual reading by the average net reading for the entire set [65,66]. The variation in the sensitivity within a batch of TLDs is the differences in mass and non-uniform mixing of dopants and non-uniform distribution of traps within the LiF [66]. A new set of TLDs manufactured from the same batch commonly exhibits a range of sensitivities from -10 to +10% of the average sensitivity of the set [65-67].

3.4.3 Pre irradiation annealing

Before TLDs can be reused they must undergo a pre- irradiation anneal. The intent of this anneal is to remove any residual trapped electrons that were not released during the reading process. If not removed by annealing the residual trapped electrons could be released during a subsequent irradiation and readout resulting in possibly a several percent inaccuracy, particularly when high doses of radiation have been used [65-67].

Even with a post-irradiation annealing, 1% residual signal remains. Variations in the annealing procedure have been tried to reduce this small possible source of error to even lower amounts.

3.4.4 Post irradiation annealing

The increased temperature in the oven increases the thermal vibrations of the molecules and the rate of electron release (Figure 3.3). The time and temperature of this so-called pre-readout anneal has been chosen to maximize the emptying of shallow traps and minimize the loss of electrons from the higher energy level dosimetric traps.



Figure 3.3 TLD Oven

3.4.5 TLD reading cycle

The common TLD reader uses a tiny metal tray (planchet), which heats up the TLD placed on it by means of an electric current passing through the planchet wires. The electric current can be precisely controlled so that the temperature of the planchet can be determined within $\pm 1^{\circ}\text{C}$ [73]. The rate of heating and length of time of heating can also be varied accurately (Figure 3.4 & 3.5).

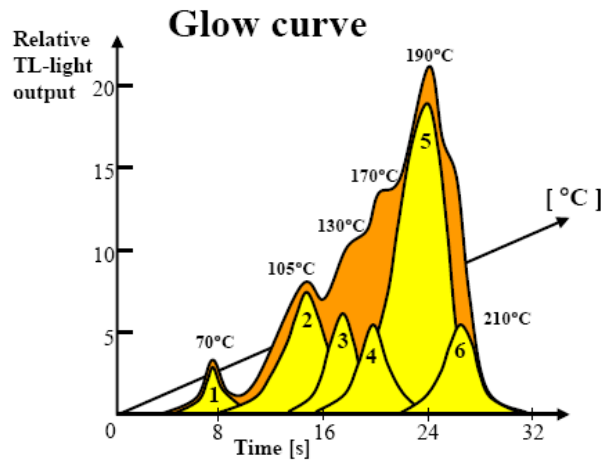


Figure 3.4: shows that the maximum amount of light from LiF:Mg,Ti is emitted at about 200°C, though there are several smaller peaks of light emission at other temperatures

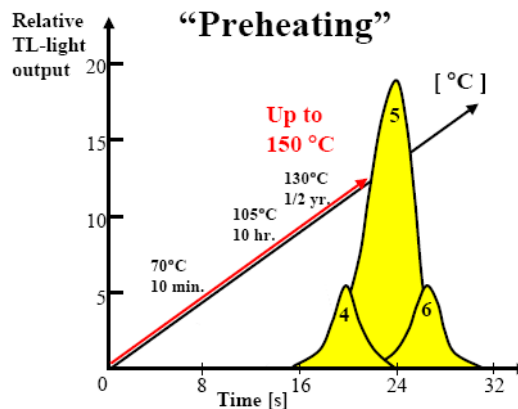


Figure 3.5: fading and pre heading effect

3.4.6 TLD Reader

The TLD system used to process TLD chips included the following component: The TLD reader consists of two main parts: the heating mechanism and the light-photon-collection components. The planchet and readout chamber are made as reflective as possible in order to make the reader more efficient. The photomultiplier tube (PMT) is used almost exclusively in TLD readers to do the light collection since it is the most sensitive known device for that purpose. The photomultiplier tube has two main parts, which are the photocathode and the dynodes.

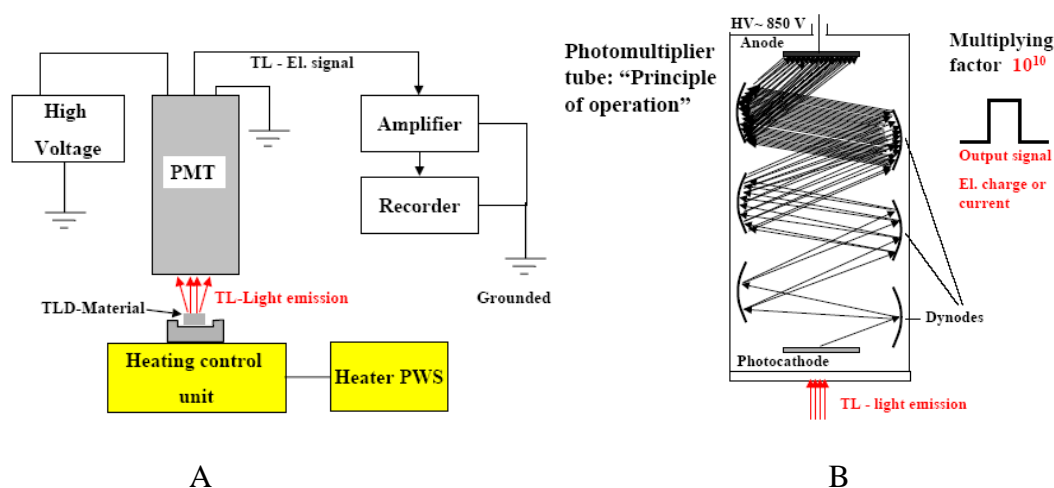


Figure 3.6 (A & B): Schematic diagram showing the typical arrangement for a TLD reader and PMT principles

The electrons released from the photocathode are proportional to the number of photons, which strike it. The number of electrons is multiplied by several stages of dynodes to produce a current, which is large enough to read. The total amount of electric current produced and integrated over the read phase yields the TLD reading, in units of nC usually, since current multiplied by time equals charge and coulombs is the unit of charge. PMT's are usually cooled to keep them at a constant temperature since their response can be affected by up to 1% per 1°C change in their temperature [74].

The electronic reference lights built into TLD readers to help check the constancy of the reader response are also somewhat affected by heat [66, 75]. It is desirable to set up the TLD reader in a climate-controlled environment to keep readouts stable. It is also important to maintain a clean working area since chalk dust, dirt, and static electricity can alter TL readings [66, 76]. In order to obtain the same amount of light at all times, the planchet was cleaned with an alcohol. However, it was found that the alcohol residue increased background, readings of the empty planchet up to as much as possible (about 7 readings to get less than 1 nC).

3.4.7 TLD dose response

The ideal dosimeter would respond proportionally over a wide range of dose. Currently used TLDs are proportional over a limited range. The Lower detection limits (LDD) depends on the particular reader used as well as the TLD type [65, 66]. LiF: Mg, Ti starts to become non-linear at about 100 cGy (Figure 2.7) and more noticeably so at 300 cGy [66, 67, 71].

The TL output may become supralinear. For LiF: Mg, Ti this supralinearity occurs at about 100 to 300 cGy [65-67]. This is explained by the track interaction density effect model [77]. The idea is that at higher ionization densities (higher doses) more of the electron traps are filled, which increases the electrons' chances of finding a recombination center, where the electron can drop down to its ground state when heated and produce thermoluminescence [66-68]. The supralinear response continues to about 10,000

cGy [66-68](Figure 3.7). At these high doses the TLD becomes saturated; most of the electron traps have now been filled with electrons, and electrons produced by additional given dose face a decreasing probability of finding an empty trap to lodge in.

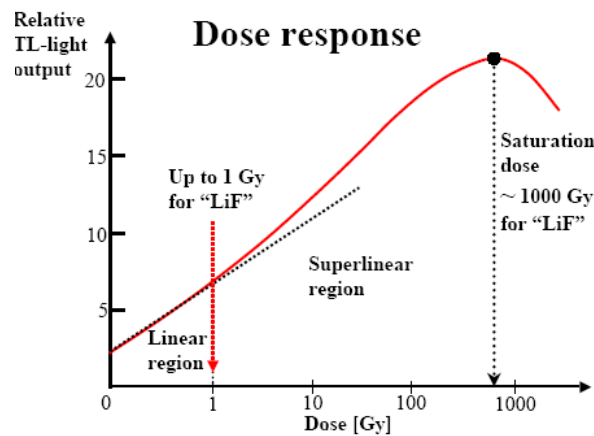


Figure 3.7: TLD response versus radiation dose.

3.4.8 TLD calibration

Because it is so difficult to compute the expected TL for dosimeters theoretically, in practical dosimetry a set of calibration TLDs are always used. Several TLDs from the set are irradiated at known doses and energies and then read out using the same procedures as for the TLDs of interest. The calibration TLDs are exposed to a range of doses surrounding the dose the TLDs of interest are expected to receive. For example, a radiotherapy patient may be receiving 200 cGy per treatment. Two or three TLDs may be irradiated at each calibration point, which might be chosen at 150 cGy, 200 cGy, and 250 cGy. Within this limited range the linear approximation is a good one. When a TLD from the patient is read its TL output is converted to dose based on the calibration information. When a larger range of patient doses is expected or when the patient dose is unknown, a calibration curve with more calibration points and greater dose width must be constructed. The amount of TL output as the result of a particular radiation dose is the result of several probabilistic processes. Thus, it has a statistical nature. Therefore, the dose computed from any one TLD is not likely to coincide with the actual dose used for the irradiation, but it should be close to the true dose within average statistical variation. [66, 67, 78].

3.4.8.1 Background signal:

The background signal is the signal obtained from unirradiated TLDs. The background TLD reading is the result of several factors. Most of the background reading comes from the natural TL of oxygen in the air [68]. This can be eliminated by reading the TLDs in a non-oxygen atmosphere. The use of nitrogen can reduce this effect. Another source of background TL reading is electronic noise from the TLD reader [65, 66]. This originates from spurious electrons released and multiplied in the PMT and is called the dark current [65-67]. This current exists because of the dynode amplification of the stray electrons emitted even when no light is impinging on the photocathode. In this study, subtraction of the background

readings was applied from all the readings. It is important that the background TLDs be stored in the same place as the other TLDs in the set so that they will all be subjected to the same background conditions.

3.4.9 TLD energy response

The photon energy response of a TL phosphor depends primarily on its effective atomic number. The TL response of a phosphor is usually normalized to particular photon energy. This is the result of photoelectric absorption, which is a function of the atomic number (Z) of the TLD material to the third power and the energy of the photon inversely to the third power (Z^3/E^3) [65-66].

The relatively low Z of TLD-100 (8.2) results in a relatively small over response in the photoelectric region since it is close to the Z of human tissue, about 7.6. For TLD-200, much higher photon energy dependence is observed because of the relatively high atomic number (16.3), compared with tissue [79]. However, the TLDs were calibrated at the same energy, as the patient TLDs, so there was no need for energy corrections.

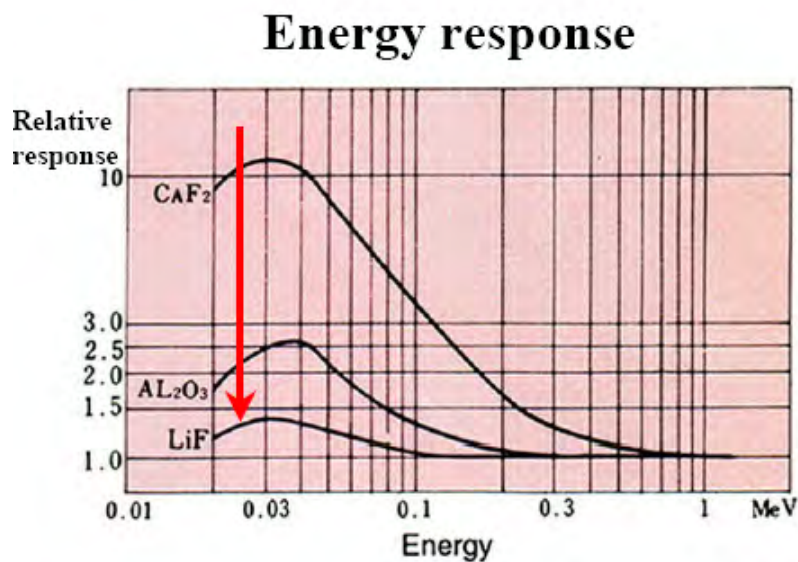


Figure 3.7. Energy response of different TLD Materials.

3.4.10. TLD response: Fading

Fading is the term given to a loss of TL output due to a chronological difference between when the TLDs are annealed, irradiated, calibrated, and read-out [65,66,79]. Some trapped electrons can escape their traps even at room temperature, particularly those in the lower energy levels. Therefore, there are differences in subsets of a batch of TLDs depending on storage time between annealing, irradiation and

readout. These widely dispersed findings suggest a medical center must conduct their own study of this TLD characteristic.

The amount of environmental light the TLDs are exposed to can also have effect the dose readout [65, 78]. Light energy, like thermal energy, can also release trapped electrons, especially ones in the lower-energy traps corresponding to ultraviolet light found in sunlight or fluorescent lights. Additional fading has been reported at between 7 to 11% loss of TL for a 3-hour exposure to the sun or to ultraviolet lights [65, 66].

However, in this study annealing, irradiating, and reading of all TLDs was performed on the same day, avoiding the requirement of fading correction.

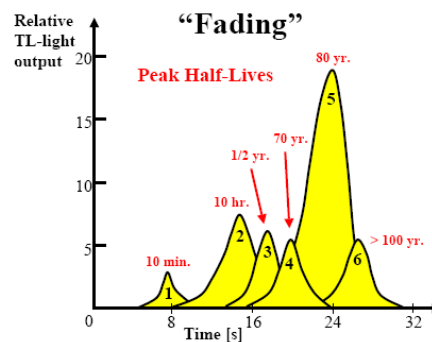


Figure 3.8: TLD-100 fading

3.4.11 TLD Response: Accuracy

The use of TLD systems, taking the aforementioned factors into account, can lead to an uncertainty of 1% to 5% in the dose readout accuracy [66, 77]. Some residual inaccuracy will always be expected because the filling and emptying of electron traps are statistical processes. It is impossible to predict which particular traps and how many will capture electrons when a given dose of radiation is given since the process is "deterministically unpredictable" [66], but the mean number given by a Gaussian curve should be highly predictable. In other words, the precision (repeatability) of TLD measurements is very good, but not perfect.

4. MATERIALS AND METHODS

4.1 TLD materials

Dose measurements were made using two groups of TL dosimeters from Harshaw TLD (Bicron-NE, Solon, Ohio, USA) of dimensions $3.1 \times 3.1 \times 0.89 \text{ mm}^3$ and mass $\sim 22.8 \text{ mg}$. TLDs made of natural lithium fluoride doped with magnesium and titanium (LiF: Mg, Ti , TLD-100). TLDs were used to measure patient dose during radiology procedures and radiotherapy treatments. Calcium fluoride TLDs doped with dysprosium ($\text{CaF}_2\text{: Dy}$, (TLD-200)) were used to measure staff doses during diagnostic and interventional radiology. Some of the TLD characteristics are presented in Table 4.1

Table 4.1 detector characteristics [65, 66]

Material Characteristics	TLD-200	TLD-100
Density (g/cm^3)	3.18	~ 2.64
Melting point ($^{\circ}\text{C}$)	1423	846
Sensitivity	300	1
Spectral emission peaks	480-577	400
Effective Z	16.3	8.2
Energy gap (eV)	12.2	10
Photon energy response (30 keV/ ^{60}Co)	13-15	1.3
Temperature of main glow peak at slow heating rate	200-240	195
Dynamic Range (Gy)	10^{-6} - 10^3	5×10^{-5} - 10^3
Toxicity	Low	High if ingested
Fading dosimetry peak at normal ambient temperature	25% in 4 weeks (10% in first 24 hours)	5 % I 3-12 month
Residual TL	-	Less than 2 %
Reusability	Indefinitely	>500 uses: <0.02% TL loss/use
TL emission spectra	250-600 nm	350 - 600 nm
Other characteristics	Optically transparent, Mechanically rugged	Inert, insoluble, relatively hard, unaffected (relatively) by environmental conditions

4.2 TLD calibration

4.2.1 TLD calibration to high energy photon beams

TLDs were calibrated in a Plexiglas phantom ($30 \times 30 \times 30 \text{ cm}^3$) at a depth of maximum dose using 6 MV ($d_{\text{max}} = 1.6 \text{ cm}$) and 15 MV ($d_{\text{max}} = 2.7 \text{ cm}$) photon beams. The first PMMA slab was used to accommodate the TLD chips in an array of slots 10×10 . Each TLD was identified by its position in the array. A field size of $10 \times 10 \text{ cm}^2$ at the phantom surface and a source to surface distance (SSD) of 100 cm was employed for the calibration. The TLDs were placed at d_{max} (1.34 cm (6 MV), 2.30 cm (15 MV)), on a Plexiglas phantom of $30 \times 30 \times 10 \text{ cm}^3$, for full backscatter (Figure 4.1). The specific density of the TL material was not considered. For each measurement, at least 4 TLD chips were irradiated and the mean value was considered as standard dose. A dose of 50 cGy at measurement depth, as determined by a calibrated ionization chamber, is given to calibrate the TLDs by applying the IAEA TRS 389 dosimetry protocol in accordance with the departmental calibration practice. The calibration was performed under reproducible reference conditions (Figure 4.1) using the same radiation source for both energies against a calibrated ionisation chamber (IC) model M30001-PTW- Freiburg, Germany. The chamber was calibrated at the National Standard Laboratory, Greek Atomic Energy Commission (EEAE). Annealing and readout procedures were performed as illustrated in section 2



Figure 4.1: TLD calibration for radiotherapy measurements.

4.2.2 TLD calibration to low energy photon beams

TLD calibration was according to international protocols for the range of energies used in the study. The TLDs were calibrated under reproducible reference conditions using the same X ray machine (Philips Diagnost 93) against an ionisation chamber model 9060/10X5-60 connected to a Radiation Monitor Controller model 9010 (Radcal Corporation, Monrovia, CA, USA) (Figure.4.2 c). Both the chamber and the electrometer were calibrated for the energy range of 30-120 kV at the National Standard Laboratory. For the TLD and chamber irradiation, a polymethylmethacrylate (PMMA) calibration test bed has been constructed having dimensions $30 \times 30 \times 6 \text{ cm}^3$, which simulates patient's lateral and backscatter

conditions (Figure 4.2). The first PMMA slab was used to accommodate the TLD chips in an array of slots 10x10. Each TLD was identified by its position in the array (Figure.4.2 a). Individual calibration factors were obtained by irradiating the entire group to the same dose.

This process was repeated three times to reduce the effect of statistical variations and to determine the stability and reproducibility of the signal. TLDs with sensitivity within 4% were used in this study. All the TLD chips had the same thermal history. Calibration cycle was carried out every month.

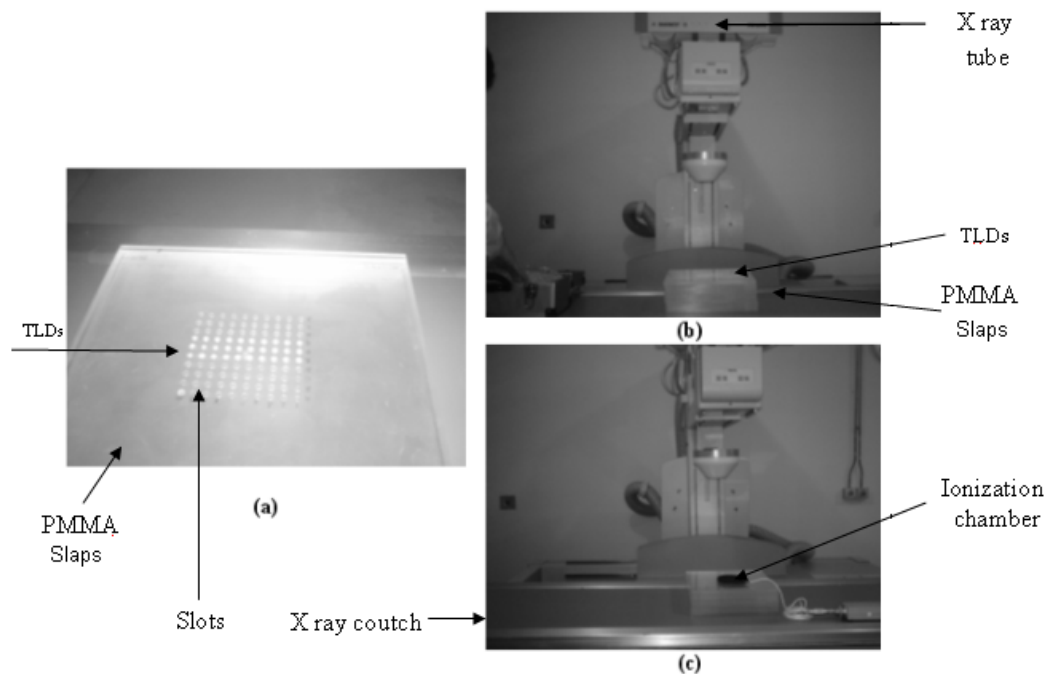


Figure 4.2: TLD calibration setup. (a) PMMA phantom with appropriate wholes for TLD measurements, (b) calibration setup to the diagnostic digital X-ray machine with the TLD phantom and (c) calibration setup to the diagnostic digital X-ray machine with the ion chamber dose measurement device.

4.4 TLD oven

An annealing oven manufactured by PTW was used (Figure 4.3). This oven has an insulated annealing chamber of approximate dimensions 11 cm x 8 cm x 10 cm² and contains a heating element producing a temperature-controlled hot air stream. A built-in fan circulates the hot air and ensures a uniform temperature distribution throughout the oven volume. For annealing, the TLDs were put on copper or stainless steel trays, which can be placed at three different levels. All TLDs were annealed (as recommended by the manufacturer) in annealing oven (TLDO, PTW, Freiburg, Germany) at 400 °C for 1 hour, followed by fan forced cool down to 100 °C which was held for 2 hours in order to optimise its characteristics and to achieve better stability of the TL signal. The annealing process removes any residual signal from previous radiation exposure and sets the sensitivity of all of the chips to a uniform Level.

Post irradiation annealing was carried out for 10 minutes at 100 °C to reduce fading effects by eliminating the unstable peaks. The average background was used because the background value was low (0.3-0.5 nC).



Figure 4.3: TLD oven

4.5 TLD Reader

The TLD system used to process TLD chips included the following component: Harshaw 3500 manual TLD reader, a personal computer with Windows NT and WinRems software. The instrument, which can be used with chips (ribbons), rods, micro cubes, or powder, includes the operational WinREMS software as a reader. The instrument allows a heating profile to be obtained. It is possible to print and export results including glow curves. Associated electronics make it possible to measure the TL light output (Figure 4.4).



Figure 4.4: TLD reader and computer system

The software stores the data in a group file that allocates an identification number. It also holds the information used by reader. The system includes a reader and a DOS-based IBM-compatible computer, connected through a standard RS-232 serial communication port. Dosimetric data storage, instrument control and operator inputs are handled by the PC, while signal acquisition and conditioning are tasks performed by the reader. The software provides real-time monitoring of the instrument's operating conditions and displays glow curves and response values. A single dosimeter is read per loading. Thereby, the TLDs are put on an interchangeable heater pan. The reader uses contact heating with a closed loop feedback system that produces linearly ramped temperatures accurate to within ± 1 °C up to 400 °C with standard 1/4" x 1/4" planchet. The time temperature profile has three segments (preheat, acquire, anneal), for each of which the user can choose time and temperature. During acquisition, the emitted light is detected by a photo-multiplier tube (PMT) connected with a 200 channel scalar to generate the glow curve. The stability of the reader was checked before any reading session. The performance of the light detection system can be monitored by a built-in test light source. Light source (light under the PMT) and dark current (the reading without TL material in the planchet) are read out to insure the consistency of the system 5 times prior the measurements. The reader provides nitrogen allowing it to flow around the heater pan. By eliminating oxygen in the pan area, the nitrogen flow eliminates unwanted oxygen-induced TL signals. However, a nitrogen source was not available during this study. Before its use, the reader was warmed up for 30 min. A typical readout cycle (time and temperature profile (TTP)) begun with preheat phase at 100°C. During the reading phase the planchet temperature is increased by 11°C/s up to 280°C (300 °C for TLD-200) in order to empty the entire electron trapped in the traps used for dosimetric purposes.

4.6 TLD Handling Accessories

TLDs were handled with vacuum tweezers to avoid contaminants and scratching, which influences the amount of the emitted light. Suction allows contact between the nozzle and the TLDs. When handling miniature TLDs, a finer nozzle with a narrower surface area was used for contact to prevent damage to the TLD and to prevent the TLD from being drawn up into the tweezers. When not in use the TLDs were stored in dedicated copper and stainless steel trays each of which could house up to 50 or 100 TLDs.

4.7 Linear accelerators

Two Philips linear accelerators, a SL-75 and a SL-18, installed in the University Hospital of Larissa (UHL) were used. The ELEKTA SL 75/5 is a single 6 MV accelerator, while the SL-18 produces 6 and 15 MV photon beams, as well as electron beams of various energies.

4.8 X ray machines

The radiological procedures were performed in two UHL X ray rooms equipped with Philips remote-controlled ($\pm 90^\circ$ tilt) fluoroscopic units with an overcouch X ray tube an undercouch image intensifier and three fluoroscopic modes. A Diagnost 93 (Philips Medical Systems, Italy) unit with three magnification levels (38/31/23cm) is installed in suit A (the 38 cm field was mainly used in this study). A Diagnost 94 unit (Philips Medical Systems, The Netherlands) with three magnification levels (38/25/17) cm, three fluoroscopic modes (low, medium, and high) and two monitors; one at examination room and one at the control room was installed in suit B. The 38 cm field of view was used frequently during HSG procedures. The resolution of the image intensifier is 1.8 lp/mm and the geometrical distortion is 6% at the centre and 11% at the periphery resulting in very good image quality. The exposure factors were selected automatically by the machine, while the phantom used was the ETR-1 (Wellhofer - Germany).

The two units were equipped with Rotalix and super Rotalix X-ray tubes, with nominal focuses 0.6 mm/1.3 mm, 0.6 mm and 1.2 mm, respectively. The available range of the kVp and mAs are 40-125 kV, 1-850 mAs .the maximum mA at 80 kV is 700 mA for machine B.

The nominal total filtration was 4.0 mm Al in both units at 80 kV. Both of the units are equipped with automatic brightness control and last image hold. The minimum screening time recorded by both machines is 0.1minute. Both machines were equipped with a pair of leg supports to be used in HSG procedures, constructed in 1996. The exposure factors were either selected manually or the kV was selected manually with the corresponding mAs and tube current selected automatically for radiography and fluoroscopy, respectively. The latter option was used during this study. Focus to Image Receptor Distance (FID) was 110 cm.

Quality assurance tests were performed regularly for exposure parameters (applied potential, tube current to the same dose level rent. and time) for both X ray machines and for image quality.

4.9 Method of dose calculations

Determination of detector correction factor (Ci):

Due to the differences in thermoluminescent efficiency of the various dosimeters, a detector correction factor, Ci, has to be assigned to each of them.. After the TLD initialization procedures (section 2), all TLDs were irradiated to the same dose level. The Detector correction factor was called the quantity.

$$Ci = \frac{TLs}{TLm} \quad (4.1)$$

Where: TLs: TLD signal in nC for individual TLD after the subtraction of the background signal

TLm : The mean value of all the signals after the subtraction of the background signal

The determination of Ci procedure was repeated three times and the mean value was used. The calibration factors were presented in annex A.

TLD dose calculation:

A group of TLDs were exposed to a series of known doses (D) in the clinical range. Two accurately known dose values were selected to represent the “standard dose” (Do) to be used for unknown dose calculations and the “Test dose” to check the accuracy of the dose measurements.

The radiation dose was determined according to the following equation:

$$D(\text{Gy}) = \left(\frac{(TL - BGR) / Ci}{(TL - BGR)_m / Do} \right) \quad (4.2)$$

Where:

TL is TLD signal.

D: dose in Gray.

Do: standard dose.

Correction factors

Correction factors had to be used. For example, a linearity correction factor, F_{lin}: had to be introduced in radiotherapy since the dose to some patients was higher than 1.0 Gy.

$$D = Do \cdot F_{\text{cal}} \cdot F_{\text{en}} \cdot F_{\text{fad}} \quad (4.4)$$

Do: Initial dose (Gy)

F_{en}: Energy correction factor

F_{fad}: Fading correction factor

In this study, there was no need for a fading correction factor, because the TLD readings were performed on the same day of exposure, and almost the same photon spectra were used for calibration and dose measurements.

4.9.1 ESD

The ESD is one of the simplest and most frequent parameters used to measure patient and staff doses from radiologic examinations. Four TLDs, packed on a thin envelope made of transparent plastic foil to protect the TLDs from any contamination were used to measure ESD. They were placed at different body sites to measure staff and co-patients doses.

The organ equivalent dose (mSv) is given by:

$$H_T = \sum_R w_R \cdot D_{T,R} \quad (4.5)$$

Where $D_{T,R}$ is the mean absorbed dose to tissue (T) from radiation (R) and w_R is the radiation-weighting factor from the recent ICRP recommendations [18], which represents the biological effectiveness of the incident radiation.

4.9.2 Equivalent Dose

A number of radiobiological quantities are used to assess the probability of induction of stochastic radiation related effects and to ensure the avoidance of deterministic effects. Most of them related to the mean absorbed dose to a tissue or an organ $D_{T,R}$, due to radiation of type R. The protection quantity equivalent dose in an organ or tissue, H_T , is defined as

$$H_T = \sum_R w_R D_{T,R} \quad (4.6)$$

Where w_R is the appropriate radiation-weighting factor. The sum is performed over all types of radiations involved. The unit of equivalent dose is J/kg (sieverts (Sv)).

Values of w_R , given by ICRP [18] are mainly based upon experimental values of the relative biological effectiveness (RBE) for various types of radiations compared to the effects of x- and γ -rays at low doses for the induction of stochastic effects (see Chapter 2).

4.9.3 Effective dose

ICRP first introduced the protection quantity, effective dose equivalent, in Publication 26 [83] as proposed by Jacobi [84]. The basic principle was to use the absorbed dose as the fundamental physical quantity, to be averaged over specified organs and tissues using weighting factors to take into account the differences in biological effectiveness of different types of radiation in inducing stochastic effects and to quantify their severity. The development of the effective dose equivalent and subsequently the effective dose made a significant contribution to radiological protection as it has enabled doses to be summed from whole and non-uniform irradiation of the human body with external radiation and from intakes of radionuclides.

The effective dose, E , is defined by ICRP as

$$E = \sum_T w_T \sum_R w_R D_{T,R} \quad (4.7)$$

Where w_T is the tissue weighting factor with $\sum w_T = 1$. The sum is performed over all organs and tissues of the human body considered in the definition of effective dose [18]. The SI unit of effective dose is the Sievert (Sv) (Figure 4.5).

While absorbed dose in a specified tissue is a physical quantity, the equivalent dose and effective dose include weighting factors, which are based on radiobiological findings. These weighting factors are selected for application in radiological protection by judgement and include simplifications, which are assumed by ICRP to be acceptable. Therefore, these quantities are not pure physical quantities. For

example, the tissue weighting factors, w_T , are based on epidemiological studies of cancer induction and mortality after radiation exposures, as well as genetic data and judgements. Furthermore they are representing mean values for humans averaged over both sexes and all ages.

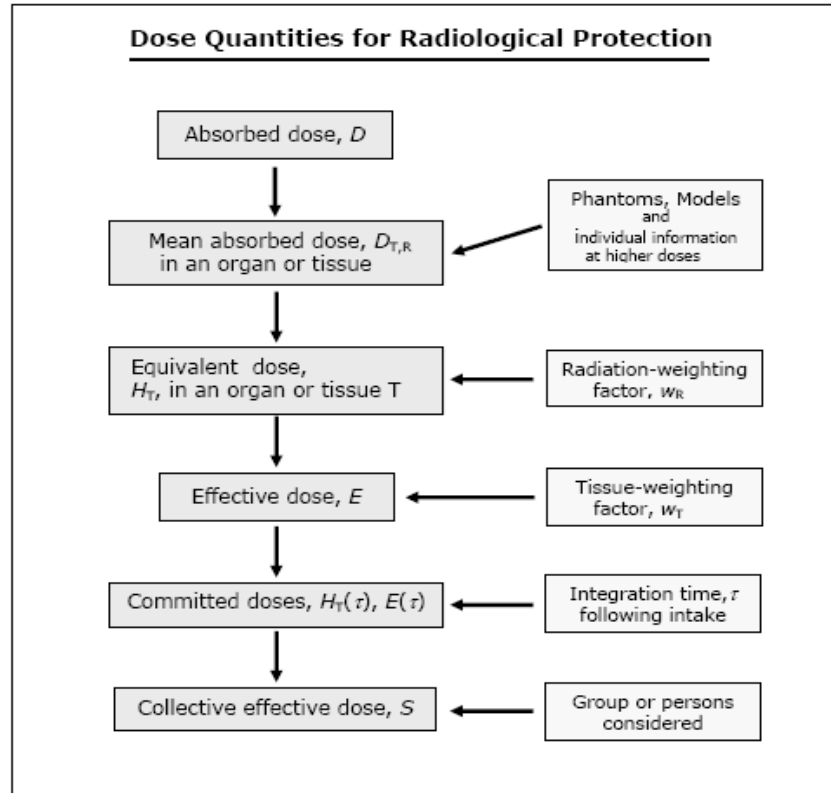


Figure 4.5: System of dose quantities for use in radiological protection

4.9.4 Occupational Exposure

4.9.4.1 Assessment of Effective Dose from Individual Monitoring Data

Individual dose monitoring is usually performed using personal dosimeters and using this value for the assessment of the occupational effective dose. In fluoroscopic guided medical practices body exposure is not uniform. For example parts of the body are protected by the lead apron and other mobile screens, or lead shields. Therefore, the evaluation of the occupational effective dose is complicated and introduces uncertainties [85]. Some algorithms requires the use of two dosimeters, one worn over a 0.5 mm Pb equivalent apron at the neck level and under the apron at the waist level. Other algorithms require the use of a single dosimeter, worn over the apron at neck level. Moreover the algorithm accounts for the use of a thyroid collar shield.

In the case of two dosimeters without a thyroid shield, [86] the effective dose is:

$$E = 0.06(H_{os} - H_u) + H_u \quad (4.8)$$

Where H_{OS} is the dose measured by the dosimeter at the neck (shallow depth), H_U is the dose measured by the dosimeter under the apron at waist level (deep).

In the case where a single dosimeter is worn at collar level, H_U is often assumed to be equal to 0.01 H_{OS} , [86] and the effective dose can be approximated as:

$$E = 0.07H_{OS} \quad (4.9)$$

When a thyroid shield, a 0.5 mm Pb equivalent, is worn:

$$E = 0.02(H_{OS} - H_U) + H_U \quad (4.10)$$

In the case where a single dosimeter worn at the collar level, again assuming $H_U < 0.01 H_{OS}$, the effective dose can be approximated by

$$E = 0.03H_{OS} \quad (4.11)$$

However, in this study, the effective dose for the second examiner was derived from the TLDs at chest level. Effective dose estimation using two dosimeters results in a slightly higher effective dose than those result from applying a correction factor for a single neck dosimeter. However, the later equation was used in effective dose estimation.

It is worth mentioning that the conditions of examiner exposure during ERCP are different from those in conventional and interventional procedures i.e., during ERCP the examiners do not face the source of the X ray (primary beam and scatter radiation), while for other procedures examiners are always facing the source of X rays. This point should be considered in the estimation of the effective dose because it underestimates the effective doses. Also the formulae overestimate the dose because no tissue attenuation was assumed.

However, occupational effective dose is calculated to be the 10% of the $H_p(10)$ dose recorded by the TLDs outside the lead apron. For the unprotected parts of the body, the absorbed dose was assumed to be the same as the dose recorded on the TLDs at chest level. The equivalent dose has been taken equal to the absorbed dose (applicable for low LET radiation). The effective dose to the organs and tissues has been calculated using the methodology and tissue weighting factors reported at ICRP 60 and NCRP 122 (18,87). A computer program was developed by (Dr Theodorou (Medical Physics Department) allowing calculation of the dose to 14 organs and tissues for co patient and radiologist during MCU and HSG respectively (Annex C).

4.10 Patient dose assessments

4.10.1 NRPB software (NRPB-SR262)

NRPB-SR262 [44] is a software report, which includes a computer disk containing files of conversion coefficients, providing estimates of organ doses and effective doses to adult patients undergoing diagnostic x-ray exposures. It contains the results of Monte Carlo calculations modelling the conditions of exposure relevant to 68 common radiographic views on a mathematical phantom representing an average adult patient (with a mass of 70.9 kg and a height of 174 cm and body mass index (BMI ($\text{weight}/\text{height}^2$)) of $23.12 \text{ kg}/\text{m}^2$, which includes the female breasts, ovaries, uterus and testes). Each Monte Carlo run tracked the pattern of energy deposition in the anthropomorphic phantom from primary and scattered photons for total 4,000,000 photons used with each x-ray projection. Normalised doses are presented for 26 organs or tissues along with the effective dose, as defined by ICRP in 1990 and the effective dose equivalent as defined by ICRP in 1977. The data are provided for 40 x-ray spectra ranging from 50 kV to 120 kVp and beam filtration 2 mm Al to 5 mm Al. The doses are normalised to both ESD (mGy) and DAP ($\text{Gy}\cdot\text{cm}^2$). Organ doses from HSG were obtained from the average value of conversion factors for anteroposterior pelvis view. However, as specific projections were not available for ERCP, organ doses (mGy) were obtained from the average value of the conversion factors for the most similar PA kidney, stomach and oblique duodenum views. These projections were selected because they simulate the ERCP exposed area within the patients, with the same exposure factors. Furthermore, during the procedure, the patient position might change from prone position to oblique or lateral position.

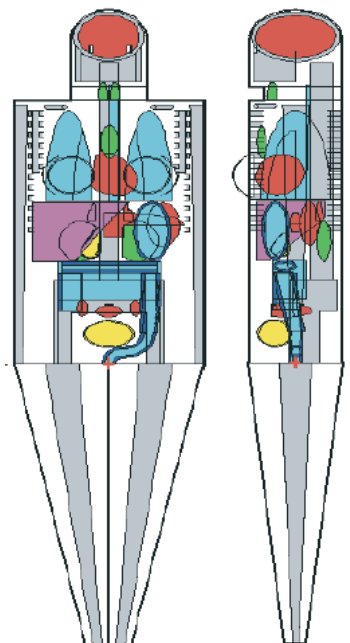


Figure 4.6 Mathematical phantoms for Monte Carlo calculations of patient dose

4.10.2 CHILDOSE -SR279

This computer data package provides estimates of organ doses and effective doses to paediatric patients undergoing diagnostic x-ray exposures. It contains the results of Monte Carlo simulations using five paediatric phantoms representing children aged 0, 1, 5, 10 and 15 years old [88]. The conditions of exposure relevant to about 20 common radiographic views were modelled, including views of the head, neck, chest, abdomen, lumbar spine, pelvis and bladder.

The data are provided for 72 x-ray spectra ranging from 50 to 120 kVp and 2 mm Al to 0.2 mm Cu with 3 mm Al total beam filtration. The doses are normalised to both entrance surface dose and dose-area

product. Organs doses from MCU were obtained from the average value of conversion factors for anteroposterior pelvis view.

4.11 Cancer risk estimation

The risk (R_T) of developing cancer in a particular organ (T) following ERCP after irradiation was estimated by multiplying the mean organ equivalent (H_T) dose with the risk coefficients (f_T) obtained from ICRP [18,89,90]

$$R_T = H_T \cdot f_T \quad (4.12)$$

The overall lifetime mortality risk (R) per procedure resulting from cancer/heritable was determined by multiplying the effective dose (E) by the risk factor (f). The risk of genetic effects in future generations was obtained by multiplying the mean dose to the ovaries by the risk factor [18, 89, 90]. The gender averaged risk coefficients were used in

$$R = E \cdot f = \sum R_T \quad (4.13)$$

Table 4. 2. Detriment adjusted nominal risk coefficients for cancer and hereditary effects (10^{-2} Sv^{-1})

Exposed population	Cancer		Heritable effects		Total	
	ICRP 2007	ICRP 60	ICRP 2007	ICRP 60	ICRP2007	ICRP 60
Whole population♣	5.5	6.0	0.2	1.3	6.0	7.3
Adult workers*	4.1	4.8	0.1	0.8	4.0	5.6
Children	-	13	0.08	0.1	-	-

♣ age between 0-90 years old

*Adult workers aged 18-64

5. IN VIVO DOSIMETRY IN HIGH ENERGY BEAMS

The scope of Chapter 5 is to present the methodology developed for in vivo dosimetry in teletherapy and the results of its clinical application at UHL. More specifically the aim of the study was to:

1. Evaluate the effect of different Buildup caps materials (Copper, Aluminum, Stainless steel and Plexiglas) in both the linear and the non-linear region of the TL efficiency of the dosimeters. Determine and the perturbation in 6 and 15 MV X-ray fields due to the presence of the build cups and the factors that modify this perturbation, such as the source to surface distance (SSD) and the field size.
2. Measure the entrance and peripheral dose (skin and thyroid) during breast, head and neck, abdomen and pelvic treatments.
3. Compare the results with the previously published values.

5.1 Dose build-up region

The dose region between the skin surface (depth = 0) and depth of maximum dose= d_{max} in high energy photon beams is referred to as the dose build-up region and results from the relatively long range of energetic secondary charged particles (electrons and positrons) ejected by photon interactions. In addition, particles produced by photonuclear reaction have energy greater than the binding energy of the neutron in the nucleus. With few exceptions, nuclei have binding energies between 7-20 MeV. Therefore, with photon energies above 7 MeV, there is likely to be neutron contamination in the beam. Neutrons can be generated at the target, collimator, build up material or the patient it self [25, 46].

The condition of charged - equilibrium (CPE) does not exist in the region immediately close to patients' skin, the absorbed dose being lower than the collision kerma. However, as the depth, d , increases, CPE is reached at depth, $= d_{max}$ approximately equal to the range of secondary charged particles and the dose becomes comparable to the collision kerma. Beyond d_{max} both the dose and collision=kerma decrease because of the photon attenuation in the patient, resulting in a transient rather than true CPE [46] (Figure 5.1).

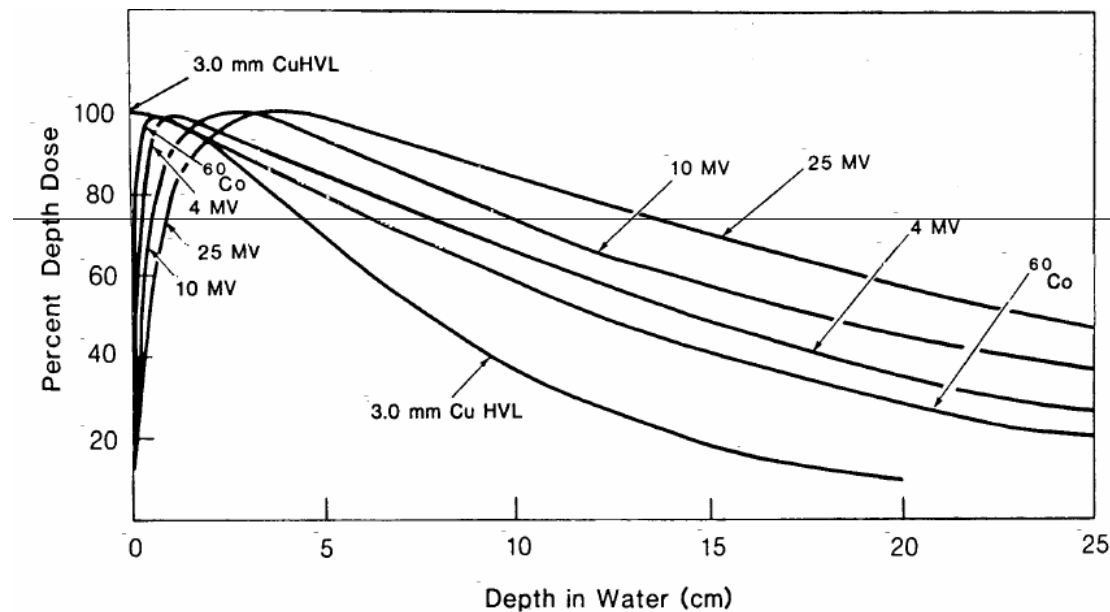


Figure 5.1: Central axis depth dose distribution for different photon beam energies. Field size is $10 \times 10 \text{ cm}^2$; SSD is 100 cm for all beams except for 3.0 mm Cu HVL, the SSD is 50 cm [46].

As the high-energy photons interact with the patient or the phantom, high-speed electrons are ejected. These electrons deposit their energy at significant distances away from their site of origin (multiple scattering).

The electron fluence - and hence the absorbed dose close to the entrance surface increase with depth until they reach a maximum. The fluence of the incoming photons decreases with depth. The net effect is that beyond a certain depth the dose eventually begins to decrease with depth [25, 46]. The advantage with high-energy photon therapy is this dose build-up effect, which gives rise to what is clinically known as the skin sparing effect. This means that larger doses can be given to tumours located deep inside the body without injuring the skin.

Head scattered electrons are produced by interactions of the primary X-rays prior to their entrance to the human body or phantom. The magnitude of electron contamination increases with an increase in the field size a decrease in the SSD or when a tray is placed [91]. Secondary electrons arise mainly from the Compton interaction and at energies above 1.022 MeV - pair production at the field flattening filter, the primary and secondary collimator jaws in the treatment head and the air column between the source and the patient or phantom surface [25, 46, 63]. The dose contribution of contaminating electrons decreases almost exponentially with depth [92]. At lower energies, the dose due to contaminating electrons decreases more rapidly with increasing depth due to the smaller electron energy. At higher-energies, the flattening filter is the main source of contaminating electrons and the dose variation in the build-up region with field size and/or treatment geometry (trays, blocks, wedges) is higher for high photon energies than at low photon energies [93]. As the presence of head scatter electrons is the cause of the d_{max} shift toward shallower depths when the field size is increased, the position of d_{max} varies more with treatment geometry at higher than at lower energies.

The larger the photon beam energy, the lower is the surface dose. For example, in $10 \times 10 \text{ cm}^2$ ^{60}Co fields it is about 30% of the dose at d_{max} , 15% of the dose in 6 MV x-ray beams and 10% of the dose in 18 MV x ray beams. For a given beam energy, the surface dose increases with field size (Table 5.1). The low surface dose compared to the maximum dose is often referred to as the skin sparing effect and represents an important advantage of megavoltage beams over orthovoltage and superficial beams when used for the treatment of deep-seated tumours.

Table 5.1: Typical depths of dose maximum for different energies and field size [25, 29, 94]

Photon energy	d_{max} (cm)		
	Field size (cm^2)		
	5 x 5	10 x 10	30 x 30
4 MV	1.0	1.0	0.8
6 MV	1.7	1.5	1.5
18 MV	3.5	3.2	2.0
25 MV	4.4	-	2.5

5.2 TLD and build up capsule

TLDs and semiconductor diodes are the most popular tools used in in vivo dosimetry in radiotherapy to date. TLD-100, compared to other detectors is composed of tissue equivalent material beside other valuable advantages [64]. TLDs with build-up caps are previously reported as being suitable for in vivo dosimetry [95-99]. With tissue equivalent material (Plexiglas) [95,], Polystyrene [96] or high atomic build up caps materials with powder, Aluminium [97], polytetrafluoroethylene (PTFE) [98] or a mixture of different materials (S.Steel, Paraffin, Perspex) [99], an accuracy of ± 2 was achieved (Table 5.2). No study as far as we know used the TLD chips with high Z build up cap material. Some published studies concerned about peripheral dose [100-104] used diodes [100], TLDs in build up caps [101-103] or pen dosimeters [104] Table 5.2.

Table 5.2. Physical data of build up caps in the literature

Author	Buildup cap	Organ and energy used	Parameters measured	Accuracy
Kalef-Ezra et al [95]	10 mm of PMMA, capsule: 30 mm diameter and 20mm thickness, 3 TLD	Pelvis (54), Breast (34). 6 MV and Co-60	Entrance dose Exit dose Midline dose Output	99%
Swinan et al [97]	2mm Cu. Cylenderical.27mm length, diameter 20 mm. 1.3 AL build up cap for Co-60.diameter7.6 mm .LiF powder.	Open field patients. 6 MV and Co-60.	Entrance dose for 18 radiotherapy centers Build up cap perturbation	98%
Amor Duch et al [96]	12 mm polystyrene buildup cap, hemispherical. Diameter 40 mm, 1 TLD	TBI, 18 MV	Entrance and exit dose	98%
Venables et al [98]	10 mm buildup cap from (PTFE), 20 mm length, 4 TLDs	6MV Co-60 Breast	Entrance dose Phantoms and 429 patients in 33 hospital	99%
Loncol et al [99]	2 mm hemispherical buildup cap for steel, 12 mm diameter, inner cavity filled with paraffin, TLDs in Perspex box	8 MV Head and neck, Brain	Entrance and exit dose 249	99%

5.2.1 Capsule design

TLDs placed at skin level may be surrounded with adequate material to avoid the initial steep gradient in the depth dose curve and thus to be reproducible, i.e. with a build-up cap of specific thickness close to that of d_{\max} [63]. However, at high photon energies the thickness of the build-up cap can be several cm of water equivalent material. This may cause patient discomfort and leads to an under-dosage of a broad part of the treatment volume, combined with loss of skin sparing close to the capsule. Moreover, the perturbation of the primary photons by the build-up cap takes place over a large area. Therefore, it is necessary to reduce build-up cap dimensions by using high-density materials, but in this case, the build-up cap can change the energy response of the detector. To reduce these errors and uncertainties, calibration should be performed by the TLD in its build-up cap. Minimal perturbation is usually achieved by materials with similar effective atomic number for photoelectric effect, pair production and Z/A to that of water [25, 46, 97].

The electron density ρ_e is given by

$$\rho_e = \rho_m x N_A x \left(\frac{Z}{A} \right) \quad (5.1)$$

ρ_m : the mass density (g/cm³) of material m

N_A : Avogadro's number (6.022 x 10²³) (atoms/mole)

Z : the atomic number

A : the atomic mass

Therefore, the following calculations are used to determine the water equivalent thickness d_{H_2O} of build up cap of material m and thickness d_m , assuming Compton interaction to be the dominant one:

$$d_m = \frac{(\rho_m)_m x(Z / A_m) /}{(\rho_m)_{H_2O} x(Z / A_{H_2O})} = d_{H_2O} \quad (5.2)$$

Table 5.3: Physical data of build up caps (all dimensions in mm).

Material	Atomic Number	Density (g/cm ³)	6 MV			15 MV		
			Diameter	Wall Thickness	Height	Diameter	Wall Thickness	Height
Copper	29.0	8.29	18.0	1.8	7.0	20.0	3.0	8.0
Stainless steel	25.6	8.20	18.0	2.3	7.5	23.0	4.0	9.0
Aluminum	13.0	2.79	25.0	5.7	12.0	33.0	9.6	20.0
Plexiglas	6.25	1.19	30	10.0	20.0	30	10	20

* The build up cap used for 6 MV

Five build up cylindrical caps for various sizes made of Plexiglas, Aluminum, Copper and Stainless steel were constructed for both energies to accommodate four TLD chips per cap (Figure 5.2, a and b, Table 5.3). The inner pocket, 14 mm in diameter was constructed to accommodate four 3.1x3.1x 0.89 mm³ TLDs per cap, but those made of Plexiglas of 10 mm pockets may accommodate up to three TLDs. The build caps were manufactured in a private workshop in Larissa, while the Plexiglas one is manufactured by Kalef-Ezra et al [95].

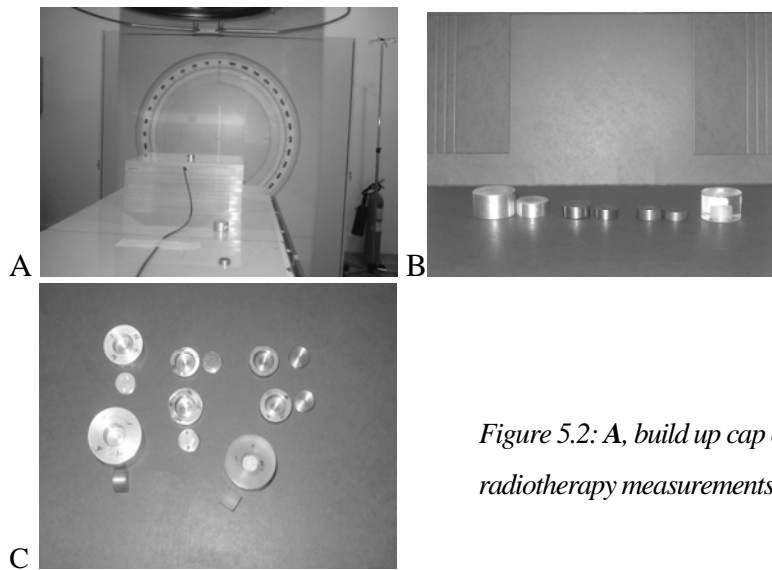


Figure 5.2: A, build up cap calibration set up for radiotherapy measurements. B, C, Build up caps

5.2.2 Testing of the capsules

A total of 33 build-up caps were manufactured, five for each high-density material (aluminium, copper and stainless steel) and three from Plexiglas.

TLDs located in the build caps attached to the upper surface of the 30 x 30 x 12 cm³ Plexiglas phantom were irradiated in the central beam axis on the phantom using a 10 x 10 cm² field at SSD of 100 cm. A dose of 500 mGy in water was given (Figure 5.2. 1,c). Each TLD was identified by its position in the cap, while each cap had specific number. The build up cap was positioned such that the beams central axis passed through its central axis. The applied dose values ranged between 0.25 cGy to 10 Gy while a dose of 0.5 Gy was used to detect the effect of geometrical settings (SSD, Field size, tray, and wedge).

To test the similarities in the construction between the capsules, all the capsules of each kind were irradiated under identical conditions and the doses registered by the TLDs in the capsules of each kind were compared.

5.3 TLD calibration for entrance dose measurements

TLDs in the build-up cap have to be calibrated to measure entrance and peripheral dose i.e. when positioned on the patient's skin the measured dose should be correlated to the dose at some location inside the human body, such as at the depth of maximum dose. Therefore, the most straightforward calibration method could consist of comparing the dose given to TLDs in capsules to the doses measured with a calibrated ionization chamber (IC) at the point of interest (Figure 5.3). Therefore, factors (F_{cal}) that correlate the doses registered at the two points have to be determined experimentally. This methodology

was proposed and used at Ioannina University Hospital by Kalef-Ezra et al [95] and other studies (e.g. [97-99]).

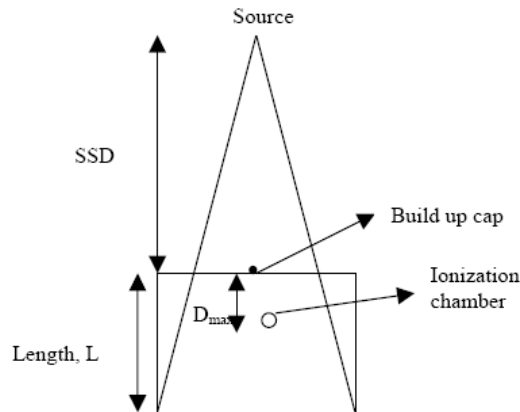


Figure 5.3: *Experimental calibration set up for entrance and exit dose*

5.3.1 TLD calibration in build-up capsules

Calibration factor (F_{cal}) is defined as the ratio of the dose in water measured with the IC in Plexiglas under reference conditions, and the dose of the TLD irradiated in build-up cap under the same conditions.

$$F_{cal} = \frac{R_{IC}}{R_{TLD}} \quad (5.3)$$

The experiments for the assessment of F_{cal} were repeated three times and the mean value was used. More specifically, TLDs in the build-up cap were placed on top of about 10 cm thick Plexiglas (PMMA), and were irradiated under reference conditions (field size 10 x 10 cm², source-surface-distance (SSD) = 100 cm, 0.5 Gy) simultaneously with an IC located at d_{max} , i.e. at 1.6 and 2.7 cm depth for 6 and 15 mV beams)(Figure 5.4), outside the shadow of the build up cap. This technique has limitations related to non-uniformities of the photon field. No trial was made by switching the locations of the TLD and the IC.



Figure 5.4. *Copper build up caps for 6 and 15 MV.*

5.3.2 Build up calibration for entrance dose measurements

5.3.2.1 Determination of geometrical correction factors

In order to obtain an accurate radiation dose in clinical conditions, a set of correction factors has to be established to account for variations in the TLD signal in situations deviating from the reference conditions. The ultimate factors influencing the TLD response are the field size, SSD, presence of beam modifiers such as filters or wedges, presence of tray and blocks and the beam incident angle. Correction factors accounting for the variations in response are determined as the ratio of the reading of IC and the reading of the TLD for a clinical irradiation situation normalized to the same ratio for the reference situation.

Correction factors were calculated for the following clinical conditions (Table 5.4):

1. SSD correction factor (CF_{SSD})
2. Field size correction factor (CF_{FS})
3. Tray correction factor (CF_{Tray})
4. Wedge correction factor (CF_{Wedge})
5. Angle correction factor (CF_{Angle})

TLD irradiations in build up cups were performed with the caps located on the top of the Plexiglas phantoms under a variety of irradiation geometries (Table 5.3).

Table 5.4: different beam geometries for calibration TLD in build up caps

SSD (cm)	Field size (cm)	Tray	Wedge (degree)	Angle
85	5x5	5x5	15	15
90	10x10	10x10	30	30
100	15x15	15x15	45	45
110	20x20	20x20	60	60
120	25x25	25x25		
130	30x30	30x30		

$$Dose = Dose_{TLD} \times F_{cal} \times CF_{SSD} \times CF_{FS} \times CF_{wedge} \times CF_{Tray} \quad (5.4)$$

$$CF_{Total} = CF_{SSD} \times CF_{FS} \times CF_{wedge} \times CF_{Tray} \quad (5.5)$$

The reference conditions influence the value of the correction factor for a second parameter (e.g. the presence of a tray). The ‘reference condition’ for the determination of this second correction factor is

adapted in order to avoid double inclusion of the first correction factor. This is made clear in the practical recommendations given below.

$$CF_{SSD,FS} = \frac{(R_{IC}/R_{ILD})_{clinical}}{(R_{IC}/R_{ILD})_{reference}} \quad (5.6)$$

Beam modifiers correction factors:

- Tray correction Factor

Inserting a tray of 5 mm thickness between the source and the patient changes the amount of electrons that reaches the patient skin. The tray correction factor varies with field size. To determine the tray correction factor, tray transmission is needed for different field sizes for TLDs and ionization chambers. To determine CF_{Tray} , we measure the tray transmission for different field sizes at the depth of dose maximum, first with an ionisation chamber and then with the build up cap placed in the surface of the Plexiglas phantom. The transmission factors measured with the ionization chamber and with the build up cap are compared, and CF_{Tray} as a function of field size is obtained

$$CF_{Tray} = \frac{ICtransmission}{TLDtransmission} \quad (5.7)$$

- Wedge correction factor

Inserting wedge in the beam results in decrease of the dose rate and a hardening of the spectrum beam. Therefore, a correction factor is needed. The wedge correction factor is defined as the ration between the wedge transmission factors for a 10x10 cm² field with the same field as that used for the TLD reading on the surface of the phantom.

$$CF_{wedge} = \frac{ICtransmission}{TLDtransmission} \quad (5.8)$$

Transmission is defined as the ration of clinical value to reference value

- Angular dependence

Different gantry angles were considered to determine the directional dependence of the build up caps to evaluate the influence of the angle in TLD accuracy.

5.3.3.2 Determination of Physical Correction Factors

Physical correction factors include: fading, energy and linearity correction factors [25, 26, 29, 64, 69]. Since the TLDs are calibrated at the same energy used for clinical investigation and the readout process

was performed in less than 24 hours, the energy and fading correction factors are considered to be equal to 1.

- Linearity correction factor

Lithium Fluoride, which is commonly used in TLDs, is linear up to 1 Gy, but after that becomes supralinear. The necessary correction factor can be established by plotting the TLD reading against dose. The dose response curves for the TLD phosphors are linear in the dose range from 10^{-5} Gy to 1Gy followed, in the case of LiF, by a supra-linear range for higher doses. At saturation region the LiF TL yield decreases.

Therefore, correction account for the supralinearity of LiF: Mg, Ti is needed.

The supralinearity correction can be defined as:

$$f(D) = \frac{TL(D)/D}{TL(D_0)/D_0} \quad (5.9)$$

TL (D): TL signal corresponding to dose D.

TL (D_0): TL signal corresponding to D_0 being in the linear region of the TL dose response curve.

The radiation dose was measured from TLD signal with build-up cap according to the following expression:

$$Dose = D_0 \times F_{Calibration} \times CF_{SSD,FS,Tray,wedge} \times CF_{linearity} \quad (5.10)$$

5.4. Thyroid surface dose measurements (TSD)

In radiotherapy it is important to measure the doses received by the critical organs, which are outside as well as inside the direct radiation field. In this work, the scattered radiation dose to the skin surface, thyroid was measured during external beam radiotherapy for breast cancer patients.

TSD were measured during breast radiotherapy, in order to evaluate the risk of radiation dose and the probability of a secondary cancer effect. The TLDs were packed in plastic envelopes and attached on the middle surface of the thyroid in presence of radiotherapist (Figure 5.5,A). The measurements were performed per field and for two fields. Doses to the thyroid can be measured directly in an anthropomorphic phantom. However, the phantom was not available. Thyroid dose can be derived from the prescribed dose using data in the literature. The TSD is measured as indicator for the thyroid surface dose.

As far as we know, there is no available data to convert the surface dose to thyroid dose during radiotherapy. Therefore, in this calculation we used surface dose as a thyroid dose. ICRP [25, 26] have quoted the probability of a fatal cancer to the general public due to irradiation of the thyroid as $20 \times 10^{-4} \text{ Sv}^{-1}$ giving a risk of fatality due to thyroid cancer per treatment course.

Secondary tumour induction may seem a relatively significant problem, since the patient has to survive the primary tumour long enough for a secondary one to become obvious [105]. It has been estimated that the probability of developing a solid tumour after receiving radiotherapy is increased by 1.4% (10 years post treatment, and compared to the surgical control group) to ≈ 1 patient out of 70 [105].

The thyroid is the largest pure endocrine gland and it normally weighs about 20 g. It consists of two lobes connected by the isthmus in the midline. Each lobe is about 3–4 cm long, about 2 cm wide, and only a few millimeters thick. The isthmus is 12–15 mm high and connects the two lobes. (Figure 5.5,A).

Radiation is one of the few accepted risk factors for thyroid cancer. Numerous studies have confirmed that the thyroid gland is one of the most radiation-sensitive human organs and that thyroid cancer is one of the most common radiogenic malignancies [106]. Thyroid cancer is the most common endocrine malignancy, accounting for 1.9% of all new malignant tumors (0.92% of cancers in men; 2.9% in women;) [106]

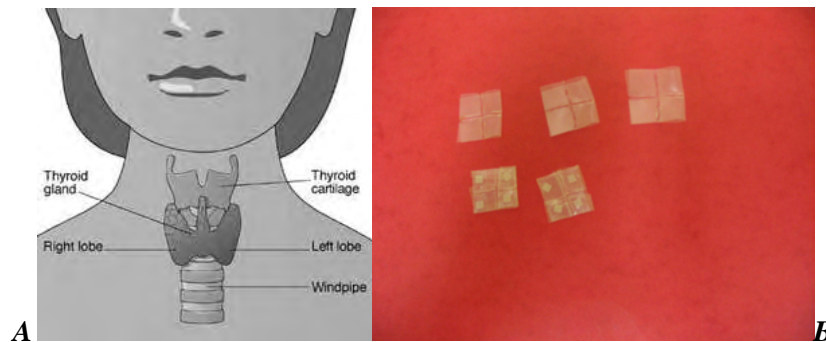


Figure 5.5. A, Thyroid position, B, TLDs in a Plastic envelope

5.5 Skin dose measurements

The dose to skin close to the treatment head can be divided into two main components, the dose from the secondary electrons produced by interactions with air, collimator jaws, beam monitor chambers, target and any other scattering material and electrons ejected under the action of the incoming beam inside the patient body.

5.6 TLD and build up caps results and discussion

The ratios of the doses registered in TLDs located in capsules to the doses given at d_{\max} and assessed with the calibrated IC under reference conditions are shown in Table 5.5. It was found that ratio of doses was close to 1.00 when the Plexiglas caps were used for both 6 and 15 MV X-ray beams. In a similar study at IUH a ratio of 1.00 was found when 6 MV X-ray beams were used [95,107]. The TLDs over responded at 6 MV fields, when located in Cu or S.S. cups but not in Al. On the other hand at 15 MV photon fields, the TLDs underresponded in Al caps and overresponded in Cu caps. This can be explained by the fact that

SS and Cu compared to Plexiglas and Al have a higher Z material and produce more pair production electrons at higher energies (See Chapter 2).

Table 5.5: Test results for build up caps according to the atomic number

Build up cap		n	Nominal Dose	Mean measured dose	Measured/Nominal dose
Copper	6MV	3	50.00	50.00	1.000
	15 MV			51.04	1.0208
S. Steel	6 MV			51.24	1.0248
	15 MV			50.42	1.0084
Aluminum	6 MV			51.01	1.0202
	15 MV			49.03	0.9806
Plexiglas	6 MV			49.84	0.9968
	15 MV			50.12	1.0024

Table 5.6 Inter-build up caps variations (nC)

Caps	Copper		Aluminum		Stainless steel		Plexiglas	
	6 MV	15 MV	6 MV	15 MV	6 MV	15 MV	6 MV	15 MV
1	1331.2	1777.0	1194.4	1396.3	1286.5	1663.7	1005.5	1011.8
2	1342.2	1765.2	1186.2	1387.2	1292.5	1660.2	1003.5	1013.3
3	1325.9	1779.2	1193.1	1378.3	1301.2	1674.3	1004.1	1018.2
4	1338.5	1772.3	1202.4	1378.4	1297.2	1667.4	-	-
5	1336.8	1767.6	1188.2	1382.6	1289.9	1669.8	-	-
Mean	1334.9	1772.3	1192.9	1384.5	1293.5	1667.1	1004.4	1014.4
Sd	6.4	5.9	6.3	7.5	5.8	5.4	1.0	3.4

5.6.1 Perturbation behind the detector

Dose perturbation was determined using a radiographic film (Kodak-X Omat) at d_{max} of the Plexiglas phantom using standard irradiation conditions. The profile was obtained using a film densitometer (VIDAR system corporation, USA). The different build-up caps were calibrated to measure entrance dose.

The relative dose ratios of TLDs in build-up caps versus the dose at d_{\max} in the corresponding open field, due attenuation and absorption in the TLDs and the capsule itself, is given in Table 5.7

Energy	Copper	Aluminum	Stainless steel	Plexiglas
6 MV	14.1%	14.7%	13.7%	16.8%
15 MV	22.6%	15.6%	22.9%	-

Table 5.7: Dose perturbation due to the presence of the TLD in the build-up capsule

These perturbation values are higher compared to results obtained by previous studies using TLDs [97,98] and diodes [26]. From these results (19%), the reduction of the dose in some areas of the treatment fields and the reduction of tissue sparing are of clinical importance and have to be taken into account. Therefore, it is preferable to be applied only few times in each patient, for example during the two initial treatment fractions and possibly twice at a later stage.

5.6.2 Calculated correction factors (Copper capsule)

The calculated entrance correction factors for field size, SSD, angle of incidence, and wedge angle are given in Tables 5.8 and 5.9. The reproducibility of the measurements has been found better than 2.0 % for the 108 beam geometries. Most of the correction factors are close to unity and fall most within the uncertainty of the measurements.

The variation in correction factors and F_{wedge} is most extreme for 15 MV energies. The correction factor increases with increasing field size, which can be explained by the electron contamination increase in function of field size [108]. Moreover, the dose contribution of contaminant electrons in high-energy beams is relatively high at 3 cm depth for field sizes $10 \times 10 \text{ cm}^2$ and larger. Compared to water, the high-atomic number build-up caps have different scattering properties for these electrons. In addition, if the field size increases, not only more head-scatter electrons but also head-scatter photons reach the cap and because of high Z , produce more pair production electrons at higher energies. Since these photons are scattered through small angles and have only small variation in energy, they have similar penetration characteristics to un-scattered components [92].

Table 5.8 Entrance dose correction factors and standard error of the mean (SEM)

Energy	6MV	SEM	15MV	SEM
Geometry	CF		CF	
FS (cm ²)	CF (FS)	0.008	CF (FS)	0.014
5x5	1.002	0.017	0.975	0.018
10x10	1.000	-	1.00	-
15x15	1.003	0.005	1.031	0.017
20x20	1.007	0.012	1.041	0.012
30x30	1.016	0.015	1.049	0.024
SSD (cm)	CF(SSD)		CF(SSD)	
85	0.989	0.018	0.987	0.022
90	0.998	0.012	0.988	0.019
100	1.000	-	1.000	-
110	1.016	0.012	1.013	0.014
120	1.022	0.014	1.029	0.019
130	1.028	0.018	1.031	0.015
Angle	Angle		Angle	
0	1.00	-	1.000	-
15	0.939	0.016	0.90.23	0.019
30	0.878	0.015	0.86.25	0.012

Table 5.8: geometrical correction factors to account for variations in TLD response in situations deviating from the reference irradiating condition in 6 MV and 15 MV photon beam energies

Wedge angle	15	30	45	60
Field size				
5x5	0.981	0.990	0.984	0.995
10x10	0.997	1.067	0.998	1.009
15x15	1.009	1.098	0.998	0.985
20x20	0.998	1.047	1.032	1.023
25x 25	1.006	1.049	0.988	1.013

5.6.3 Effect of the atomic number on the TLD signal

The TLD signals measured in the copper, aluminum, stainless steel and plexiglas increase with beam energy (Figure 5.6). A qualitative explanation can be based on the following argumentation [97,107]. The mass densities of copper, stainless steel, aluminum, and Plexiglas are 8.29, 8.20 2.70 and 1.17 to 1.19 (depending on the production technique) g/cm^3 respectively, i.e. larger than that of water, 1.00 [109,110]. On the other hand, for the mass weighted (Z/A ratio), plexiglas (polymethyl methacrylate) has Z/A 0.53937, water 0.55509, aluminum 0.4818, copper 0.45636, SS (it depends on the way of its production), however is quite similar to that of Cu. The TLD signal for Cu and SS are higher than the one for Plexiglas and Al.

From the higher number of electrons per volume in Cu it follows that the number of scattered electrons is higher, which results in a higher TL signal in Cu and SS than in water (Figure 5.6). When the beam energy increases (15 MV X-rays), the probability of pair production rises. Pair production is almost proportional to Z . As the atomic number of Cu is high, even more secondary electrons are set in motion and can get to the LiF TL chips, which results in a higher signal.

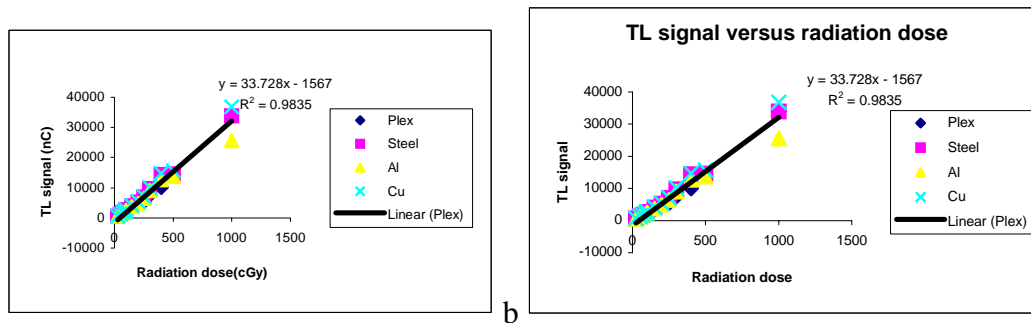


Figure 5.6. Correlation between TLD-100 signal and radiation dose. (a) for 6 MV and (b) for 15 MV.

The TL supra-linearity effects are illustrated in Figure 5.7, A and B, for both energies. The onset of supralinearity occurred clearly above 1 Gy. This can be explained by the fact that an increase of TL signal per unit dose for high Z material is not accompanied by decrease the linearity region compared with low Z materials.

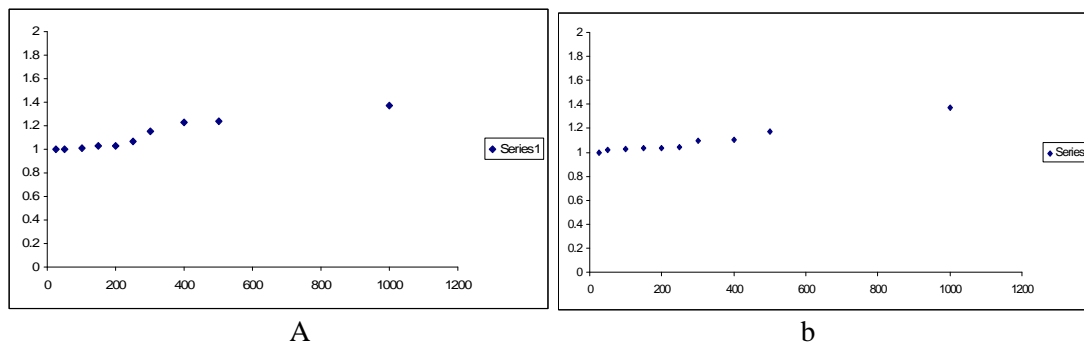


Figure 5.7. A, TLD linearity for Copper build up cap for 6 MV, and B for 15 MV

5.7 In vivo dose measurements

In vivo dosimetry was performed after the commissioning of the build up capsules, in 69 patients (183 fields Table 5.11) to assess the accuracy in dose delivery, to evaluate and improve the accuracy in dose calculation and delivery. The measured quantities were entrance and peripheral dose using 6 and 15 MV X-ray photon beams. At least two fields were tested per treatment. More specifically, four fields were tested in prostate patients (Anteroposterior (AP), Posteroanterior (PA), Right lateral (RL) and Left Lateral (LL). For tangential breast treatments both fields were measured. Therefore, repetitive in vivo dose measurements on a limited number of patients yield information on the influence of patient anatomy on the accuracy of the dose delivery as well as on the reproducibility of the treatment method in daily practice.

The delivery of radiation according to a specific treatment plan is important to maximize tumor control and minimize normal tissue complications (26, 69). The limitation of QA procedures to one or a few sessions of a fractionated treatment is usually required due to a number of factors [69], such field perturbation. Therefore, it might be more important to concentrate the efforts on the detection of systematic errors, which will be repeated by definition (and thus need corrective action). However, in the present study in vivo dosimetry was performed in patients treated for breast, head and neck, pelvis and abdominal cancer of a fractionated treatment, for two of the treatment fields in minimum.(Table 5.9) .

5.7.1 Patient Setup

The build up capsule was secured on patient skin with tape at centre of the field. In PA treatments the beam has to pass first through the treatment couch. The SSD to the surface of the couch was therefore taken and the build up cap placed on the posterior side of the treatment couch (for patient comfort). The initial measurements in each patient were performed in presence of a radiotherapist. Annex B, shows the Patient data documents for each patient.

The contribution of systemic errors can be calculated by comparing the mean of measurements of specific patients to corresponding planned values. By comparing the mean of the measured value, random daily variations may be cancelled out [26]. The expected dose at d_{max} was calculated using a TPS and the dosimetric data obtained from linear accelerator calibration for each field. Isocentric and non-isocentric irradiation techniques have been used.

Before starting patient measurements, patient set-ups were simulated using a phantom. The irradiations and TLDs within build up capsules measurements were performed in identical conditions as in the clinical situation.

Initial patient measurements were made using treatment fields, where there was easy fixation of the Build up cap in the field centre (head and neck, pelvis and abdomen). Later, the measurements were also performed in breast and wedged fields, because these techniques are complex and require excellent modeling from the planning system and accurate placement of the build up caps (Table 5.9).

Table 5.9: Number of measurements in vivo per anatomic region and per type of the treatment.

Anatomic Region	Field	No of Patients	No of Measurements
Head and neck	LL, RL	16	45
Abdomen	AP, PA	8	24
Breast	Field in, field out	24	70
Pelvis	AP, PA, LL, RL	21	44
Total		69	183

5.7.2 Action thresholds set in literature

The choice of tolerance/action levels is very important since they will in practice determine the number of "errors" detected and will influence the associated workload to implement or to maintain in vivo entrance dose measurements at a departmental level.

When in vivo dosimetry is used to check particular treatments, the value of the levels can vary according to the treatment type. Treatments with high dose - high precision techniques require narrow tolerance windows, while other treatments have less stringent accuracy demands. In certain centres, it could be realistic to set higher tolerance/action levels for patients treated with palliative intent in order to minimize the number of second measurements, paying more attention to the patients treated with curative or adjuvant intent. The determination of the actual value of the level is based on different factors, first of all on the uncertainty of the detector measurement method [111].

Tolerance Level: For a performance parameter that can be measured, a tolerance level is defined. If the difference between the measured value and its expected or defined value is at or below the stated tolerance level then no further action is required as regards that performance parameter.

Action Level. If the difference between the measured value and its expected or defined value exceeds the action level then a response is required immediately. The ideal response is to bring the system back to a state of functioning that meets all tolerance levels [112].

In order to implement a proper in vivo dosimetry programme, the clinical setting uncertainties involved in the measurement should be defined. For this reason two thresholds are generally given. An investigation threshold above which, a repeat of the in vivo dosimetry measurements is made, and, an action threshold, above which patient setup and treatment delivery is checked [111,113]. The action threshold should not be chosen arbitrarily as choosing the wrong action threshold can lead to time wasted on investigations into treatment errors, which do not exist [114]. This in turn leads to lack of confidence in the new techniques being offered. Action levels are based on 2 standard deviations from the mean measurement [111,114]. For a centre with calibrated diodes and a program in place to implement in vivo dosimetry regularly this is about 5 to 8% [111]. Even though Leunens et al [114] found the average standard deviation for all

measurements was 3.1% (1SD) for corrected tangential breast treatments they chose 5% as the tolerance level. Not surprisingly 10% of patients had deviations greater than 5% (the chosen threshold). Wedged and blocked fields had higher standard deviations. Breasts had higher standard deviations than vertebrae [111].

Action levels set in literature vary between the various studies for example ranging in Europe between 2.5% to 10% (Table 5.10). Action levels also depend on the complexity of techniques. In general, techniques using tangential fields with wedges are hard to check and generally have higher action levels [111].

Table 5.10: Action Levels for different radiotherapy departments [111]

Institution	Technique	Action Level 1	Action Level 2
Leuven	All Techniques	5 -10%	5 -10% (6 MV -18 MV)
Barcelona	All Techniques	5%	5%
Nancy	All Techniques	5%	10%
Copenhagen	Tangential Breast	8%	8%
Copenhagen	Prostate	5%	5%
Amsterdam	Prostate	2.5%	2.5%
Milano	Tangential Wedge	7%	7%
Edinburgh	Conformal prostate	2.5%	2.5%
Edinburgh	General Entrance	5%	5%

5.8 *In vivo dosimetry results and discussion*

10 build up cylindrical caps made of copper were used for both energies to accommodate four TLD chips per cap. The cap dimensions and physical construction are demonstrated in Table 5.2, Build-up caps made of Cu were found to be optimum for high-energy photon fields due to copper having a high density (8.29 g/cm^3) and high atomic number ($Z= 29$); copper provides the minimal amount of metal needed to achieve full buildup at d_{max} . To prevent friction from the metallic build up cap, a piece of plastic was placed over the TLD's in the build up cap. This was used in all steps of the dosimetry to ensure uniformity across the measurements.

5.8.1 Head and neck

Forty-five entrance dose measurements were carried out in 16 patients who received fractionated radiotherapy treatments applying either isocentric or non-isocentric irradiation techniques with opposed lateral 6 MV fields at UHL. Due to the limited number of patients per group (larynx, nasopharynx and brain) the data was grouped together. Patients were treated in the supine position with a fixed individual thermoplastic mask for immobilization. Markers for patient set-up, field center and fields' edges were indicated on this mask. Figure 5.8 illustrates a TLD capsule made of copper, attached to the patient's mask in the central beam axis for the assessment of the entrance dose of the left field. The entrance dose for the studied fields ranged between 0.90 and 1.87 Gy in water. Beam modifiers (trays and wedges) were used for some of the fields.



Figure 5.8: Placement of copper build up cap for in vivo entrance dose measurements, attached in a patient mask in central axis of the beam for entrance dose measurements.

The mean value of the all dose measurement is presented in Figure 5.9.

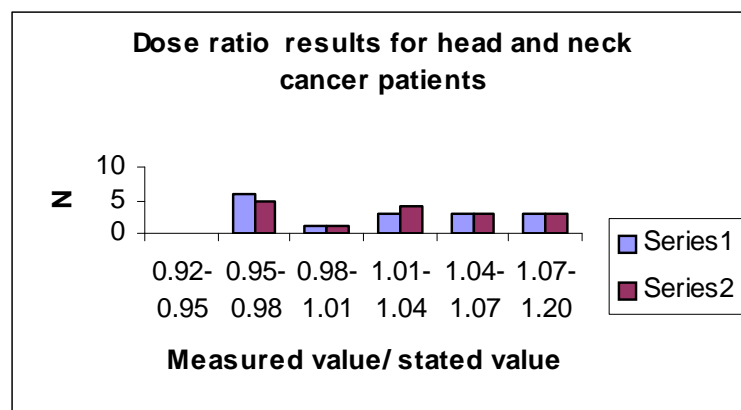


Figure 5.9: Entrance dose ratio for head and neck cancer patients (left and right lateral fields)

The global mean of all measured ratios of measured to stated entrance dose per patient during the two series of measurements are shown in Fig. 5.6 (series 1(right lateral)) and series 2(left lateral) The mean ratio is 1.017 ± 0.05 , and 1.016 ± 0.06 for left and right lateral fields respectively .The number of patients are

16 patients with 32 fields, and because of some patients were measured more than two times, the total of fields are 45 (annex D.1 shows the details of dose measurements). The mean value of the fields is presented. No patient received a dose less than 5% percent of the prescribed one. The large deviation can be explained by in accuracy in SSD, since the TLDs are placed in the masks a better accuracy is expected with analyzing all source of errors.

Table 5.11 illustrates the accuracy obtained from different reported studies in the literature. The results are comparable to our results.

The main reported reasons for the higher doses are (i) patient set up, (ii) error in indicator of the treatment couch (iii) inaccurate acquisition of body contours [9,57,108] and (iv) when the beam axis passed through air cavities or when the on-axis point was near bony structures (Inhomogeneous structures)[69]. Better fixation is going to reduce the random errors but not the systematic.

Table 5.11: Results of in vivo dosimetry performed in head and neck cancer patients.

Authors	Number of patients	No. Setups	Detector	Measurements	Errors <5%
Present study	16	45	TLD	Entrance dose	5%
Leunens et al[115]	17	554	TLD/Diodes	Entrance dose	3%
Leunens et al[116]	47	230	TLD/Diodes	Entrance dose	20%
Essers [117]	23	261	Diodes	Entrance +exit	9%
Broggi et al [118]	16	116	Portal detectors/Diodes	Midline dose	3.5%
Tung et al [119]	Phantoms	-	TLD/Diodes	Midline dose	8%

In conclusion, these initial clinical tests demonstrated that high Z build up caps can be implemented in practice without an excessive increase in workload. Accurate positioning of build up cap during treatment takes approximately 1 min and estimation of the agreement between estimated and calculated entrance doses need to be improved by further investigations although, the results are within the acceptable limits.

5.8.2 Breast

Seventy entrance dose measurements were carried out in 24 patients, which received fractionated breast radiotherapy treatments at LUH. 6 MV wedged tangential X-ray fields were used in all patients, but in patients with large breast that were treated with 15 MV X fields (Figure 5.10, A&B).

After patient set-up, a pair of build up capsule was placed on the beam axis at the entrance and exit surface. The mean ratios of the measured to the expected entrance dose per patient ranged between 0.92

and 1.20 with mean values and standard deviation 1.011 ± 0.04 and 1.002 ± 0.04 for external and internal fields respectively (Figure 5.11) (Annex D.2). These findings are lower with those reported by other investigators using TLDs in capsules, taking into account the high Z build up caps characteristics [95,97,98] (Table 5.14). The entire breast in vivo dose measurements has an error of 0.4%, which indicates a problem in a placing the TLDs.

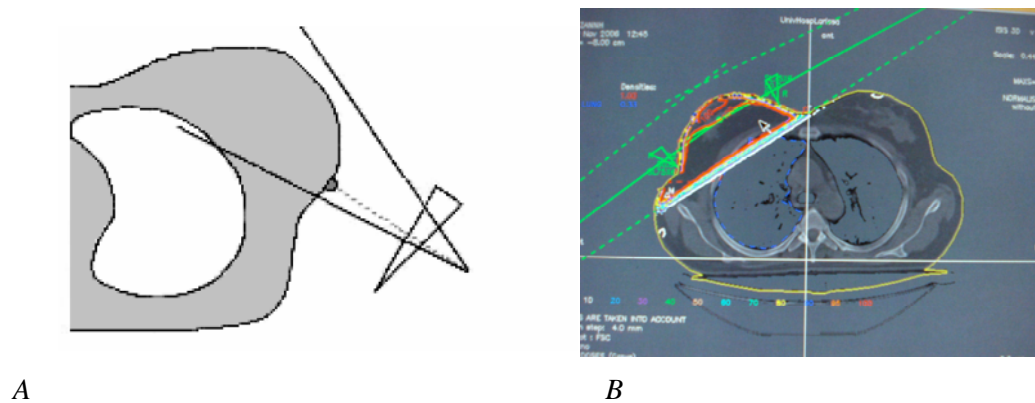


Figure 5.10 , A Schematically representation of build-up cap positioning in lateral breast treatment field, B, Breast treatment plan using tangential fields

Table 5.1.: Breast dose results in some studies in literature (Mean value \pm SD), ratio of measured to prescribed doses.

Authors	Number of patients	Detector	Measurements	(Mean value \pm SD).
Present study	24	TLD	Entrance	1.011 ± 0.04
Kalef-Ezra et al [95]	69	TLD	Entrance dose (Internal)	1.013 ± 0.041
	67	(Plexiglas capsule)	Entrance dose (External)	1.030 ± 0.041
Venables et al [98]	429	TLD	Entrance, exit	0.99 ± 0.04

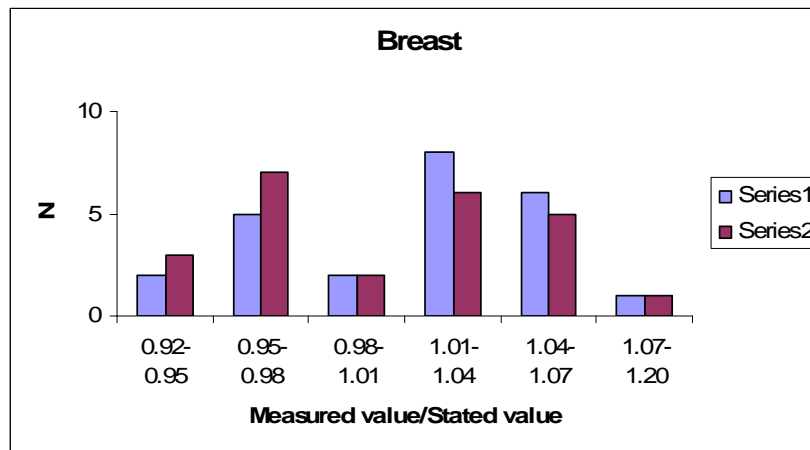


Figure 5.11: Entrance dose ratio breast cancer patients

5.8.2.1 Thyroid surface dose measurements

In radiotherapy it is important to know the doses received by the critical organs. Recent developments in radiotherapy increase patient survival rate. For example, survival rates for breast cancer have been improving for more than twenty years and more women are being successfully treated than ever before [120]. These developments increase the importance of reducing the probability of induction of radiation late effects in the thyroid gland, such clinical hypothyroidism and thyroid cancer. For these reasons we have studied the thyroid dose due to scattered and leakage radiation in patients undergoing therapy with wedged tangential breast fields at UHL.

Thyroid and skin doses were measured during breast radiation therapy of 24 patients using TLDs placed in a thin plastic film at center of the thyroid gland. The measurements were performed for single fields and for two fields. Table 5.15 illustrates the percentage of thyroid dose per radiation field and skin dose due to primary, head scatter and leakage radiation. (The measurements were expressed as a percentages of the of the prescribed dose. Measurements were made during 2- 3 treatment sessions in minimum using TLD detectors taped appropriately to the neck.

An average skin dose of 3.7% of the prescribed dose, which ranged between 90 to 133 cGy per field, was found (Table 5.13). These results are comparable in those of the in vivo of reported by Besbes et al [100]. Chougule [121] reduced the thyroid dose by 10 to 40 percent by using a 0.5 mm thick lead rubber cover over the thyroid during radiotherapy to breast.

Table 5.13: Breast entrance, exit and peripheral dose

Parameter	Thyroid surface dose	Skin dose (total)	Field internal		Field external	
			Entrance dose	Skin dose per field	Entrance dose 2	Skin dose per field
Dose (cGy)	6.165	138.53	167.20	66.06	165.34	64.125
% of entrance dose	3.7%	83.95 %	1.013	40.03	1.002	38.86
sd	0.132	1.235	0.142	1.42	0.213	1.642

Besbes et al [100] measured the thyroid dose with diodes during breast and nasopharynx radiotherapy for 12 and 18 patients respectively. The patients were treated with a Co-60 unit. The dose was 1.14 Gy during the treatment. The prescribed dose Gy was 50 or 51.2. Stevens et al [101] determined the absorbed dose received by thyroid during prophylactic cranial irradiation in childhood leukemia and the factors that affect the dose. The dosimetry was performed in a phantom for both energies; 6MV and Co-60. They estimated that the thyroid depth was 1-2 cm. The dose ranged between 0.7- 7.3% (13-132 cGy) of the prescribed dose. Thyroid superficial dose was also measured to be only 1.5% of the prescribed dose. Porlaluri et al [103] measured the scattered radiation during breast cancer radiation therapy using TLDs. The dose was measured for thyroid using Perspex holders. The measurements were performed for two lobes of the thyroid. The average scattered dose was 0.53-2.15 Gys for the thyroid and 0.14-0.19 Gy for the gonads (Table 5.15). Cigna et al [104] measured the radiation-scattered dose for 11 organs during breast radiotherapy. The mean equivalent dose was 91 mSv for the thyroid (Table 5.14).

Table 5.14: Peripheral dose results and dose descriptor used in different studies

Author	Organ	Technique	Dose descriptor
Besbes et al [100]	Thyroid	18 Nasopharynx, 12 breast	Diodes, Co-60
Stevens et al [101]	Thyroid	Prophylactic cranial irradiation (Children) Phantom study	TLD, 6 MV and Co-60
Van der Geissen [102]	Fetus	Breast cancer And phantom	Build up caps with 3 TLD.
Mazonakis et al [122]	Thyroid	Phantom study Brain tumour	TLD 6 MV
Portaluri et al [111]	thyroid and gonads	Breast	3TLDs in a hemispherical caps of polystyrene placed
Cigna et al [103]	11 organ, thyroid, etc...	Prostate	Pen dosimeters 6 MV

From previous studies, it is clear that the thyroid received a significant dose during breast radiotherapy. Therefore, the routine evaluation of the thyroid function is important in patients who have been treated with radiotherapy and whose treatment portals have included a large part of the thyroid gland. A suitable protection of the thyroid gland is important to be provided specially for the patient performing radical radiotherapy when young. A reduction in the thyroid function often occurs without any significant symptoms, and often remains clinically undetected. The incidence of thyroid dysfunction may be decreased by reducing the field size or the irradiated volume of the thyroid gland and by using modern radiation equipment with high precision.

3.8.3 Abdomen

In vivo entrance dose measurements were carried out on 8 patients with a total of 20 treatments fields, using 6 MV X ray beam for different treatment conditions.

The reproducibility of TLD dose measurements was within 2%. Figure 5.12 represents the ratio of measured to expected entrance dose, treated for abdominal cancer, with the mean ratio of 1.0035 and standard deviation of ± 0.04 and 1.009 with standard deviation of ± 0.04 for Anteroposterior and PA fields, respectively (Figure 5.12(Annex D.3)). The measurements show good agreement between measured and expected dose in general. Large errors were detected on some patients assumed to be related with patient movement and respiratory motion. The maximum displacement was measured to be 24.0 mm and 34.0

for intrafractional motion for pelvic and abdominal region respectively [123] and the difficulty of placement of the capsule in PA field, which decreases the distance between the source to the surface of the build up cap and consequently might result in a higher dose.

Table 5.15 illustrates the accuracy obtained from different reported studies in the literature. The results are comparable to our results.

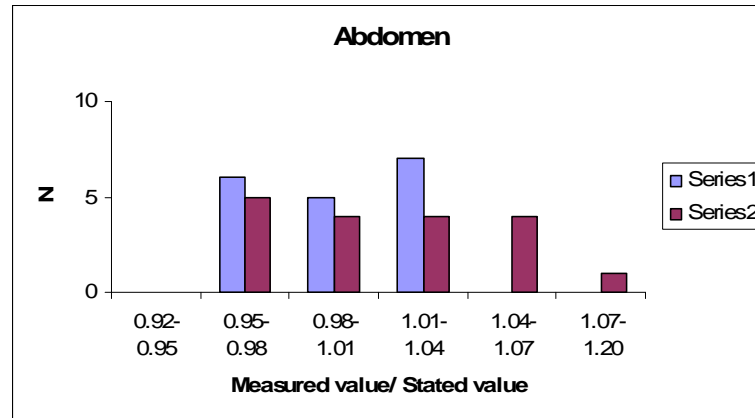


Figure 5.12: Entrance dose ratio for abdominal cancer patients

Table 5.15. Abdominal dose results in some studies in literature (Mean value \pm SD)

Authors	Number of patients	No.setups	Detector	Measurements	Errors <5%
Present study	8	24	TLD	Entrance	4%
Briot et al [124]*	28	-	TLD	Entrance+Exit	4% 8-12%
Greig et al [125]*	8	-	Diodes	Entrance	3-4%
Appleyard et al [126]	-	712	Diodes	Entrance	5%
ESTRO [111]	46	640	Diodes	Entrance	5%
Adeyemi et al [127]	550	-	Dides	Entrance	5%
Fiorino et al [128]	33	437	Diodes	Entrance	7.6%

* Total body irradiation

3.8.4 Pelvis

Patients with pelvic tumours are treated in supine or prone position according to the malignancy site. Pelvis treatments had results, which include different clinical conditions (prostate, cervix and rectum) distributed around a mean, with an average of 0.99 for all fields (AP, PA, RL and LL) with standard deviation of 3.6 %. In vivo entrance dose measurements were carried out on 21 patients, with a total of 44 treatments fields, which received fractionated radiotherapy treatments using 6 MV and 15 MV X ray beams.

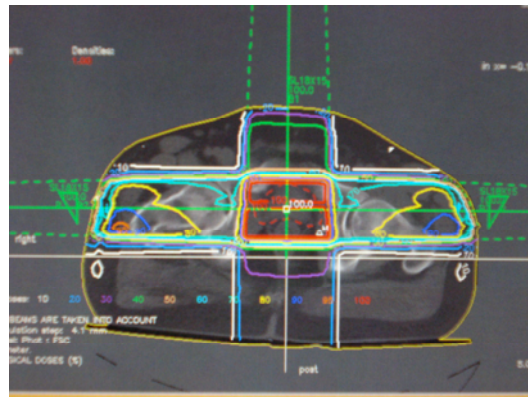


Figure 5.14. Treatment plan for prostate

The reproducibility of TLD dose measurements is within 2%. Figure 5.15 represents the ratio of measured to expected entrance dose of 21 patients, treated for abdominal cancer, with the mean ratio of 0.9963 and standard deviation of ± 0.0364 and 0.9902 with standard deviation of ± 0.0546 . The measurements show good agreement between measured and expected dose in general. Some patients have a big error, due to respiratory motion and the difficulty of placement the build up cap in PA field, which decreases the SSD and consequently results in a higher dose.

This is higher compared to results found in other institutions ($SD = 2.7\%$ and 3.0% for Leuven and Milan respectively, Table 5.10). To avoid the shadow effect, either the entrance detector or the exit detector should be shifted slightly off the beam axis. Since the exit dose is more sensitive to the position displacement, it is recommended to keep the exit detector on the axis and shift the entrance detector off the axis.

For a dose this small build up cap would have a larger standard deviation. If all 3 fields are considered per treatment the mean is 1% and the standard deviation is 1.9%. This is comparable to the 1.5% S.D. reported by other studies [117].

Table 5.16 illustrates the accuracy obtained from different reported studies in the literature. The results are comparable to our results

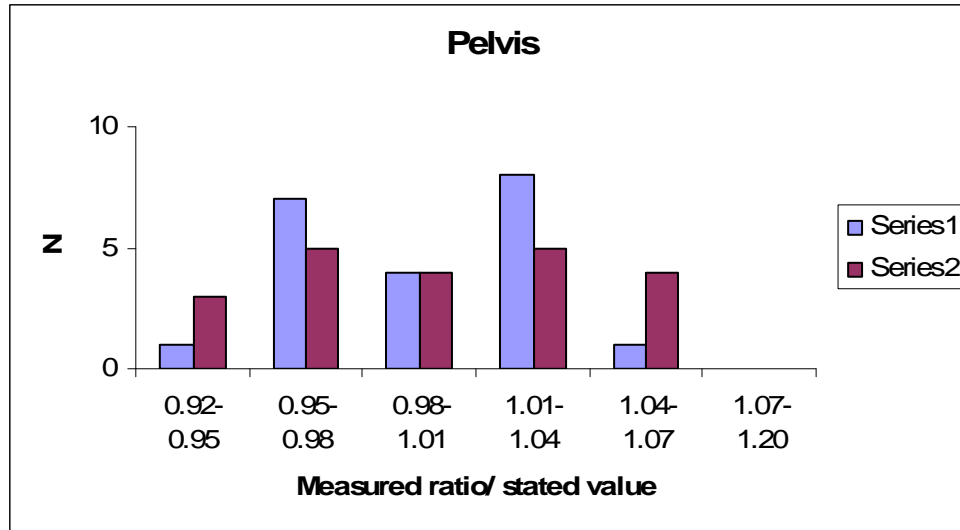


Figure 5.15: Entrance dose ratio for pelvic cancer patients

Table 5.16. Pelvic dose results in some studies in literature (Mean value \pm SD)

Authors	Number of patients	No.setups	Detector	Measurements	Errors >5%
Present study	21	44	TLD	Entrance	0.9963 \pm 0.04
Kalef-Ezra et al[95] *	35	160	TLD (Plexiglas capsule)	PA/AP	1.011 \pm 0.016
	19	80		Lateral	1.009 \pm 0.017
Heukelom et al[129]	11	35	Diode	Entrance	0.9%
Scarantino et al[130]	18	64	MOSFET	Entrance	5-8%
Lanson et al[131]*	27	318	Diodes	Entrance	1.005 \pm 0.013
Fontenla et al [132]	6	-	Diodes	Entrance+Exit	\pm 4

*(Mean value \pm SD).

5.8.5 Thyroid surface dose and cancer risks

Thyroid cancer is one of the least frequent causes of death from cancer. In the general population, it accounts for approximately 1% of the total cancer incidence [133]. The choice of energy also plays an

important role, because lower energies have been shown to result in lower risk for second malignancies [134]. In the case of higher energies, the neutron dose should be included in the calculation of the whole-body dose, because it can contribute an increase of 4% – 10% to the risk for secondary cancer. If lower energies are used, more MUs are required because of the lesser penetrating power of these beams; hence, radiation leakage is increased.

An average thyroid skin dose of 3.7% of the prescribed dose was measured. In order to estimate the total dose delivered over an entire treatment course (50 Gy over 25 fractions). The skin dose overlying the thyroid will be ~1.85 Gy. As far as we know, no available data to convert the surface dose to thyroid dose during radiotherapy.

Previous studies have shown that adjacent organs can receive a dose of radiation from both internal or external scatter as well as machine-dependent leakage when radiation is used to treat cancer [135]

It therefore is of increasing importance to determine the possible carcinogenic effects of RT as a result of scattered radiation among patients with breast carcinoma. Previous studies have focused mainly on the possible increase in the incidence of carcinoma in the contralateral breast due to this scatter [135].

Reda et al [136] measured radiation dose to the left breast during radiotherapy using anthropomorphic phantoms and Monte Carlo calculations. The thyroid dose was estimated to be 0.4% (0.213) Gy of the breast of total dose (50Gy) using cobalt 60. However, to our knowledge no data was available for higher energies. By using the same conversion factor used in a previous study, thyroid dose can be 0.2 Gy of the prescribed dose. The risk for radiotherapy-induced thyroid malignancies can be estimated equal to 2×10^{-5} .

Therefore, such risks should be considered during treatment and certain precautions such as shielding, should be taken to reduce the treatment- related complications.

Fortunately, Age at exposure can modify the effectiveness of radiation to cause cancer; for example, radiogenic thyroid cancer is not apparent among adults exposed after age 20 and radiogenic breast cancer is not seen among women exposed past menopause [135]

In the literature, many studies are published concerning thyroid risk due to head and neck cancer especially in children.

Mazonakis et al [122] estimated the risk of the radiation-induced cancer from treatment of brain tumours in adults and children using a phantom. Thyroid dose was varied between 9.6 to 89.4 cGy depending in the field size and thyroid location. They estimated the excess of relative risk of thyroid cancer irradiation for exposed children to be 0.6 – 14.9 while the adults risk is 0.1-1.1. Mazonakis et al [122] also measured the radiation dose to unshielded thyroid and found it to vary between 2.6 and 4.4% of the prescribed dose depending upon the age of the child. The placement of a couch block reduced the thyroid dose to 1.2– 2.7% of the cranial dose.

In contradicted study Haung et al [135] reported that, there was no significant increase in the risk of thyroid carcinoma in either the radiotherapy cohort or the non- radiotherapy cohort compared with the

general population; therefore, women who have received radiotherapy for breast carcinoma require no special surveillance for their thyroid gland.

Careful consideration should be paid to treatment setup, as collimator orientation and the use of shadow trays with shielding blocks can alter scattered radiation, increasing the thyroid dose significantly. Due to the linear dose response relationship for induction of thyroid cancer at doses exceeding 10 cGy, attention to these steps will result in a significant reduction in the risk of thyroid cancer.

5.8.4 Skin dose and risks

High-energy photon beams, which are used for treating deep-seated tumors, have a skin-sparing effect but are contaminated with secondary electrons. Unacceptable normal tissue reactions remain in many cases and this is the limiting factor for delivering a tumorcidal dose in radiotherapy [25]. Acute radiation reactions typically appear between 10 and 14 days after the commencement of radiotherapy and continue to increase in severity until the completion of treatment [137].

In this study, measurement of skin dose of patients treated for breast cancer was performed using 4 TLDs placed in a plastic film. Skin dose can be measured with better accuracy using extra thin thermoluminescent dosimeters. However, the TLDs were used according to the availability.

The mean skin dose for a breast treatment session was estimated to be 42% of d_{\max} in tangential breast fields. Therefore, the total skin dose delivered over an entire treatment course will be 2 Gy, which is higher than the threshold of erythema. Radiation thresholds are presented in Chapter 2, Table 2.12

These results are similar to findings reported in the literature. Harber et al [138] estimated that 90% of patients treated with radiotherapy for breast cancer would develop a degree of radiation-induced dermatitis (radiation dermatitis). Acute skin reactions can range from mild erythema to moist desquamation in which the dermal injury is severe enough to cause skin slough (Figure 5.16) [139].

Before the development of modern megavoltage x-ray capability, skin toxicity limited the doses that could be safely delivered to the breast. However, the dose of megavoltage x-rays builds up at a depth below the skin [139].

These early effects such as erythema and desquamation usually appear during or immediately after radiotherapy therapy, whereas late effects develop some years afterwards. The acute side effects resolve rapidly without treatment [46, 95]. However, in a substantial group of patients, radiation-induced fibrosis, telangiectasia, and skin pigmentation disorders appear at different times after radiotherapy.



Figure 5.16. A photo skin reactions taken at 6 weeks of treatment [139]

Generally, during the course of radiation sequelae follow a distinct clinical pattern. An erythematous rash can develop on the skin of treated patients within a few hours of exposure and can persist or slowly worsen until the end of radiotherapy treatment.

The severity of skin reactions during and following breast irradiation is influenced by both treatment-related factors and patient-related factors. Treatment-related factors include the fraction size (the dose delivered with each treatment), the total dose delivered, the volume of tissue treated, the type of radiation, and the addition of chemotherapy. Patient-related factors include breast size, axillary lymphocele drainage before treatment (suggesting poor lymphatic drainage), age, and infection of any surgical wound. [103,121,122] A patient's genomic constitution also influences their risk of normal tissue toxicity [138].

5.9 General discussion and conclusions

The use of high Z material build up caps resulted in relatively high TL signal, but no affect was seen on the incidence of supra-linearity or the accuracy of the dose. Accuracy better or equal to $>5\%$ on all measured fields was achieved (Table 5.17). Tissue equivalent material and low Z material gave better results, but the size of the build up cap is not suitable for small fields and high energies. The results also showed that copper and steel are more suitable for in vivo dosimetry of small fields, while aluminum and Plexiglas can be used for large fields with a better accuracy due to their low atomic number but higher perturbation. The perturbation area, a circle of 18 mm diameter of the buildup cap, illustrated that it could be a limiting factor in entrance dose in-vivo dosimetry measurements by underdosing the tumour up to 24%.

Therefore, in agreement with previous suggestions, in vivo measurements of entrance dose can be performed three times during the course of treatment.

In vivo entrance dose results for head and neck, breast abdomen and pelvis are comparable with the previous studies. Our results show lower values than previous studies. This can be attributed to the fact that we measured the dose only, while other studies measured the dose including setup errors, etc. It is important to note that the patient movement or any change on capsule angle can underestimate the dose.

Table 5.17: Summery of the in vivo dosimetry results compared with action levels

Anatomic Region	Results from this study Global dose ratio	No. patients >5%	No. Patients >8%
Head and neck	1.017±0.05	13	3
Breast	1.011±0.04	21	3
Abdomen	1.004±0.04	6	2
Pelvis	0.996±0.04	17	4

The limitations of build up caps are time and effort required to set a calibration, and set the geometrical and physical correction factors. Furthermore, during this work, the TLDs might break or scratch due to friction with the metallic build up cap.

The risk of thyroid dose due to breast cancer is considerable, due to increased life span of cancer patients. Therefore, a suitable protection of the thyroid gland is important and needs to be provided especially for patients receiving radical radiotherapy when young.

Although, the patient risk due to radiotherapy is unavoidable, it is important to ensure that exposure of normal tissue during radiotherapy be kept as low as reasonably achievable (ALARA) consistent with delivering the required dose to the planning target volume (PTV).

6. IN VIVO DOSIMETRY IN LOW ENERGY BEAMS

6.1 *In vivo dosimetry in radiology*

The medical use of ionizing radiation continues to develop and more complex examinations now entail higher exposures. The average annual per caput effective dose is 1.3 mSv in level 1 of health care countries [19].

Council Directive 97/43/Euratom [20] on the health protection of individuals against the dangers of ionizing radiation in relation to medical exposures recognizes these facts and, therefore, requests careful justification and optimization of radiological procedures. The latter means that the requested diagnostic information is obtained at the lowest possible dose. Practical implementation of this principle is only possible when suitable tools, such as diagnostic reference levels for radiological diagnostic examinations, are available. The ethics and research committee at UHL approved this study and informed consent was obtained from all patients prior to the procedure.

The aim of this part is to:

- i. Quantify and evaluate the radiation doses for children and women undergoing Micturating cystourethrography (MCU), Hysterosalpingography (HSG) and Endoscopic retrograde cholangiopancreatography (ERCP) patients according to the protocol used at the Radiology Department.
- ii. Optimise the radiation dose for patients and staff.
- iii. Compare the doses based on available data obtained by other researchers and reference levels recommended by international organizations.
- iv. Evaluate the techniques applied in order to reduce patient and co-patient doses, and staff doses.
- v. Estimate the radiation risk to the sensitive organs, thyroid surface dose for both patients
- vi. Estimate the radiation risk to co-patients and staff.
- vii. To propose a local diagnostic reference level.

6.1.1 Specific radiological procedures:

Radiation doses were measured for frequent procedures and considered as gold standard techniques for some sensitive groups. The first procedure is performed for infants and children. The dose to patients and co-patients was measured during MCU because it is the most frequent examination and represents about 30–50% of all fluoroscopic examinations performed in children [140]. Infants and children constitute 10% of the total number of radiological examinations [18, 19]. Neonates and children are more sensitive to ionizing radiation than adults. The risk of them developing a radiation-induced cancer, hereditary effects or other serious disorders is 2 to 3 times that of adults due to their greater cell proliferation rate and long life span expectancy.

The second procedure, is performed for women in childbearing age, and involves unavoidable radiation dose to the ovaries and genital organs of patient as well as to the staff. It has been estimated that HSG is performed in

90 % of female patients who undergo for infertility consultation. Infertility, which is defined as an inability to conceive after one year of unprotected intercourse, has been estimated to occur in 8-20 % of couples [141,142]. The third procedure is performed for the evaluation of pancreaticobiliary disorders and the treatment of many clinical situations with a high successful rate of up to 90% [143,144]. Gallstones are a common indication for ERCP with 5% to 20 % prevalence in the general population, increasing with age. Considerable radiation doses are delivered to entire patients groups. The examiners have always been required to stand close to the patient in order to oversee the procedure. As a consequence, the unprotected parts by the lead apron (hands, eye lens, thyroid), may receive significant radiation dose from scattered X-rays, which might later translate to tissue reaction (deterministic effects, (cataract)) and cancer/heritable effects (stochastic effects). Although the radiation dose to examiners is very low, no radiation dose can be considered safe. Furthermore this low dose accumulates with time when a high workload coexists [18, 19].

6.1.1.1 MCU

MCU is X-ray examination used to visualize the urethra and urinary bladder that takes place during micturating (voiding). MCU or voiding cystourethrography (VCUG in USA) has been performed since 1914, by Kretschmer to detect the reflux. Urinary tract infection (UTI) is one of the most common sources of infection in children under 5 years of age. UTI incidence during childhood has been estimated to be 8% for girls and 2% for boys. A large number of children may be considered for radiological investigation [142,145]. Vesicoureteric reflux (VUR), the retrograde flow of urine from the bladder to the ureters and renal pelvis, has been identified as the most important risk factor for the development of UTI. The prevalence of VUR has been estimated to be 18-40 % of the child population investigated for their first episode of UTI [145,146]. In uncircumcised boys there is a 10-fold increased incidence [147].

6.1.1.1.1 Investigation procedure:

A standard protocol for MCU was established in order to ensure consistency of performance and application of radiation protection principles. An Ultrasound (U/S) was usually performed of the urinary system before the investigation. 200 ml of contrast medium (50 ml of ionised contrast medium (Ultravist) diluted in 150 ml of normal saline solution (0.9%)) was administered via urethral catheter using a gravity drip. Catheterisation was performed under strict septic conditions: the skin was carefully cleaned with anti septic solution (Bethadine) and then a 6F feeding tube was inserted in the urethra with the help of a sterile anaesthetic gel (Xylocine gel 2%). After urine egression the catheter was advanced a few centimetres more and was secured to the skin surface with tape. The catheter was taped in the left inner thigh of the child, in order to avoid its projection over the male urethra in the lateral views.

Intermittent fluoroscopy was performed with automatically selected kV and mAs exposure parameters to detect VUR or other abnormality. Radiographic images were taken in cases where there was a presence of reflux or of difficulty in evaluating a finding such as air filled intestinal loops obscuring the area of interest.

A fluoroscopic image was obtained before the administration of contrast to ensure the correct position of the catheter (scout view). After contrast administration, the examination has two phases, filling of the bladder and voiding. Fluoroscopic images are taken during early filling of the bladder (valuable in case of ureteroceles and grade 1 reflux that can be obscured by fully filled bladder), and with a full bladder (Figure 6.1).

During voiding, fluoroscopic images of the urethra were taken (in the lateral position for males and supine position for females). Fluoroscopic images of the renal area and the bladder view were taken following voiding (for neurogenic bladder). Most small children (< 1 year) do not empty their bladder completely. Occasionally right of left oblique views were performed. Since VUR is an intermittent phenomenon, filling and voiding of the bladder is repeated at least three times.

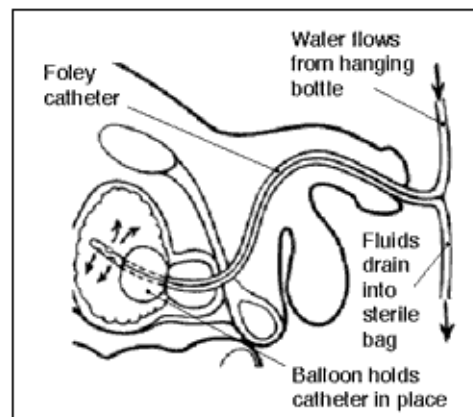


Figure 6.1: *A simple description of MCU procedure*

6.1.1.1.2 Patient dosimetry

A total of 52 children (35 male and 17 female) were examined at UHL, with a mean age of 0.36 years (0.02-2 years), and weight between 2.28 and 16.4 Kg. They were divided into two reference groups: Group 1, newborn (0-6 month) and Group 2, from 6 months to 2 years old. For each patient all the following parameters were recorded: radiographic data (kV, mAs and exposure time), fluoroscopic data (minimum and maximum kV and mA and total screening time) and patient data (name, gender, age, weight, height, date of birth, clinical indication, and radiologist, start and end time). The mean and the range of the patients' physical data and the number of radiographic and fluoroscopic images are presented in Table 6.1. The radiographic and fluoroscopic exposure factors for each age group are shown in Table 6.1 and Table 6.2.

Table 6.1: Number of patients included in the study, the mean and range values of weight, thickness, screening time and number of radiographic and fluoroscopic images.

Age Group	n	Weight (kg) Mean (range)	Height (cm) Mean (range)	Screening time (s) Mean (range)	No. radiographic images Mean (range)	No. fluoroscopic images Mean (range)
Newborn (all)	39	6.0 (2.8-16.4)	61.1 (49-89)	42.7 (24-84)	1.70 (0-6)	6.4 (1-11)
Male	29	5.6 (2.8-10.9)	60.2 (49-82)	42.6 (24-82)	1.60 (0-6)	6.3 (1-11)
Female	10	7.7 (3.4-16.4)	65.7 (51-89)	44.0 (30-84)	1.60 (0-4)	6.5 (3-11)
2 years old (all)	13	8.6 (6.5-11.5)	75.2 (66-80)	46.9 (24-126)	0.66 (0-3)	6.9 (4-10)
Male	6	7.9 (6.5-10.8)	73.6 (66-80)	40.5 (24-48)	0.68 (0-2)	7.3 (5-10)
Female	7	8.9 (7.1-11.5)	76.1 (69-80)	50.6 (24-126)	0.68 (0-3)	6.4 (4-8)

Table 6.2: Exposure factors used for radiography and fluoroscopy during MCU examinations

Age Group	Radiography		Fluoroscopy	
	kVp	mAs	kVp	mA
	Mean (range)	Mean (range)	Mean (range)	Mean (range)
Newborn	70 (65-80)	12.3 (4-21)	59 (40-78)	0.66 (0.1-1.6)
2 years old	75 (70-80)	14 (14-16)	58 (40-77)	0.72 (0.1-1.2)

6.1.1.1.3 Co-patient dosimetry

TLDs were placed on the outside of the lead apron (0.5 mm thick lead equivalent) at the level of left breast towards the child's head. The absorbed dose by the co-patient is calculated using specific software (see chapter 3).



Figure 6.2 a photo explains the patient's position, TLDs locations and co-patient

6.1.1.2 Hysterosalpingography

Hysterosalpingography (HSG), also called uterosalpingography, is an efficient, quick and non-invasive reliable radiologic procedure for evaluating the anatomy of the female genital tract and assessing the function of the fallopian tubes and structural abnormalities that can contribute to infertility [141,142]. Blockage of one or both fallopian tubes causes about 35% of cases of infertility in women. Infertility, which is defined as an inability to conceive after one year of unprotected intercourse, has been estimated to occur in 8-20 % of couples [142]. HSG, which is performed only for diagnostic purposes, can restore fertility due to the passage of the contrast medium under pressure into the tubes via uterine cavity and therefore enhance the fertility [141,142].

6.1.1.2.1 Investigation procedure

HSG was performed by two experienced radiologists, according to a standard protocol in order to ensure the consistency of the performance. In all patients, fluoroscopic digital images were mainly obtained (Figure 1a&b).

The patient was placed in the lithotomy position at the end of the X-ray couch in sterile towels. A scout image was obtained prior to the administration of the contrast solution to ensure the correct position of the cannula and patient preparation. Subsequently, digital images were acquired after each phase of contrast medium injection until the diagnosis was obtained or intraperitoneal spill was documented. Oblique images were acquired only if indicated.

6.1.1.2.2 Patient dose measurement

Thirty-seven patients were included in this study. The main indication for HSG was infertility (97%). i.e. primary infertility (91%) (no previous pregnancy) and secondary infertility (6%)(with previous history of pregnancy) and previous tubal surgery (3%). Findings were normal in 29 of the cases (78.4%). Tubal obstruction was found in 6 patients (16.2%) and uterine adhesions were found in 2 patients (5.4%). This result shows that most of the HSGs were simple without any need for further therapeutic procedures. Patient demographic data (age, weight, Height and BMI), screening time and number of radiographic and fluoroscopic images are presented in Table 6.1.

Patients were divided into two groups according to the digital X-ray machine used. 23 patients were examined in the first machine (A), while 14 patients were examined in the second machine (B). The patients were randomly examined to machines A and B according to availability.

The indications for the investigation that were included, specifically, infertility, follow up after tubal surgery, and women prior to in vitro fertilization. TLDs were packed on a thin envelope made of transparent plastic foil to protect the TLDs from any contamination. Each envelope contained 4 TLDs. Moreover, an envelope was placed directly on the thyroid to measure the TSD. TSD was measured because thyroid is radiosensitive organ and it lies on the surface of the patient. The mean ESD was measured using 4 TLD envelopes placed at the following positions: at the center of the initial field, symphysis pubis and at the mid-point between symphysis pubis and antero-superior iliac spine (ASIS). These positions were selected in order to obtain accurate measurements because the center of the radiation field is not always constant. During the procedure, the TLDs were kept in place with adhesive tape.

For each patient the following parameters were recorded i.e. radiographic data: tube voltage, product of tube current and exposure time, fluoroscopic data: tube voltage, tube current and total screening time and patient data: name, age, weight, height, clinical indication, and radiologist name, start and end time.

Patient demographic data (age, weight, Height and BMI), screening time and number of radiographic and fluoroscopic images are presented in Table 6.1. The radiographic and fluoroscopic exposure factors for each group are also shown in Table 6.3 and 6.4.

Table 6.3: Patient physical characteristics (age, Height, BMI and weight), screening time and number of radiographic and fluoroscopic images. (Mean and the range in the parentheses)

Group	n	Patient age (years)	Height (cm)	Weight (Kg)	BMI (Kg/m ²)	Screening time (second)	No. of radiograph ic	No. of fluoroscopic images
All	3	34.0	165.8	66.3	24.1	18.2	0.2	6.0
	7	(20-43)	(153-178)	(52-85)	(20-31)	(6-66)	(0-1)	(3-9)
A	2	34.2	164.7	66.6	24.5	17.4	0.2	5.3
	3	(20-43)	(153-175)	(52-85)	(20-31)	(12-36)	(0-1)	(3-8)
B	1	29.3	166.3	61.7	22.1	19.3	0.2	7.6
	4	(23-39)	(155-178)	(52-73)	(20.3-30.8)	(6-66)	(0-1)	(6-9)

Table 6.4: The mean and range of the exposure parameters for radiography and fluoroscopy for both machines during HSG examination

Machine	Radiography		Fluoroscopy	
	Tube voltage (kVp)	Current time product (mAs)	Tube voltage (kVp)	Tube current (mA)
A	90 (80-110)	30 (25-45)	80 (70-110)	1.7 (0.8-3.2)
B	85 (80-110)	20 (15-40)	81 (79-84)	1.6 (1.1-2.8)

6.1.1.2.3 Staff dose measurement

An envelope containing TLDs was attached outside the lead apron (0.5 mm Lead equivalent thickness) at the chest level. Protective eyeglasses were worn frequently while the thyroid collar was always worn.

6.1.1.2.4 Endoscopic Retrograde cholangiopancreatography

Endoscopic Retrograde Cholangiopancreatography (ERCP) is considered the gold standard procedure in the evaluation of pancreaticobiliary disorders and the treatment of many clinical situations with a high successful rate of up to 90% [143,144-148]. ERCP was developed in the late 1960's. Gallstones are a common indication for ERCP with 5% to 20 % prevalence in the general population, increasing with age [144]. ERCP has evolved from a diagnostic to an almost exclusively therapeutic procedure after the introduction of new, non invasive imaging techniques, such as magnetic resonance cholangiopancreatography (MRCP), computed tomography (CT) and endoscopic ultrasonography (EUS), which provide diagnostic information that allows the selection of patients for therapeutic ERCP [143].

6.1.1.2. 4.1 ERCP technique

All cases were performed for therapeutic purposes. ERCP was performed with a duodenoscope (Olympus, exera CLE 145(Olympus Medical System Corp, Japan)). Prior procedural antibiotics coverage was usually administered in order to reduce the risk of infection. The patient was placed on an X-ray couch in the left anterior oblique position with right leg flexion. A mouth guard was placed to protect the patient's teeth and the endoscope. A pulse oximeter (NPB-40) with finger clip sensor, or (BCI 3301) hand-held pulse oximeters were used for measurement of functional oxygen saturation of arterial haemoglobin and to monitor the patient's vital signs.

A Buscopan (Eoscine) injection was routinely given intravenously in order to decrease duodenal motility and facilitate visualization. Intravenous sedatives were also administered for comfort and relaxation prior to the procedure (Midazolam / Propofol). Intermittent fluoroscopy was always used for radiation dose optimization. During the procedure, radiographic and fluoroscopic images were obtained after injection of a contrast medium. Since the contrast medium normally remained in the biliary tree for several minutes following removal of the duodenoscope, a post procedure anteroposterior projection was also obtained, if required, for further evaluation of the stent placement or residual stones. The results of the ERCP procedure were classified into three categories: (1) Successful (satisfactory performance and completion of planned therapeutic measures) (2) partial success (the cannulation was successful, but patient condition or other factors did not allow the completion of the procedure) and (3) unsuccessful (failed cannulation).

6.1.1.2.4.2 Patient dose measurement

One hundred and fifty three consecutive ERCP procedures were evaluated, involving 62 males (40.5%) and 91 females (59.5%) for both patient groups. One hundred and eleven patients underwent ERCP in group A, 43 males (38.7%) and 68 females (61.3%). Forty-two patients underwent ERCP in-group B, 19 (45.2%) males and 23 (54.8%) females. Clinical indications for the investigation of ERCP for both groups are presented in Table 6.5.

Table 6.5: ERCP indications

Indications	Group A	Group B	Total	%
CBD stones	66	20	86	56.2
Post operation leakage	5	1	6	3.90
Cholangitis	4	7	11	7.2
Malignancy	22	6	28	18.3
Benign CBD stricture	1	3	4	2.6
Stent removal or exchange	4	2	6	3.9
Pancreatitis	9	3	12	7.8
Total	111	42	153	100

TLDs were packed on a thin envelope made of transparent plastic film, to protect them from any contamination. Each envelope contained 3 TLDs. Three envelopes were used to measure the ESD, exit dose and thyroid surface dose accurately for each patient. It was considered important to determine the exit dose since it reflects the transmission of the radiation and the radiation dose to the anterior organs. During the procedure the TLDs were kept in the required positions and were stuck in place with adhesive tape. The examiners performed the investigations as their daily practice with a protocol that is designed to minimize patient and examiner dose (intermittent fluoroscopy, the fluoroscopic captured images, reduction of radiographic images, well patient positioning prior to procedure and optimum exposure factors).

The data recorded for all procedures included demographic data, tube voltage (kV), tube load (mAs), fluoroscopic data: kV, tube current (mA), total screening time, clinical indication, start and end time.

Patients' demographic data, screening time, number of radiographic and fluoroscopic images, and the procedure duration are presented in Table 6.6. Considerable variations were observed among patient populations in terms of radiation dose, and fluoroscopic time. These variations are due to the different indications, patient characteristics and pathological findings (Table 6.7).

Table 6.6: Patient physical characteristics (age, Height, BMI and weight), screening time and number of radiographic and fluoroscopic images. (Mean and the range in the parentheses)

Age Group	n	Patient age (year)	Height (cm)	Weight (Kg)	BMI (Kg/m ²)	Screening time (minute)	No. of radiographic	Procedure duration (Minutes)
All	153	66.8 (26-91)	165.5 (149-186)	74.6 (47-110)	27.3 (17.9-2.9)	2.9 (0.3-12.3)	2.6 (1-6)	27 (15-55)
A	111	64.9 (26-86)	165.4 (149-186)	74.9 (47-106)	27.5 (17.9-0.6)	2.6 (0.3-12.3)	2.3 (1-5)	25 (15-50)
B	42	71.7 (27-91)	165.6 (150-185)	73.5 (50-110)	26.8 (18.6-2.9)	3.8 (0.7-10)	3.8 (1-6)	30 (20-55)

Table 6.7: The mean and range of the exposure parameters for radiography and fluoroscopy for both patients group.

Group	Radiography		Fluoroscopy	
	KV	mAs	KV	mA
A	84(70-100)	44(12-141)	75(52-110)	1.6(0.4-3.1)
B	80(70-104)	58(10-171)	75(55-110)	2.2(1.3-3.1)

6.1.1.3.4 Examiner dose measurement

Two experienced gastroenterologists in group A and three in group B performed all the procedures. For the first examiner, the radiation dose was monitored at 7 sites: the forehead (eye lens), thyroid, chest, and left hand, waist (left side), back shoulder at the scapula and the left leg. The examiner used a 0.25 mm lead equivalent thick apron, full wrap-around protection (Dr. Goos-Suprema GmbH, Heidelberg, Germany). The second and the third examiners used 0.50 mm lead equivalent thickness, frontal protection (Rheix-srl, Milan, Italy). TLDs were attached outside the lead apron at the chest level and at the left hand side of the second examiner, while for the third examiner; the radiation dose was monitored for the hand, chest, thyroid and forehead. Neither a protective eyeglass nor a thyroid collar was worn by either of the examiners. The examiner radiation dose in gastroenterology departments is routinely monitored by TLD dosimeters.

During the procedure, the first examiner stood on the right side of the typical position of the patient. A lead apron (100 x 60 cm²) of 0.50 mm lead equivalent was placed on the side of the first examiner to reduce radiation scatter to the examiners standing to the side of the fluoroscopy couch.

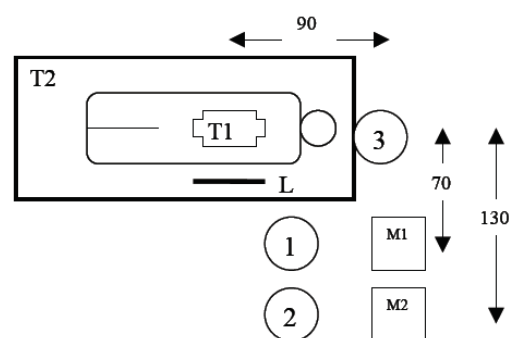


Figure.6.3: Patient setup, lead apron and examiners positions during ERCP examination. 1., first examiner; 2., second examiner; 3., third examiner; M1., endoscopic monitor; M2., fluoroscopic monitor., T1 X ray tube., T2, Table, and L lead apron.

The second examiner, who controlled the radiation exposure, stood on the right side of the first examiner. A fellow stood near the patient head to monitor the patient (group B). All procedures were performed with the examiners at the same locations (Figure 6.3). The nurses remained outside the X-ray room during the exposure; therefore, there was no need for radiation dose measurements for them.

The transmission through 0.25 mm and 0.50 mm lead equivalent aprons was measured with different radiation qualities ranging from 50 kVp to 100 kVp. The aprons were placed in the primary beam and the entrance and exit doses were measured at source surface distance (SSD) of 1 meter using the ionisation chamber (Figure 6.3).

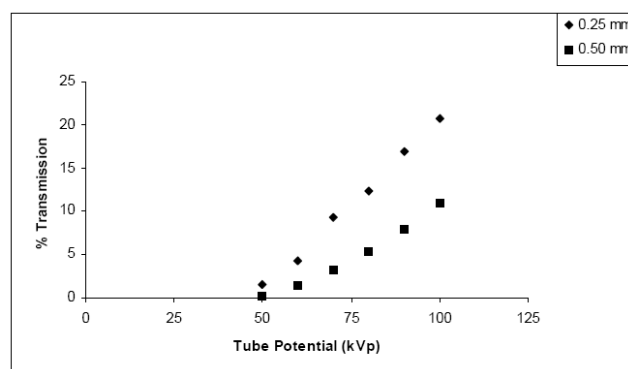


Figure. 6.4: Shows the transmission ratio versus the tube potential (kVp).

6.2 Results and discussion

This part describes results of in vivo dosimetry in radiology for patient and staff.

6.2.1 Micturating cystourethrography

The mean and the range value of ESD obtained by TLD for MCU examination are presented in Table 6.8. The ESD and surface scattered doses to the thyroid, testes, ovaries and co-patient's radiation dose values are also presented in the same table. Radiation dose values varied widely with X-ray tube potential, patient size, source to image receptor distance and filtration applied Table (6.9).

Table 6.8: MCU entrance surface dose and surface dose to the thyroid, testes and co-patient (mGy)

Age group	n	ESD Mean (range)	Thyroid Mean (range)	Testes/ovaries Mean (range)	Co-patient Mean (range)
All patients	52	1.13 (0.37-2.36)	0.15 (0.02-0.53)	0.47 (0.05-1.78)	0.14 (0.03-0.50)
Newborn (All)	39	1.15 (0.37-2.36)	0.15 (0.03-0.35)	0.43 (0.05-1.78)	0.15 (0.03-0.50)
Male	29	1.12 (0.37-2.36)	0.15 (0.03-0.53)	0.36 (0.05-1.52)	0.14 (0.03-0.48)
Female	10	1.28 (0.86-2.21)	0.19 (0.05-0.38)	0.65 (0.13-1.78)	0.21 (0.06-0.50)
2 years old (All)	13	1.18 (0.41-2.05)	0.14 (0.02-0.38)	0.64 (0.14-1.25)	0.13 (0.03-0.27)
Male	6	1.13 (0.55-1.33)	0.15 (0.04-0.38)	0.52 (0.14-1.09)	0.16 (0.03-0.27)
Female	7	1.23 (0.41-2.05)	0.12 (0.02-0.22)	0.75 (0.26-1.25)	0.10 (0.05-0.22)

Table 6.9: Radiation dose to the patients with negative and positive VUR (mGy)

Category	n	ESD Mean (range)	Thyroid Mean (range)	Testes/Ovaries Mean (range)	Co-patient Mean (range)
Positive	11	1.45 (0.57-2.36)	0.22 (0.04-0.53)	0.44 (0.11-1.52)	0.17 (0.03-0.48)
Negative	41	1.05 (0.37-2.21)	0.14 (0.02-0.38)	0.57 (0.05-1.78)	0.14 (0.03-0.50)

The risk probability of radiation induced cancer and the risk of genetic effects for MCU examination; thyroid, ovaries and testes are presented in Table 6.10. The risk coefficients and organ equivalent dose (mSv) values for previous mentioned organs are also presented at the same table. The risks are very small especially when compared with the benefits which accurate diagnosis and treatment can provide.

Table 6.10: Risk estimation for gonads and thyroid. The risk for radiation induced fatal cancer and hereditary effects was taken for whole population for each organ from ICRP 60.

Organ	Organ equivalent dose (mSv)	Risk factor 10^{-2} Sv^{-1}	Risk of malignancy $\times 10^{-7}$	Genetic effect * $\times 10^{-7}$
Thyroid	0.006	0.08	0.04	-
Ovaries	0.44	0.1	4.4	44
Testes	0.33	0.1	3.3	33

*Probability for genetic effects = $1.0 \times 10^{-2} \text{ Sv}^{-1}$ (ICRP 60)

Medical exposures to external radiation are commonly concerned with only limited parts of the body and it is important that operators should be fully aware of the doses to normal tissue in the irradiated fields. Fortunately, tissue-weighting factors for the skin and extremities exist. In addition to this relatively low values for a number of other body tissues means that partial body exposure can result in appreciable equivalent doses to local tissues even though the overall effective dose may be small. Higher considerations are always made when the patients involved are infants and children.

The potential risk from radiation exposure of the patients must be balanced against the diagnostic information. Attention to radiation risk for children has increased in recent years and several studies have been performed in the field of dose calculation and the related risk. [148-155].

Paediatric ESD during MCU depends on patient parameters and exposure factors. Pediatrics physical parameters are subjected to large variations. Although, child size increases with age, individual variations can be great (Table 6.1).

Radiographic exposure factors used in this study ranged from 65 to 80 kVp and from 4 to 16 mAs during the examination. Fluoroscopic applied voltage ranged from 40 to 78 kVp and tube current from 0.1 to 1.6 mA during image acquisition (Table 6.2). The applied voltages of the current study are comparable with the values reported in literature [150,152].

In this study, the mean ESD was 1.13 mGy for the all-patient populations. The mean radiation dose for the newborn group was found to be 1.15 mGy, whereas the mean measured value for the 2 years group was 1.05 mGy (Table 6.8). ESD was lower by 50% compared to other studies. The difference could be due to imaging protocols, equipment and the number of radiographic images per MCU examination. This result indicates that a high degree of patient dose optimisation was achieved in this study. The mean ESD per AP radiographic image ranged between 0.54-0.73 mGy per exposure, which is slightly lower than the corresponding values reported in literature [152, 165,157]. In most non-reflux cases (negative) 45% the patients were examined using only fluoroscopic images.

The mean ESD for patients with positive VUR is 1.45 mGy and for patients with negative VUR is 1.05 mGy (Table 6.9). ESD is higher for patients with positive VUR because the mean number of radiographic images is 2.0, while the mean number of radiographic images is 0.5 for patients with negative VUR, for both sexes.

Estimation of ovarian dose is very important because the ovaries contribute 20 % of the effective dose based on the weighting factor from ICRP 60 [18].

The mean organ equivalent dose was assessed from ESD using NRPB software [43], and was found to be for thyroid, ovaries, and testes, 0.006 mSv, 0.44 mSv and 0.33 mSv, respectively. The surface dose for ovaries (0.7 mGy) and testes (0.47 mGy) is similar to the equivalent dose, while there is a significant difference for the thyroid dose (0.15 mGy) (Table 6.9). This difference can be easily explained since the thyroid is away from the radiation field, while the gonads are always inside the field.

For male patients, the European guidelines for paediatric radiology [159] recommended the use of testicle protective shielding during MCU. The ESD to the gonads is high because most of time they were inside the radiation field.

The mean effective dose per procedure assessed using the same software from NRPB [43] is 0.20 mSv, while in the literature; Shultz et al [156] report a mean effective dose of 0.2 mSv for newborn and 0.4 mSv for 5 years old child. Fotakis et al [152] reported a mean effective dose of 0.91mSv for male and 0.71 mSv for females of the newborn group while the effective doses for a 1-year-old child were 0.89 and 0.83 mSv for male and female, respectively.

The mean co-patient dose was 0.14mGy, with a range 0.03-0.5 mGy. The equivalent doses for thyroid and skin outside the lead apron are estimated to be 0.72 and 0.072 μ Sv respectively. Mantovani & Giroletti [150] reported a mean effective dose to the co-patient of 4 ± 7 μ Sv, while the equivalent doses to the thyroid and eye lens were estimated to be 20 ± 19 μ Gy.

The overcouch X-ray tube is associated with a higher exposure to the hands and eyes of the co-patient compared with an undercouch X ray tube, which produces higher scatter beneath the couch arising from primary beam interactions from the bottom of the couch and patient [160]. Overcouch X-ray machines are

primarily intended for remote operation from the protected control area, or from behind a mobile protective screen. However, overcouch systems generally provide better access to the patient. In our study, this was the only type of equipment available.

The risk, of thyroid, ovaries and testes malignancy and hereditary effects to the children, was both less than 1.0 per million (Table 6.10). The radiation risk per examination was estimated from the effective dose to be 26 per million. Therefore the risk of radiation-induced cancer can be considered to be negligible.

The radiation dose results of this study are appropriate for adoption as local initial DRL values for this technique. Following the recommendations of the European guide [159] and ICRP [18]. We proposed a DRL of 1.7 mGy for ESD based on the third quartile for newborn and children up to 2 years old.

In this study, MCU radiation dose was optimized using mainly fluoroscopic images. The main advantage of this is radiation dose reduction whilst maintaining the same level of VUR detection. The number of diagnosed cases with VUR is 21.15 % and is similar compared to those reported by Mantovani & Giroletti (20%) [150]. The MCU examination technique depends on the co-operation of the co-patient resulting in an increased examination time (20-24 minutes). The increase in examination time is also related to the difficulty in obtaining prompt micturation for children and due to the repetition of bladder filling (this disadvantage is avoided in adults). It is very important that the radiologist who performs this technique has adequate training in paediatric fluoroscopy and MCU procedure.



Figure 6.5 Radiograph of MCU examination with Radiography, illustrates VUR

6.2.2 Hysterosalpingography

The radiographic and fluoroscopic exposure factors for each group are also shown in Table 6.4.

Table 6.11 presents the minimum, median, mean, third quartile and the maximum values of the ESD. The mean and range of thyroid surface dose and staff doses per procedure for both patients groups are presented at the same Table. The mean ESD values received by patients in group B are relatively higher than those for group A. This is due to the X ray machine characteristics and filtration.

Table 6.11. Minimum, median, mean third quartile and maximum values of ESD. The mean and range of TSD and staff radiation doses (mGy) during HSG are also presented.

Group	n	ESD (mGy)						
		Minimum	Media n	Mean	3rd quartile	Maxi mum	TSD Mean (range)	Staff dose
All	37	0.7	3.40	3.60	4.94	8.17	0.17 (0.06-0.51)	0.18 (0.04-0.46)
Group A	23	0.7	3.16	3.30	3.40	6.98	0.19 (0.06-0.51)	0.21 (0.05-0.46)
Group B	14	1.11	4.01	3.90	5.48	8.17	0.14 (0.06-0.14)	0.14 (0.04-0.25)

Table 6.12: The mean patient parameters, number of fluoroscopic and radiographic images, ESD, ovarian dose and effective dose in various studies. The range in is presented in the parenthesis. ND: not detected.

Author	n	Age (year)	BMI (Kg/m ²)	Screening time (second)	No. of Radiogr aphic images	ESD (mGy)	Ovarian dose (mGy)	Effectiv e dose (mSv)
Present study	37	34.0 (20-43)	24.1 (20-31)	18.2 (6-36)	0.2 (0-1)	3.60 (0.7-8.17)	0.91	0.43
Perisinakis et al [168]	78	27 (18-39)	24.8 (17.6-35.8)	20	3.2	9.7±4.2	2.7	1.2
Calicchia et al [162]	37	32 (22-40)	ND	13 (6-30)	6.5 (6-7)	25.2±3.8	4.66	1.95
Gregan et al [163]	21	31.6 (24-39)	ND	15 (5-45)	2 (2-4)	14.6 (1.4-45.7)	3.4	ND
Khouri et al [164]	25	21-45	ND	ND	4-15	12.6 (4.99-36.6)	2.94	ND

Table 6.13 shows the doses for some radiosensitive organs and risk factors probabilities of the radiation induced cancer and hereditary effects from the recent ICRP recommendations (16,17). This group of patient is considered to be on a

higher risk due to the repetition of the exam. Organs and tissues that received relatively high doses are uterus, ovaries and bone marrow. Organ dose equivalent was extrapolated from ESD using Monte Carlo calculation from NRPB (21). The radiation risk for cancer and hereditary effects due to the mean ESD for HSG procedure was estimated to be 24×10^{-6} . The radiation risk for hereditary effects for the future generation was found to be 2×10^{-6} . Furthermore, the radiation risk for ovaries, bladder, bone marrow, uterus and thyroid is shown in Table 6.13

Table 6.13 Mean and range of organ radiation dose (mSv) and radiation risk per HSG procedure.

Organ	Organ equivalent dose (mSv)	Risk factor $\times 10^{-4} \text{Sv}^{-1}$	Cancer probability $\times 10^{-6}$
Ovaries	0.91	16	1.46
Uterus	1.28	6.3	0.81
Bone marrow	0.14	22	0.31
Bladder	1.22	39	4.76
Breast	0.04	116	0.46
Thyroid	0.03	20	0.06

The main factors affecting patient dose in HSG are: exposure factors, filtration, source to surface distance (SSD), collimation, pathology and patient size. There were no significant differences between the two patients groups in terms of height, weight, BMI and number of radiographic and fluoroscopic images. Both excess and low BMI and increased age are associated with infertility in women (1). A correlation was found between ESD and patient weight and BMI (Fig.2a&b). The patients demographic data were comparable to the mean values reported in the literature (142,161-170) and also comparable to NRPB (44) standard phantom used for Monte Carlo modeling. Therefore, the anatomical differences between the two patients groups and the phantom is not significant and did not affect the estimated doses and risks, because the BMI for the phantom is 23.12 kg/m² and for both groups of patients are 24.1.

The mean screening time was estimated to be 18.2 seconds, 17.4 seconds for group A and 12 seconds for the group B as shown in Table 6.3. The mean screening time is less than previously reported studies (161-166). Merkle et al (165) reported that, on average, fluoroscopy contributed 69% of total radiation dose during HSG, using of a computer program permitted accurate differentiation of the dose obtained by fluoroscopy and radiography. Abdullah et al (166) obtained a similar contribution of the fluoroscopy (70-90%) of the total dose. However, Fernandez et al (167) estimated the fluoroscopic contribution to be 26.8% of the total dose. This can be easily understood since they used a mean of 7 radiographic images per procedure. Therefore, reduction of

screening time will reduce the radiation dose significantly since it contributes most of the radiation dose. In addition, selection of low dose fluoroscopic mode also reduces the radiation dose.

The mean radiographic images in this study were 0.2 images. The range was from 0-1 image per procedure and the mean fluoroscopic images were 6 images with a range of 3-9 images. The number of radiographic images is lower compared to various studies in the literature, which ranged between 2 –15 image per procedure (161-165). This value also explains the higher ESD per procedure among previous studies. The number of X-ray images depends on the technique used in various departments. However, this study was designed to use the fluoroscopic image instead of radiologic image in order to reduce the patient and staff radiation dose without significantly affecting the image quality (Fig.1a&b).



Figure. 6.6:Radiographs of HSG examination with fluoroscopy, which illustrates fallopian tubes for A and B machines.

The quality of the radiation depends on the tube voltage and the total filtration of the X-ray beam. X-ray beam filtration in both machines is relatively high compared with other studies in literature, which range between 2.5 mm aluminum [164] and 3.9 mm aluminum [168].

However, the exposure factors (tube voltage and tube current) for both patient groups in this study were comparable as shown in Table 6.4. As expected, correlation was found between applied voltage and patient weight (Fig.2c). The mean exposure factors for both machines are higher than exposure factors reported by Calicchia et al [162], Gregan et al [163] and Khoury et al [164] and comparable to those reported by Perisinakis et al [168].

High tube voltage and low tube current are preferred in fluoroscopy in order to produce reasonable quality images with low patient radiation exposure since increasing of the photons energy results in more penetrating radiation [166].

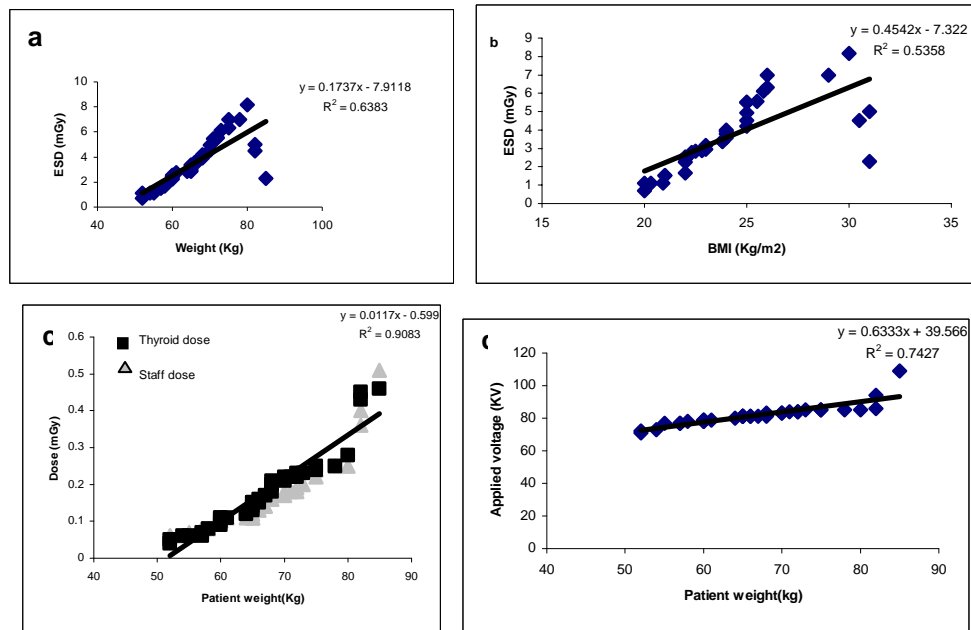


Figure 6.7: correlation between patient weight, BMI, ESD and staff dose. (a) Correlation between patient dose and weigh. (b) Correlation between BMI and ESD.(c) Correlation between patient weight thyroid and staff dose and (d) Correlation between patient weight and applied voltage.

In literature, many attempts were made in order to reduce the radiation dose during HSG. Kushner et al [161] studied the radiation dose reduction using low-mode scanning beam digital imaging system. A mean ESD of 2.2 mGy per image was obtained. The number of images was ranged between 4 to 10 images per procedure. Haussler et al (14) achieved 47% dose reduction when digital images were used with no lack of diagnostic details when compared with conventional 100 mm films. In addition, Abdullah et al [166] made a comparison between conventional and high voltage techniques during HSG using conventional X-ray machine. The results showed that the DAP values for high voltage technique reduced the dose by only 5% and 2.5 % for the effective dose. However, Shultz et al [169] reported that, the implementation of digital radiography for HSG resulted in a reduction of 20% for effective dose when automatic mode was used. An overall reduction of 60 % was achieved by manual selection of higher tube voltage and when lower tube current was used. The previous trials indicate that radiation protection of patient still allows for wide margins of optimization.

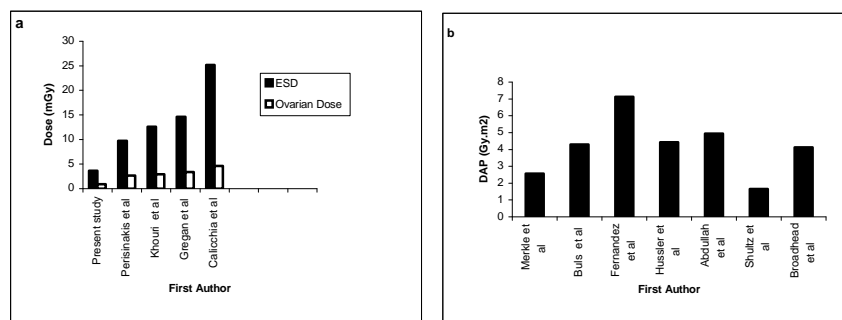


Figure 6.8 (a) A comparison of ESD and ovarian dose for HSG with those published, previously.(b) Comparison of DAP values for HSG for previously published studies

In this study the mean ESD was found to be 3.60 mGy for the total patient population. The mean radiation dose for group A was found to be 3.30 mGy, whereas the mean measured value for group B was 3.90 mGy (Table 6.11). The ESD per procedure depends, among other factors, on the fluoroscopic mode used. Machine B presented 30% higher values than machine A in all fields of views. The mean ESD result for both groups of patients is significantly lower compared to previous studies in literature, which were 3 to 7 times higher (Table 6.12). This result indicates that a high degree on patients' dose optimisation was achieved in this study. However, Gregan et al [163] reported an ESD of 2.5 mGy and 13.5 mGy using digital and conventional X ray machines, respectively. The digital value is lower than this study, but no details were reported about the technique used. Khouri et al [164] measured the ESD during HSG procedure in three different departments. The mean dose for each department was 8.44mGy, 17.36mGy and 31.74mGy. The use of different equipment and protocols by the various departments is sure to have influenced the radiation dose (Table 6.12).

Effective doses were assessed from the ESD value using the NRPB software (44). The mean value of the effective dose for both groups was estimated to be 0.43 mSv. In comparison between effective doses from previous studies, these values are lower. The effective dose value from the literature ranged between 1.2 mSv and 3.1 mSv (162-164).

HSG involves direct irradiation of the pelvic organs; therefore organ doses were estimated for the ovaries, uterus, bladder and bone marrow and to radiosensitive organs such as the thyroid and breast, (Table 6.13). These values are significantly lower than in previous studies (2,6). TSD was estimated by direct placement of the TLDs onto the organ site. A correlation was found between thyroid surface dose and patient weight (Fig.2d). The thyroid dose was found to be 3 times lower than TSD.

Estimation of ovarian dose is very important because all patients are in childbearing age. The mean ovarian dose was estimated at 0.91 mGy (Table 6.13). Comparing this result with the previous data (Table 6.11), it is clear that this study reports the successful reduction of the radiation dose to the ovaries as well as all other dose values. However, the ovarian equivalent dose estimation, which is a good indicator for the expected stochastic risk of the HSG procedure, might contain some uncertainties. These uncertainties are related to the ovaries position, which varied in different patients and in the same patients at different times [161,168]. Kushner et al [161] assessed ovarian dose to be 30% of the ESD during HSG. In present study, ovarian dose was estimated to be 25% of the ESD, which is comparable with previous studies. The results obtained by Perisinakis et al [168] indicated the ovarian dose to be 28% and Gregan et al [163] 23 % of the ESD (Fig.3a). This approximation allows the estimation of the ovarian dose directly from ESD. On the other hand, Calicchia et al [163] estimated the uterus dose to be 5.7 mGy by placing TLDs inside the uterus. Uterus dose was also estimated at 4.03 mGy by Khouri et al [164] and at 4.06 mGy by Buls et al [170], which are also higher than this study.

Staff absorbed doses are principally due to scattered radiation, and leakage from the X ray tube housing. Despite the fact that scatter radiation is only a small fraction of the dose that patient receives, it becomes significant over the working life [18,20,44]. The staff dose for group A (0.21mGy) is relatively higher than group B (0.14mGy) because machine B offered better access to the patient than machine A. The mean ESD for

the staff was measured to be 0.14 mGy per procedure, while eye lens dose and thyroid dose was estimated to be 140 μ Sv, 0.6 μ Sv, respectively. In literature, as far as we know, staff dose was measured only by Buls et al [170] during HSG procedure on an overcouch X ray machine. The ESD for the eye, thyroid and hand of the radiologist was measured by direct placing the TLDs at organ's site. The absorbed dose was found to be 0.22mGy, 0.15 mGy and 0.19 mGy for the eye, thyroid and hand, respectively.

It is important to note that various operators performed HSG in literature. i.e. Radiologists in the present study, gynecologists [170], trainee doctors [164,166] and both radiologists and gynecologists [163]. However, HSG is operator dependent and the mean screening time was observed to be higher when gynecologist (58 seconds) [170] and trainee doctors (119 seconds) [166] performed the examination. Generally, Gynecologists and trainee doctors are not fully trained in radiation protection (clinically directing) while radiologists are physically directing, i.e. well trained in radiation protection [153].

The use of an over couch X ray tube increases the scatter dose to the face, neck and the upper parts of the body, while undercouch X ray tube have higher exposure to the legs and lower parts of abdomen. Staff dose is very low under protective shielding, since the radiologists wear lead aprons with 0.5 mm lead equivalent with transmission 3.2% at 100 tube voltage and 0.36% at 70 tube voltages [171].

Radiation risk estimation for fatal cancer and hereditary effects per procedure was found to be 24×10^{-6} while the hereditary risk is estimated to be 2×10^{-6} . This risk is lower than the risk estimated by Perisinakis et al [168]. They estimated a risk of radiation induced cancer between 145×10^{-6} to 86×10^{-6} . Using aged related risk factors, they also estimated the hereditary effect per procedure to be 27×10^{-6} . To obtain a reasonable assessment of radiological risk for the patient, account should be taken of the irradiation of all the radiosensitive organs of the body.

The estimated risk values for the uterus offer a better understanding of the radiation dose for the fetus and associated risks, because the reported prevalence of unexpected pregnancy during HSG is 0.6% [172] The radiation risk per HSG procedure for the radiologist is negligible. Further dose reduction could be achieved by wearing protective eyeglasses and thyroid shields which significantly attenuate scatter radiation.

Despite these problems and the uncertainties involved, the estimation of the probability of radiation-induced cancers is needed for use in radiation protection to increase the awareness of medical personnel.

Both the hereditary and somatic risks of diagnostic X-ray exposure are enhanced when the average patient age is lower, i.e. the younger the patient has higher child expectancy and a longer subsequent life expectancy [167,173]. Generally, the risk of tissue reactions is very small compared with the benefit of the examination. This allows a good safety margins for patient to proceed with further infertility investigations if needed, without significant risk.

Our study protocol was designed to use intermittent fluoroscopy with fluoroscopic image with last image hold to minimize exposures. Radiographic images were taken in cases that were not possible to evaluate a finding. Murase et al [174] noted that fluoroscopic images are adequate for detecting the tubal patency, although these images generally have inferior image quality compared with radiography. Patient radiation dose reduction was achieved in this study by using the fluoroscopic image technique, higher X ray machine filtration, precise

collimation of the radiation beam and radiologist experience. Further dose and screening time reductions were observed when the number of procedures increased. Techniques used for optimization of image quality to meet clinical requirements allow patient dose reduction without the loss of diagnostic accuracy, and are therefore of great interest (Fig.1a&b).

The advantage of these techniques is the dose reduction up to 3 times less than the reported in aforementioned studies. This reduction also reduces the risk of the tissue reactions and offer further margins for further investigations and follows up. The disadvantage of this technique is that it needs a good level of clinical experience. Nevertheless, it is still advisable to avoid radiation exposure where possible for both patient and staff, by other alternatives, i.e., laparoscopy, hysteroscopy, transvaginal, sonography and magnetic resonance imaging (MRI) when equivalent information can be obtained.

DRLs can be used to verify the practices for typical examinations for groups of standardized patients in order to ensure that the dose should not be exceeded in normal practice without adequate justification (6). Nevertheless, the available data is still not enough to establish national reference levels, but this could be a baseline for further studies concerning dose optimisation.

To the best of our knowledge, no values have been proposed to date for ESD during HSG procedure, while Broadhead et al [175] proposed a DAP value of 4.12 Gy.cm^2 . Therefore, a third quartile value of 4.94 mGy for ESD and 1.0 radiographic image associated with screening time of 30 seconds can be used as DRL in a local basis for HSG procedure.

6.2.3 Endoscopic Retrograde cholangiopancreatography

A total of 153 ERCP procedures were performed over 5 months. The total number of successful procedures was for 142 patients (93.5%) for both groups. In group A, the ERCP procedure was successful in 106 patients (95.5%), 2 procedures were partially successful (1.8%) and 3 procedures were unsuccessful (2.7%). Similarly, in group B, the procedure was successful in 38 patients (90.5%) and 4 procedures were partially successful. The above results lie within the range for successful procedures [143,144]. Patients' demographic data, screening time, number of radiographic and fluoroscopic images, and the procedure duration are presented in Table 6.3. Considerable variations were observed among patient populations in terms of radiation dose, and fluoroscopic time. These variations are due to the different indications, patient characteristics and pathological findings.

Although the vast majority of patients were elderly, it is interesting to note that 14% of patients in this study were below 50 years. Radiation risk may be significant for this age group. The mean exposure factors used during fluoroscopy screening and (radiography) image acquisition for both groups are shown in Table 6.6. The patient characteristics and exposure factors are comparable for both groups.

Table 6.11 presents the ESD (mGy) values for both patients groups. This data shows asymmetry in distribution. The mean, median, minimum, third quartile and the maximum values are presented. The ESD for

group A is 15% lower than group B. This can be attributed to inter-examiner differences, since the examiners were using the same X-ray machine.



Figure. 6.9: Radiographs of HSG examination with fluoroscopy, which illustrates fallopian tubes for A and B machines.

Table 6.14. Minimum, median, mean third quartile and maximum values of ESD. The mean and range of TSD and staff radiation doses (mGy)

Patient group	n	Mean	Minimum	Median	3rd quartile	Maximum
All	153	68.75	10.17	44.79	86.81	289.1
Group A	111	65.89	10.17	36.77	74.59	277.1
Group B	42	77.4	14.44	59.41	88.81	289.1
Exit dose	153	3.45	0.19	1.76	5.89	14.91
Group A	111	2.43	0.19	1.56	4.32	32.27
Group B	42	4.56	0.49	2.18	6.48	44.91
TSD	153	0.67	0.10	0.46	0.89	5.03
Group A	111	0.55	0.06	0.34	0.67	3.56
Group B	42	0.82	0.10	0.57	1.04	5.03

The mean transmission ratio between ESD and exit dose is 5%. Exit dose value is higher compared to the values range in diagnostic radiology. However this results can be explained by the patient position, which changes from prone, oblique or lateral. The examiners dose (μGy) per procedure for both groups is presented in Table 6.15. The dose values received by both groups are comparable. The higher doses were for the waist and the shoulder, because the source of the scatter radiation is behind the examiner and also the attached lead apron does not reach the X-ray couch, so a considerable amount of stray radiation is expected. Table 6.17 shows the estimated organ dose using the conversion factors from NRPB software [44], risk factors from ICRP [87,88] and the estimated risk values.

Table 6.15: Minimum, Mean, median, third quartile and maximum values of staff radiation doses (μGy) both groups

First examiner	Group	n	Minimum	Mean	Median	3rd quartile	Maximum
Chest	All	153	0.2	6.2	3.6	6.6	32.5
	A	111	0.2	6.1	3.5	6.6	32.5
	B	42	1.1	6.4	3.6	7.1	30.1
Thyroid	All	153	0.2	5.40	2.9	5.6	27.6
	A	111	0.2	5.40	3.8	6.7	27.6
	B	42	1.03	5.52	2.6	5.6	26.1
Forehead	All	153	0.2	3.81	2.4	6.6	26.3
	A	111	0.2	3.51	2.2	6.6	26.3
	B	42	0.7	4.45	3.2	3.9	21.0
Hand	All	153	1.02	27.2	13.8	53.1	223.2
	A	111	1.02	27.3	21.4	49.2	223.2
	B	42	2.9	26.9	21.3	49.3	171.5
Back shoulder	All	85	0.70	38.7	59.1	54.1	282.3
	A	61	0.70	60.1	35.6	56.1	282.3
	B	36	1.25	39.3	42.1	52.3	191.2
Waist	All	85	13.6	100.5	77.8	120.9	381.3
	A	61	13.6	101.2	79.1	123.5	381.3
	B	36	14.7	99.5	54.38	113.7	291.0
Leg	All	54	0.20	1.60	3.50	8.20	17.10
	A	30	0.20	1.50	3.80	6.40	15.90
	B	24	0.20	2.00	4.20	10.0	17.10
Second examiner							
Chest	All	153	0.2	3.2	2.1	3.4	17.3
	A	111	0.2	2.5	2.1	3.9	17.3
	B	42	1.1	5.1	1.7	2.6	15.8
Hand	All	153	0.2	7.2	3.2	12.2	32.5
	A	111	0.2	8.4	3.6	12.3	32.5
	B	42	0.2	4.3	2.6	10.3	25.8
Third examiner							
Chest	B	24	12.8	72	106	301	429.1
Thyroid	B	24	16.1	63	108	243	382.1
Forehead	B	24	13.4	65	114	242	317.8
Hand	B	24	32.1	162	259	421	739.5

Table 6.16 provides an estimation of the cancer risks associated with the organ dose. Not surprisingly, the pancreas had the highest dose due to its position always inside the radiation field. The risk of radiation-induced cancer for different organs was in the magnitude of 10^{-5} and 10^{-6} per procedure, whilst the annual examiner risk was in the magnitude of 10^{-3} and 10^{-4} .

Table 6.17: Mean organ radiation equivalent dose (mSv), risk factors and radiation risk per ERCP procedure.

Organ	Organ equivalent dose (mSv)	Risk Factor $\times 10^{-4}\text{Sv}^{-1}$	Cancer probability $\times 10^{-6}$
Ovaries	1.29	16	2
Uterus	1.42	6.3	1
Breast	0.28	116	3.2
Red bone marrow	0.91	23*	2.1
Pancreas	8.52	6.3	5.4
Bladder	0.36	39.5*	1.4
Spleen	4.78	6.3	3
Lung	0.83	129*	10.7
Skin	1.91	670	128
Effective dose	3.44	550	190

* Gender average value

This part of the study is intended to optimize and provide a detailed evaluation of radiation dose during ERCP and to analyse factors that might affect the radiation dose for both examiners and patients. Since techniques and equipment influence patient dose, fluoroscopy time and the number of images, and exposure factors were evaluated.

In comparison with patient characteristics obtained by other studies [176-178], this study showed no significant differences between the two patients groups in terms of height, weight, BMI and number of radiographic and fluoroscopic images (Table 6.7). The patient demographic data were comparable to the mean values reported in the literature [176,178,179,180] and these values were higher compared to those of the NRPB standard phantom [44]. In general, variations in BMI and exposure factors influence the patient dose and image contrast.

The mean screening time (2.9 minutes) as shown in Table 6.7, was less than that previously reported, which ranged between 6 to 14 minutes [176,178,179,180]. The total fluoroscopic time is a good indicator for the radiation dose to both patients and examiners. It is important to note that; Larkin et al [176], Singhal et al [181] and Buls et al [178] estimated that fluoroscopic exposure contributes 90% of patient total dose during ERCP. In agreement with the aforementioned studies, strong correlation was found between the ESD and screening time ($R^2=0.91$). Therefore, fluoroscopic time can be a good indicator of dose if radiographic images are controlled. Uradomo et al [182] achieved a reduction in screening time of 10% with pulsed fluoroscopy (5.2 minutes), which was adjusted to terminate the exposure in 3 seconds, compared to continuous fluoroscopy (4.7 minutes), while Singhal et al [181] reported a mean screening time of 1.6 minutes in 247 therapeutic ERCP. Unfortunately, they did not report the number of films taken.

The exposure factors (kVp, mA) for both patient groups were comparable to exposure factors reported in previous studies [176,178,179,180]. In general, High kVp increases the scatter radiation thus also the examiners dose, while decreasing the contrast of the image [174]. Consequently, Heyd et al [183] reported that, a high kVp technique (80 kVp -100 kVp) could reduce the dose to a patient up to 50%, compared to the conventional technique (75 kVp -96 kVp). The mean number of radiographs in this study was 2.6 per procedure, which is also lower than in previous studies [176,178,179,180,183]. As expected, no significant correlation was found between patient dose, demographic characteristics, and exposure factors, but it should be noted that dose does depend on the complexity of the procedure. Storing fluoroscopic images could reduce the number of radiographs; this may decrease the image quality but not the yield of the procedure. Selection of the low dose fluoroscopic mode and good patient positioning prior to the procedure could also reduce the radiation dose. Moreover, adequate filtration of an x-ray beam can substantially reduce patient dose up to 70% by improving the quality of the beam whilst largely maintaining adequate image quality [184]. The filtration of our machine (4.0 mm Al) was higher than that used in other studies (Buls et al [178] 2.9 mm AL and Tsalaftoutas et al [179] 3.5 mm Al). Therefore, a significant radiation dose reduction can be achieved by optimizing the aforementioned factors.

In this study, the mean ESD, resulting from an ERCP procedure has been estimated to be 68.89 mGy for the total patient population. The mean ESD for group A was 65.89 mGy, whereas the mean measured value for group B was 77.4 mGy (Table 6.14). Examiner A has a lower dose by 15% compared to examiner B, which reflect the high degree of optimization. The mean ESD result for both groups of patients was significantly lower compared to previous studies for therapeutic ERCP (Table 6.18). However, the majority of the previous studies were mainly for dose surveys [76,178,179,180] and examiner protection [177,178,180]. Heyd et al [183] reported the highest ESD (733 mGy), number of radiographs (16 radiographs) and screening time (14 minutes). Our results are 60% lower than the lowest value (178.9 mGy) [178] of the reported studies. In addition, continuous considerable radiation dose reduction was observed concerning the recent published studies compared to the previous ones. This result indicates that a high degree of patient dose optimisation was achieved in the present study. This could be attributed to the presence of two experienced gastroenterologists, offering quick interpretation and decision-making, and to the low screening time, fluoroscopic captured images

and radiographs reduction. Interpretation of an image can produce a dilemma for the first examiner whose attention is divided between endoscopic and fluoroscopic monitors and patient [185] The first examiner always concentrates on the endoscopic screen, whilst the second one monitors the fluoroscopic screen and controls the radiation. Conversely, Buls et al [178] reported that the communication problem between the gastroenterologist and the radiographer affects the radiation dose.

Effective dose enables us to evaluate the expected risk from the procedure and make a comparison between different studies using different dose descriptors (TLD, Dose Area Product (DAP), or IC). The mean value of the effective dose for both groups was estimated to be 3.44 mSv.

As ERCP involves direct irradiation of some of the internal and radiosensitive organs, equivalent doses for specific organs were estimated as shown in Table 6.19. In comparison with Buls et al [178], the radiation organ doses were also significantly lower. TSD was estimated by direct placement of the TLDs to organ site. Ovary dose, which has special concern due to the hereditary effect of radiation, was estimated to be 1.29 mGy while testis dose was negligible. The exit dose value was much higher than estimated dose values for the breast, while it was slightly higher than total skin dose.

Previous authors have used different values of conversion factors to derive effective dose from ESD. Buls et al [178] ($0.0.03 \text{ mSv.mGy}^{-1}$) used NRPB software [44] whereas Tsalafoutas et al [179] ($0.0.05 \text{ mSv.mGy}^{-1}$) used a mean value derived from the conversion factors between the two studies [176, 179], which is similar to our result. These variations could be attributed to the X-ray machine characteristics and to projections used to derive the effective dose from ESD. However, it offers a good and simple indicator of the effective dose estimation.

Variation of patient dose is in general due to differences in the protocols and exposure factors, X-ray equipment, patient pathology, field of view, geometry and examiners experience.

In this study, the protocol was designed to use intermittent fluoroscopy with fluoroscopic image with last image hold to minimize exposures significantly without compromising clinical outcome. Even if these images generally have inferior image quality compared with radiography, they still contain the required information for diagnosis. This reduction also reduces the risk of the radiation effects and offers further margins for further investigations and follow-ups especially for young and pregnant patients.

The measured examiner dose (μGy) for both groups is comparable as presented in Table 6.15. As expected, the first examiner was more exposed than the second one, while the radiation dose for the fellow was the highest because no protective shield was used in that direction and he was always facing the primary beam. The back shoulder and the waist were points of the highest dose for the first examiner, because these parts are always facing the source of the scatter radiation, although it can be considered not detrimental because they are protected by a lead apron and no radiosensitive organs are involved. The use of full wrap-around apron is more effective due to the full coverage of the back and waist area, than the frontal protection one. It should be noted that, the radiation dose for the first examiner was measured for 5 procedures without a protective shield. The mean and the range for waist and shoulder doses were measured to be 775.8 (387-1681) μGy and 615(229-1518) μGy , respectively. Conversely, the examiner's chest and thyroid dose has a lesser increment since the examiners are always concentrating on the fluoroscopic monitor during the screening. A dosimeter worn at the

front side will not appropriately assess the effective dose. Also in cases of partial body exposures the reading of a personal dosimeter may not provide a representative value for the assessment of effective dose. Therefore, the current effective dose estimation method is underestimating the dose, since the TLD should be placed on areas of the body with the highest exposure rate [87, 88,185].

Table 6.18: The mean patient parameters, screening time, number of radiographic images, ESD and effective dose in various therapeutic studies (range is in parenthesis).

Author	n	Age (year)	BMI (Kg/m ²)	Screening time (Minutes)	No. of Radiograph ic images	DAP Gy.cm ²	ESD (mGy)	Effective dose (mSv)
Present study	153	66.8 (26-91)	27.3 (17.9-42.9)	2.9 (0.3-12.3)	2.6 (1-6)	NR	68.75	3.44
Larkin et al [176]	12	74.8 (60-89)	NR	10.5 (5.9-16.6)	3.7	66.8	NR	12.4
Tsalafoutas et al [179]	21	66 34-92)	NR	6 (1.3-23.5)	2.9 (2-4)	41.8	178.9	8.7
Heyd et al [183]*	72	53.6 (20.6- 86.5)	26.11 (17.5-61)	14 (2-63)	16 (6-45)	NR	80	NR
Chen et al [180]	12	60 (22-89)	NR	5.9	4	NR	262	NR
Buls et al [178]	54	66.5 (41.5-81)	NR	6	4	49.9	347	9.9
Singhal et al [181]	247	NR	NR	1.38	NR	8.1	NR	NR

NR: not reported

* Diagnostic procedures

Table 6.19. The mean radiation doses for the first examiner during ERCP procedure (mGy).

First examiner	Hand	Thyroid	Eye lens	Chest	No. of Film	Exposure time (min)	X-ray tube location
Present study	0.027	0.005	0.003	0.006	2.6	2.9	Overcouch
Buls et al [178]	0.64	0.45	0.55	nd	4	6	Overcouch
Chen et al [180]*	NR	NR	NR	0.0003	4	5.9	Overcouch
Heyd et al [183]	NR	NR	NR	0.0007	17	13.6	Undercouch
Naidu et al[177]**	NR	0.2	0.04	NR	4.6	5.97	Overcouch
Johlin et al[186] ♣	NR	NR	NR	1.3	NR	60	Undercouch

♣Phantom study

*1 meter from the patient (1 R=0.087 mGy).

** Extrapolated from annual effective dose (mSv) for 400 procedures per year. NR: not reported

The mean radiation dose to the unprotected parts was higher for the hand (27.2 μ Gy) due to the stray radiation from the protective barrier (lead apron). As expected, the mean thyroid dose (5.40 μ Gy) was higher than the eye lens (3.81 μ Gy) because the thyroid is near to the field scatter radiation, while the lowest dose was seen for the leg (1.60 μ Gy), Table 6.15. It is clearly considered that the radiation dose inside the lead apron is insignificant and the examiners are adequately protected. Transmissions through the lead apron (0.25 mm and 0.50 mm lead equivalent) were 12.6 % and 5% at 80 kVp respectively, which was determined experimentally. Since scatter radiation is considered a very low energy, there could be even less transmission through the apron. However, in the current study the effective dose per procedure was estimated to be 2.04 μ Sv 1.0 μ Sv and 7.14 μ Sv, for the first, second and third examiners respectively. In agreement with Johlin et al [186], the third examiner receives higher dose because he always facing the radiation source. In contrast with Heyd et al [183] and Buls et al [178], the third examiner received a higher dose than the first one. Buls et al [178] reported the mean second examiner (nurse) doses as 260 μ Gy, 200 μ Gy and 270 μ Gy for eye, neck (thyroid) and hand, respectively. The third examiner dose was higher up to 25% more than that for the second one. A lower value was reported by Chen et al [180] 0.1 μ Gy for the third examiner without protection barrier. In a phantom study, Johlin et al [186] estimated the dose to examiners during 1 hour of fluoroscopy at 1 meter. The dose to the first, second and third examiner was 13 μ Gy, 12 μ Gy and 270 μ Gy, respectively. A reduction of dose up to 95% was obtained with rubberized 0.50 mm equivalent lead shield.

Dose differences to examiners can be explained in the light of patient dose differences, examiners location and the utility of radiation barriers. Phantom results are higher due to use of prolonged fluoroscopic exposure. Nevertheless, regarding the dose limits, examiners can perform over 1000 procedures annually without exceeding the limits [6] (20 mSv per year).

It is worth noting that, if we used the mean hand dose (tissue reactions) as a reference value, the equivalent dose would exceed the limits (500 mSv/year) in 20,000 procedures, whilst for the eye lens the dose would exceed the limits (150 mSv/year) in 40,000 the procedures. Assuming that each examiner could perform 500 procedures throughout the year, the annual effective doses are 1.02 mSv, 0.50 mSv and 3.57 mSv for the first, second and third examiners, respectively.

Published data have shown higher dose values (mGy) for the first examiners chest and unprotected thyroid, hand and eye lens compared with this study as shown in Table 6.19. The absorbed dose for gastroenterologists and the two assistants was significantly higher compared to our results. Limitation of staff number (group A) and adequate training in radiation protection is essential. Therefore, a greater need for further protection seems justified. We recommend the use of thyroid shield, and an additional barrier to protect the third examiner. Although, it might not offer good access to the patient, the risk of radiation due to chronic exposure must be considered.

The effect of radiation dose differs widely between cases of exposure over a short time (acute irradiation-patient) and those of slow and steady irradiation extended over a long period of time (chronic irradiation-examiners) [6]. However, in this study, the patient radiation risk estimation for fatal cancer per procedure was found to be 19×10^{-5} while the female hereditary risk was estimated to be negligible (1×10^{-8}). Larkin et al [176] and Nidu et al [177] estimated the risk of radiation-induced cancer between 1 in 1700 (3×10^{-4}) to 1 in 3500 (6×10^{-4}) per procedure. The annual radiogenic risk to examiners in this study (500 procedures/year) was estimated to be 56×10^{-6} , 28×10^{-6} and 196×10^{-6} for the first, second and third examiners, respectively. The probability of cancer due to radiation dose depends on organ dose, age and tissue weighting factor, which represent the relative contribution of that organ or tissue to these effects. Radiation induced cancer probability is shown in Table 6.17. Generally, the risk of cancer is very small compared with the benefit of the examination.

From previous studies, we can conclude that the radiation risk per ERCP procedure for the gastroenterologist can be significant especially in the busy departments for both patients and examiners unless optimization and dose reduction methods are applied. Further dose reduction can be achieved by wearing the protective eyeglasses and thyroid shields that significantly attenuate scatter radiation. However, the examiners believe that the use of lead glasses impairs vision and so increases the exposure time and that lead gloves are inconvenient for the first and the second examiners. Avoidance of unnecessary exposure is the best way to reduce the radiation risk.

Reference dose levels may be used to verify the practices for typical examinations, for groups of standardized patients, in order to ensure that the dose is not exceeded in normal practice without adequate justification [18,20]. However, a reference dose for Therapeutic ERCP is complicated. The duration and complexity of the

fluoroscopic exposure is strongly dependent on the individual clinical conditions. Usually, procedures are clinically open-ended, continuing until the procedure is complete.

However, the observed distribution of patient doses in this study is very broad (Table 6.6. Dose reference levels are not applicable to the management of tissue reaction risks from fluoroscopically guided interventional procedures. The objective is to avoid tissue reaction effects in individual patients undergoing justified, but long and complex procedures [6].

Therefore, we propose a local reference dose level by using the 3rd quartile value (86.81 mGy associated with 2 radiographs and 3.5 minutes screening time) as shown in the Tables 6.6 & 6.7, as a first step towards dose optimisation. The available data is still not enough to establish dose reference levels, but this could be a baseline for further studies concerning the optimisation of dose with regard to avoiding unnecessary cancer/heritable risks.

6.3 Conclusion

The results of this study provide valuable data for establishing reference dose levels for previous examinations by a direct method using TLDs. However, additional measurements are necessary to improve the technique and the statistical information by including children of other age groups. Fluoroscopic captured image technique accompanied by reduced number of images has the lowest radiation dose without compromising the diagnostic findings. The radiation risks associated with staff and co-patient are negligible. The data presented in this work showed our doses to be lower by approximately up to three times lower compared to the lower mean values presented in the literature. We recommend fluoroscopic images technique is adequate to reduce the radiation dose to the patient. In agreement with published studies our study showed that ovarian dose to be equal to 25% of ESD. The unnecessary radiation detriment can be reduced significantly during ERCP by the presence of two experienced examiners. The radiation dose to the examiners is well within established safety limits, in light of the current practice. Furthermore, the first examiner should put on a lead wrap-around protective apron, since he is not facing the scattered radiation. We believe that the available formulae to evaluate effective dose to examiners underestimates the effective dose for ERCP examiners. The results encourage examiners for further dose optimisation. Additional studies need to be conducted in order to establish reference dose levels for patients and effective dose estimation for examiners involved in radiologic procedures.

General conclusion

In vivo dose measurements provide an estimate of the dose received by the patient during radiotherapy. For entrance dose measurements, the TLDs are enclosed with a high-density material build-up cap to enable measurements at a depth, corresponding to the build-up depth of the photon beam quality in use. The build-up caps of the TLDs perturb the radiation beam, but their effect is limited as the in vivo measurements are repeated only three times in maximum. The perturbation value can reach up to 20% of the Dmax. Kalef-Ezra et al proposed deliver of 50 cGy to the patient to verify the entrance dose, and then remove the detector to continue the treatment session. This is an excellent solution to overcome the perturbation issue, although it will increase the time required for in vivo dosimetry.

By means of an IC at depth of build-up in a Plexiglas phantom, correction factors for various non-reference conditions were derived to verify if the build-up cap is of suitable thickness.

In vivo entrance dose measurements have been performed in our radiotherapy department in order to test the build up caps and corresponding entrance dose determination methodology at the patient level.

Regarding the in vivo study in the radiotherapy department of UH Larissa it was in only 10 out of the 69 patients where the absorbed entrance dose deviated more than $\pm 5\%$ from the prescribed dose. It is worth noting that, some of the poor dosimetric results reflect deficiencies in the build up placement in the patient or TLD placement inside the build up caps.

High Z material Build up caps are useful and feasible to perform in vivo dosimetry with TLDs and this methodology is ready to be applied by Kalef-Ezra [95]. The limitations of build up caps are time and efforts need to set a calibration, geometrical and physical correction factors. Further more, during this work, the TLD might break or scratch due to the friction with metallic build up cap.

Patients undergoing radiological procedures receive significant radiation doses due to the complexity of such procedures and the amount of diagnostic information required to evaluate the pathologic findings. The median values for the recorded surface doses to the patients ranged between 1.13 mGy for paediatric patients up to 68.9 mGy for ERCP patients. None of the patients exceeded the dose taken to be the threshold surface dose (2 Gy) for deterministic injuries of the skin. Most of the surface dose was contributed by radiographic acquisitions, which accounted for the 60% of the total dose. Fluoroscopy contributed only 40% to the total surface dose.

Using the recent risk coefficient from ICRP [18, 19], the effective doses computed in this study can be converted to a stochastic detriment. In general, these stochastic risks are low compared to the life saving benefits the patients receive by undergoing radiographic procedures.

The fact that stochastic risks associated with children are higher than the risks associated with adults requires that we should focus our attention to reducing doses to pediatric patients undergoing MCU procedures.

The results of this study provide valuable data for dose optimisation and establishing reference dose levels for the mentioned examinations by a direct method using TLDs. However, additional measurements are necessary to improve the technique and the statistical information by including patients from different hospitals in order to

establish national reference levels. Fluoroscopic captured image techniques accompanied by reduced number of images results in the lowest radiation dose without compromising the capability of the diagnostic findings. However, some dose reduction does affect image quality, thus it is important not just to reduce doses but also to optimise each imaging technique, maximizing its efficiency and determine the right balance between dose and image quality.

The radiation risks associated with staff and co-patient are negligible. Although the radiation dose to examiners is very low, no radiation dose can be considered safe and in addition it is accumulated when a high workload coexists.

The data presented in this work showed our doses to be lower by approximately 50% to 300% compared to the lower mean values presented in the literature.

Future work

This project is complete for photons with high build up caps, electrons could be investigated for different build up caps materials and the design can be improved in order to be more convenient for mail dosimetry. Exit dose and midline dose is also recommended. Further studies are needed to improve the results for different energies. In radiology applications, it is clear that a lot of radiographic examinations and interventional procedures need to be optimized by introducing DRL and by encouraging staff to concentrate on more dose reduction. Further studies are required for CT scanning and interventional radiology for both patients and staff.

References

1. Committee on the biological effects of ionizing radiation (BIER V). Health effects of exposure to low levels of ionizing radiation. Washington, DC: National Academy Press, 1990.
2. Ulrich H. The incidence of leukemia in radiologists. *New England Journal of medicine* 1946; 234:45-46.
3. IARC monographs on the evaluation of carcinogenic risks to humans. Ionizing radiation, part I: X- and gamma-radiation, and neutrons. Vol.75. Lyon, France: IARC, 2000.
4. Pelling JC, Slaga TJ. Cellular mechanisms for tumor promotion and enhancement. In: *Mass Med. Carcinogenesis*. New York, NY: Raven Press, 1985:369-393.
5. Mijnheer, B.J., Battermann, J.J., Wambersie, A. What degree of accuracy is required and can be achieved in photon and neutron therapy? *Radiother Oncol.* 1987; 8:237-252.
6. International Commission on Radiological Protection (ICRP). Publication 26: *Annals of the ICRP* 1(3). Recommendations of the International Commission on Radiological Protection. Pergamon Press, Oxford, England 1977.
7. Leksell Gamma Knife – Instruction for Use. 1998.
8. Moskvina, V., DesRosiers, C., Papiez, L., Timmerman, R., Randall, M., and DesRosiers, P., Monte Carlo simulation of the Leksell Gamma Knife: In. *Source modeling and calculations in homogeneous media,* *Phys. Med. Biol.* 2002 47, 1995-2011.
9. International Commission on Radiological Protection (ICRP). Publication 34: *Protection of the Patient in Diagnostic Radiology*. Pergamon Press, Oxford 1982.
10. United Nations Scientific Committee on the Effects of Atomic Radiation (UNSCEAR). 1993 Report to the General Assembly: *Medical Radiation Exposures*. United Nations, New York, NY 1993.
11. Puskin JS, Nelson CB. "Estimates of radiogenic cancer risks. *Health Physics* 1996 69: 93-101.
12. Fry RJM. Effects of low doses of radiation. *Health Physics* 1996 70: 823-827.
13. Jones D, Wall B. NRPB Report 186: *Organ Doses from Medical X-Ray Examinations Calculated Using Monte Carlo Techniques*. National Radiological Protection Board, Chilton, UK 1985.
14. Padovani R, Contento G, Fabretto M, Malisan MR, Barbina V, Gozzi G. Patient doses and risks from diagnostic radiology in North-east Italy. *Br J Radiol* 1987;60: 155-165.
15. Wagner, L. "Absorbed dose in imaging: Why measure it? *Radiology* 1991 178: 622-623.
16. International Commission of Radiological Protection (ICRP). *Radiological Protection and Safety in Medicine*. ICRP Publication 73 Oxford: Elsevier Science 1996.
17. Williams JR. The interdependence of staff and patient doses in interventional radiology. *Br J Radiol* 1997 70; 833 498-503.
18. International Commission of Radiological Protection. *Recommendations of the International Commission of Radiological Protection*. ICRP 60. Oxford: Pergamon press 1991.
19. United nations scientific committee on Effects of Atomic Radiation. *Sources and Effects of Ionizing Radiation*. UNSCEAR 2000 Vol. 1, Report to the general assembly. New York. 2000.

20. European Commission. Council Directive 97/43 EURATOM of 13 May 1997 on health protection of individuals against the dangers of ionising radiation in relation to medical exposure. Official J Eur Commun 1997;40:L180.
21. RCR, NRPB. Patient dose reduction in diagnostic radiology. Documents of the NRPB, Vol. 1, No. 3. Chilton: NRPB, 1990.
22. International Organisation for Standardisation (ISO), “Quality management and quality assurance standards—part I, guidelines for selection and use”, ISO 9000, ISO, Geneva, Switzerland 1994.
23. Perez, C., Brady, A. Principles and practice in radiotherapy and oncology. Philadelphia: J.B. Lippincott Co. 1992.
24. Perez, JP. Quality management in the imaging sciences. Mosby, Inc. Missouri, USA. 1998.
25. Khan, F.M. The Physics of Radiation Therapy. Second edition. Lippincott Williams & Wilkins, 1994.
26. Van Dam J., Marinello G. Methods for in vivo dosimetry in external radiotherapy. ESTRO (European Society for Therapeutic Radiology and Oncology) Booklet No. 1 (Physics for Clinical Radiotherapy), Leuven-Apeldoorn: Garant, 1994.
27. Williamson JF, Meigooni AS.: Quantitative Dosimetry Methods in Brachytherapy. Brachytherapy Physics: AAPM Summer School. San Diego. Madison: Medical Physics Publishing Corporation; 1995.
28. Kron T. Dose Measuring Tools. Van Dyk J. The Modern Technology of Radiation Oncology. 1st ed. Madison, USA: 1999.
29. Metcalfe P, Kron T, Hoban P. The Physics of Radiotherapy X-Rays From Linear Accelerators. Wisconsin: Medical Physics Publishing; 1997.
30. Laub WU, Kaulich TW, Nüsslin F. A diamond detector in the dosimetry of high-energy electron and photon beams. Phys Med Biol. 1999; 44:2183-2192.
31. Peet DJ, Pryor MD. Evaluation of a MOSFET radiation sensor for the measurement of entrance surface dose in diagnostic radiology. Br J Radiol. 1999; 72:562-568.
32. <http://hyperphysics.phy-astr.gsu.edu/hbase/nuclear/radrisk.html>. Accessed on 14 March 2006.
33. Perez, C.A. and Brady, L.W. Principles and practice of radiation oncology. 3rd ed. Philadelphia: Lippincott-Raven Publishers 1998.
34. Karzmark C J, Nunan C S and Tanabe E. Medical electron accelerators, McGraw-Hill Health Professions Division, New York. 1993.
35. United Nations, Sources and Effects of Ionizing Radiation (Report to the General Assembly), Scientific Committee on the Effects of Atomic Radiation (UNSCEAR), UN, New York 1993.
36. Laughlin JS. Development of the technology of radiation therapy. In: The technical history of radiology. Radiographics 1989; 9:1245–66.
37. International Commission on radiation units and measurements (ICRU). Determination of absorbed dose in a patient irradiated by beams of X and Gamma rays in radiotherapy procedures. ICRU Report 24, (WashingtonD.C.,1976.
38. Shirato H, Shimizu S, Kunieda T, et al. Physical aspects of a linear accelerator synchronized with real-time tumor tracking system, Int J Radiat Oncol Biol Phys 2000 48, 1187-1195 .

39. Schlegel, W.; Bortfeld, T.; Grosu, A.-L. (Eds.) *New Technologies in 3D Conformal Radiation Therapy: Introduction and Overview*. Springer Berlin Heidelberg. 2006.
40. Dutreix A. When and how can we improve precision in radiotherapy? *Radiother Oncol* 1984 2, 275-292.
41. Martin CJ. Effective dose: how it should be applied to medical exposures. *Br J Radiol* 2007 80; 369-647,
42. Almen A, Mattsson S. "On the calculation of effective doses to children and adolescents. *J Radiat Prot* 1996 16;81-89.
43. Hart D, Jones DG, Wall BF. NRPB Report 279: Estimation of Effective Dose in Diagnostic Radiology from Entrance Surface Dose and Dose-Area Product Measurements. National Radiological Protection Board, Chilton, Oxon, UK 1996.
44. Hart D, Jones DG, Wall BF. NRPB Software SR262: Normalized Organ Doses for Medical X-Ray Examinations Calculated Using Monte Carlo Techniques. National Radiological Protection Board, Didcot, Oxon 1998.
45. ICRU. Determination of absorbed dose in a patient irradiated by beams of x or gamma rays in radiotherapy procedures. ICRU report 24, Bethesda, Maryland 1976.
46. Podgorsak. EB. *Radiation oncology physics: A handbook for teachers and students*. IAEA, Vienna, 2005.
47. Duggan. L. Clinical use of LiF:Mg,Cu,P: Critical evaluation of an ultra-sensitive material for thermoluminescence dosimetry. PhD thesis. Faculty of Science and Mathematics, University of Newcastle. Australia. 2002.
48. Kron T applications of the thermoluminescence dosimetry in medicine. *Radiat Prot Dosim.* 1999 85;1-4. 333-340.
49. Mahadevappa M. Fluoroscopy: Patient radiation exposure issues. *RadioGraphics* 2001 21:1033-1045.
50. Draft for Consultation: Recommendations of the International Commission on Radiological Protection (Online at <http://www.icrp.org>). 2005.
51. Institute of Physical Sciences in Medicine (IPSM), National Radiological Protection Board and College of Radiographers. National Protocol for Patient Dose Measurements in Diagnostic Radiology. Chilton: NRPB; 1992.
52. Kyriou JC, Fitzgerald M, Pettett A, Cook JV, Pablott SM. A comparison of doses and techniques between specialist and non-specialist centres in the diagnostic x-ray imaging of children. *Br J Radiol.* 1996; 69:437-450.
53. European Commission. European guidelines on quality criteria for diagnostic radiographic images. EUR 16260 EN. Brussels; 1996.
54. Kron T. Dose Measuring Tools. Van Dyk J. *The Modern Technology of Radiation Oncology*. 1st ed. Madison, USA: 1999.
55. Butson MJ, Rozenfeld A, Mathur JN, Carolan M, Wong TPY, Metcalfe PE. A new radiotherapy surface dose detector: The MOSFET. *Med Phys.* 1996; 23, 5:655-658.
56. Ramani R, Russell S, O'Brien P. Clinical dosimetry using MOSFETs. *Int J Radiat Oncol Biol Phys.* 1997; 37:959-964.
57. Nam, T., Keddy, R., and Burns, R.. Synthetic diamonds as in vivo detectors. *Med Phys* 1987 14 4: 596-601.
58. Laub, W. and Wong, T. The volume effect of detectors in the dosimetry of small fields used in IMRT. *Med Phys* 2003 30,3 : 341-347.

59. Buccioli, M., Buonamici, F., Mazzochi, S., De Angelis, C., Onori, S., and Cirrone, G. Diamond detector versus silicon diode and ion chamber in photon beams of different energy and field size. *Med Phys* 2003 30 8: 2149-2154.
60. Beddar, A., Law, S., Suchowerska, N., and Mackie, T. Plastic scintillation dosimetry: optimisation of light collection efficiency. *Phys Med Biol* 2003 48:1141-1152.
61. Huston, A., Justus, B., Falkenstein, P., Miller, R., Ning, H., and Altemus, R.. Remote optical fibre dosimetry. *Nucl Instrum Meth* 2001 B, 184:55-67.
62. David I Thwaites and John B Tuohy. Back to the future: the history and development of the clinical linear accelerator. *Phys. Med. Biol.* 51 2006 R343–R362.
63. Metcalfe P, Kron T, Hoban P. The Physics of Radiotherapy X-rays: Problems and Solutions. Medical Physics Pub Corp.1998.
64. Kalef-Ezra J. work shop on Radiation Therapy Physics, Dose measurements techniques in radiation therapy, Thermoluminescence dosimetry in radiotherapy. University of Ioannina .1997.
65. Frutta C and Weng P. Operational Thermoluminescence dosimetry. World Scientific Publishing.1998.
66. McKeever, S., Moskovitch, M., and Townsend, P., Thermoluminescence Dosimetry Materials: Properties and Uses. Nuclear Technology Publishing, Ashford Kent, England. 1995.
67. Randall JT and Wilkins MHF. Phosphorescence and electron traps: I. The study of trap distributions. *Proceedings of the Royal Society* 1945 184A:366-389.
68. Nakajima, T., Murayama, Y., and Murayama, T. Preparation and Dosimetric Properties of a Highly Sensitive LiF Thermoluminescent Dosimeter, *Health Physics* 1979 36 79-82.
69. Kron, T. Thermoluminescence Dosimetry and Its Application in Medicine -Part 1: Physics, Materials and Equipment. *Australas Phys Eng Sci Med* 1994, 17; 4 175- 199.
70. Pradhan A.S. Thermoluminescence Dosimetry (TLD) in Radiation Protection. Bhabha Atomic Research Centre, Mumbai 400 085, India.
71. Harshaw TLD, Materials and Assemblies for Thermoluminescence Dosimetry, Catalogue-Harshaw/Bicron Thermoluminescence Dosimetry (TLD), Materials and Assambles, 1999.
72. Glennie GD.A comparison of TLD dosimeters:LiF:Mg,Ti and LiF:Mg,Cu,P for measurement of radiation therapy doses. PhD Dissertation. Faculty of Engineering and Applied Science. University of Virginia.2003.
73. Harshaw /Bicron Radiation Measurement Products, Model 3500 Manual TLD Reader User's Manual Saint-Gobain/Norton Industrial Ceramics Corporation, Solon, OH 1993.
74. Spanne, P., TL Readout Instrumentation in Thermoluminescence and Thermoluminescent Dosimetry. Edited by Y.S. Horowitz, CRC Press, Boca Ratan, Florida. 1984.
75. Horowitz, Y., and Horowitz, A. Characterisation of LiF:Cu,Mg,P (GR-200) for Personnel Thermoluminescence Dosimetry. *Radiat Prot Dosim* 1990 33, 279-282.
76. Horowitz, Y., LiF: Mg, Ti versus LiF:Mg,Cu,P: the Competition Heats Up, *Radiat Prot Dosim* 1993 47,135-141.
77. Horowitz, Y.S., LiF - TLD Methodology, Invited paper delivered to the European Society for Therapeutic Radiology and Oncology, 1984.

78. Horowitz, Y.S., editor, Thermoluminescence and Thermoluminescent Dosimetry. 1-3, CRC Press, Boca Raton, Florida. 1984.
79. McKinlay, A. Thermoluminescent Dosimetry. Medical Physics Handbook 5. Adam Hilger, Bristol England, 1981.
80. Banjade D.P, Tajuddin A.A. and A. Shukri., Determination of absorbed dose from photon and electron beams from a linear accelerator comparing different protocols in different phantoms. Appl Radiat Isot 2001 55, 235-243.
81. Ma C, Coffey CW, DeWerd A, Liu C, Nath R, Seltzer SM, Seuntjens JP. AAPM protocol for 40–300 KV x-ray beam dosimetry in radiotherapy and radiobiology. Med Phys 2001; 28:868-93.
82. Martin CJ, Sutton DG, Workman A, Shaw AJ, Temperton D. Protocol for measurement of patient entrance surface dose rates for fluoroscopic X-ray equipment. Br J Radiol 1998; 71:1283-87.
83. International Commission on Radiological Protection (ICRP). Publication 26: Annals of the ICRP 1(3). Recommendations of the International Commission on Radiological Protection. Pergamon Press, Oxford, England 1977.
84. Jacobi W. The concept of the Effective Dose; a proposal for the combination of organ doses. Radiat Environ Biophys 1975 12:101–109.
85. Niklason LT, Marx MV, Chan HP. The estimation of occupational effective dose in diagnostic radiology with two dosimeters. Health Phys 1994; 67:611-5.
86. Padovani R, Rodella CA Staff dosimetry in interventional cardiology. Radiat Prot Dosim 2001 94:99-103.
87. National Council on Radiation Protection and Measurements. Use of Personal Monitors to Estimate Effective Dose Equivalent and Effective Dose to Workers for External Exposure to Low LET Radiation. NCRP Report No. 122. Bethesda, 1995.
88. Hart D, Jones DG, Wall BF. Normalized organ dose for paediatric x-ray examinations calculated using Monte-Carlo techniques. NRPB-SR279 NRPB Chilton, 1996.
89. International Commission of Radiological Protection. Draft Recommendations of the International Commission of Radiological Protection, available online at http://www.icrp.org/docs/ICRP_Recs_02_276_06_web_cons_5_June.pdf. Accessed on 11.04.07.
90. International Commission of Radiological Protection. Recommendations of the International Commission of Radiological Protection. Biological and Epidemiological Information on Health Risks Attributable to Ionising Radiation: A Summary of Judgements for the Purposes of Radiological Protection of Humans available online at http://www.icrp.org/Health_risks.pdf. Accessed on 12.04.07.
91. Zhu TC, Palta JR. Electron contamination in 8 and 18 MV photon beams. Med Phys 1998 25, 1, 12-19.
92. Dietmar Georga, Bie De Ostb, Marie-TheÂreÂse Hoornaertb, Pierre Piletteb, Jan Van Damb, Michel Van Dyckeb,1, Dominique Huyskens. Build-up modification of commercial diodes for entrance dose measurements in 'higher energy' photon beams. Radiother. Oncol 1999 51;249-256.
93. Johansson, K.A. , Horiot, J.C., Van Dam, J., Lepinoy, D., Sentenac, I., Sernbo, G. Quality assurance control in the EORTC cooperative group of radiotherapy. 2. Dosimetric comparison. Radiother. Oncol. 1986;7 ,3:269-279.

94. Thwaites, DI. Quality assurance of external beam radiotherapy: In E. B. Podgorsak. Radiation oncology physics: A handbook for teachers and students. IAEA, Vienna, 2005.
95. Kalef-Ezra JA, Boziari A, Litsas J, Tsekeris P, Koligliatis T. Thermoluminescence dosimetry for quality assurance in radiation therapy. *Radiat Prot Dosim* 2002;101(1-4):403-5.
96. Duch MA, Ginjaume M, Chakkor H, Ortega X, Jornet N, Ribas M. Thermoluminescence dosimetry applied to in vivo dose measurements for total body irradiation techniques. *Radiother Oncol* 1998 47, 3:319-24.
97. Swinnen A, Verstraete J, Huyskens DP. Feasibility study of entrance in vivo dose measurements with mailed thermoluminescence detectors. *Radiother Oncol* 2004, 73 1 89-96.
98. Venables K, Miles E, Aird E, Hoskin P. The use of in vivo thermoluminescent dosimeters in the quality assurance programme for the START breast fractionation trial. *Radiother Oncol* 2004 71 303–310.
99. Loncol T, Greffe JL, Vynckier S, Scalliet P. Entrance and exit dose measurements with semiconductors and thermoluminescent dosimeters: a comparison of methods and in vivo results. *Radiother Oncol* 1996 41 2:179-87.
100. Besbes M, Siala B, J. Daoud. Absorbed dose evaluation of thyroid during nasopharynx and breast carcinoma irradiation by in vivo dosimetry. *Cancer/Radiothérapie* 2003 7 297–301.
101. Stevens G, Downes S, and Ralston A. Thyroid dose in children undergoing prophylactic cranial irradiation. *Int. J. Radiation Oncology Biol. Phys.*, 1998 42 2 385–390.
102. Van der Giessen P. measurement of peripheral dose for tangential breast treatment technique with Co-60 gamma radiation and high energy X-rays. *Radiother Oncol* 1997 257-264.
103. Portaluri M, Maiorana A, Corsa P, Fusco V, Lauriola P, Parisi S, Raguso A, Sanzo A, Giacco G. An in-vivo dosimetric study of the scattered radiation during the treatment of breast carcinoma. *Radiol Med (Torino)*. 1996 91, 1-2:122-5.
104. Cigna A, D. Nassisi, D. Masenga, R. Raffo and P. Rotta. Dose due to scattered radiation in external radiotherapy: a prostate cancer case history. *Radiat Prot Dosim* 2004 108:27-32.
105. Rijke A. G, Zoetelief. J, Raaijmakers C. P. J, Van Der Marck S. C. and Van Der Zee W. Assessment of induction of secondary tumours due to various radiotherapy modalities. *Radiat Prot Dosim* 2006 118 2 :219-226.
106. Fraass BA, Roberson PL, Lichter AS. Dose to the contralateral breast due to primary breast irradiation. *Int J Radiat Oncol Biol Phys* 1985;11:485–97.
107. Boziari A. in vivo dosimetry in radiotherapy. PhD thesis. University of Ioannina, Medical Physics Department 2002.
108. Swinnen A. Quality assurance in radiotherapy: Development and validation of mailed dosimetry procedure for external audit using a multipurpose phantom and in vivo dosimetry. PhD Thesis. Department of Oncology. University of Leuven. 2005.
109. Johns, H.E. and Cunningham, J.R. The Physics of Radiology. Charles C. Thomas, Springfield, Illinois. 1983.
110. Horowitz. Y.S.. Theory of luminescence gamma dose response: The unified interaction model. *Nuclear instruments and methods in physics research* 2001 B 184 68-84.
111. ESTRO booklet No 5. practical guidelines for implementation of in vivo dosimetry with diodes in external radiotherapy with photon beams (entrance dose), Physics for clinical radiotherapy, ESTRO, 2001.

112. Dunscombe P, Johnson H, Arsenault C, Mawko G, Bissonnette JP, Seuntjens J. Development of quality control standards for radiation therapy equipment in Canada. *J Appl Cl Med Phys.* 8 1 2007.
113. AAPM Report 87, Diode in vivo dosimetry for patients receiving external beam radiation therapy. Published for the American Association of Medical Physicists in Medicine, medical physics publishing. 2005.
114. Leunens G, Van Dam J, Dutreix A, Van der Schueren E. Importance of in vivo dosimetry as part of a quality assurance program in tangential breast treatments. *Int J Radiat Oncol Biol Phys* 1994 1; 28 1:285-96.
115. Leunens G, Van Dam J, Dutreix A, et al. Quality assurance in radiotherapy by in vivo dosimetry. 1. Entrance dose measurements, a reliable procedure. *Radiother Oncol* 1990;17:141–151.
116. Leunens G, Van Dam J, Dutreix A, et al. Quality assurance in radiotherapy by in vivo dosimetry. 2. Determination of the target absorbed dose. *Radiother Oncol* 1990; 19:73– 87.
117. Essers M, Lanson JH, Mijnheer BJ. In vivo dosimetry during conformal therapy of prostatic cancer. *Radiother Oncol* 1993;29:271–279.
118. Broggi S, Fiorino C and Calandrino R. In vivo estimation of midline dose maps by transit dosimetry in head and neck radiotherapy. *Br J Radiol* 2002 75 ,974-981
119. Tung I, CJ.. Wang, H. C Lo, S. H.. Wu J. M and Wang. C. J.. In vivo dosimetry for external photon treatments of head and neck cancers by diodes and TLDS. *Radiat Prot Dosim* 2004 111, 1, 45–50.
120. Ron E, Lubin J H, Shore R E, Mabuchi K, Modan B, Pottern L M, Schneider A B, Tucker M A and Boice J D . Thyroid cancer after exposure to external radiation: a pooled analysis of seven studies. *Radiat Res* 1995 141 259–77.
121. Chougule A. Surface dose over eye, thyroid, breast and gonads during external beam therapy of pelvis, abdomen and thorax. *Journal of Clinical Radiother Oncol.* 1993 8 2 : 31-3.
122. Mazonakis M, Damilakis J, Varveris H, Fasoulaki M, Gourtsoyiannis N. Risk estimation of radiation-induced thyroid cancer from treatment of brain tumors in adults and children. *Int J Oncol.* 2003 22 1:221-5.
123. Sulieman A, Omer H, Theodorou K, Kappas C. Review on Intra and interfractional tumour organ motion measurement for radiotherapy. *Int.J.Sci.Res.*, 2006 15 44-55.
124. Briot E, Dutreix A, Bridier A. Dosimetry for total body irradiation. *Radiother Oncol* 1990 1:16–29.
125. Greig JR, Miller RW, Okunieff P. An approach to dose measurement for total body irradiation. *Int J Radiat Oncol Biol Phys* 1996 36:463– 468.
126. Appleyard A, Ball K Hughes F. E. Kilby W, Nicholls R. Rabett V, Sage J, Smith M., Thomson E. Systematic in vivo dosimetry for quality assurance using diodes: Assessing radiotherapy techniques and developing an appropriate action protocol. *J Radiother Pract* 2005 ,4, 143–154.
127. Adeyemi A. Lord J. An audit of radiotherapy patient doses measured with in vivo semiconductor detectors dosimetry in head and neck radiotherapy. *Br J Radiol* 2002 75,974-981.
128. Fiorino C, Corletto D, Mangili P, Broggi S, Bonini A, Mauro G, Parisi R, Rosso A, Signorotto P, Villa E Calandrino R. Quality assurance by systematic in vivo dosimetry: results on a large cohort of patients. *Radiotherapy and Oncology* 2000 56 85-95.
129. Heukelom, S Lanson JH and Mijnheer BJ. In vivo dosimetry during pelvic treatment. *Radiother Oncol* 1992 25 111-120.

130. Scarantino C.W, Rini C., Aquino M., Carrea T., Ornitz R, Anscher M., Black R.. A pilot study on in vivo dosimetry during external beam radiation therapy. *Int. J. Radiat Oncol Biol Phys* 2004 60, 1, S587-S587.
131. Lanson, JH, Essers M, Meijer, GJ. Minken, WH Uiterwaal, GJ.. Mijnheer BJ. In vivo dosimetry during conformal radiotherapy Requirements for and findings of a routine procedure. *Radiother Oncol* 1999 52 51-59.
132. Fontenla D, Yaparpalvi, R. Chen-Shou Chui, , Briot,E. The use of diode dosimetry in quality improvement of patient care in radiation therapy. *Med Dosim* 1996 21 4 235-241.
133. Figge JJ. Epidemiology of Thyroid Cancer: In *Thyroid Cancer: Leonard Wartofsky and Douglas Van Nostrand*, Humana Press Inc.2006.
134. Stathakis S Jinsheng Li, and Charlie C.M. Ma. Monte Carlo determination of radiation-induced cancer risks for prostate patients undergoing intensity-modulated radiation therapy. *J Appl Cl Med Phys*, 2007 8, 4 14-26.
135. Huang J, Walker R, Patty G. Groome, Wendy Shelley, William J. Mackillop. Risk of Thyroid Carcinoma in a Female Population after Radiotherapy for Breast Carcinoma. *CANCER* 2001 15 92 96.
136. Reda S, Massoud E, Hanafy ,MS. Bashter I and Amin E. Monte Carlo dose calculations for breast radiotherapy using ⁶⁰Co gamma rays. *J Nucl Radiat Phys* 2006,1,1 61-72.
137. Porock D, Kristjanson L. Skin reactions during radiotherapy for breast cancer: the use and impact of topical agents and dressings. *Eur J Cancer Care* 1999;8:143-153.
138. Harper J, Lynette E. Franklin, MSN; Joseph M. Jenrette, MD; Eric G. Aguero, MD Skin Toxicity During Breast Irradiation: Pathophysiology and Management. *South Med J* 2004 97 10: 989-993.
139. Enomoto T, Johnson T, Peterson N, Homer L, Walts D, Johnson N. Combination glutathione and anthocyanins as an alternative for skin care during external-beam radiation. *Am J of Surg* 2005 189 627–631.
140. Schneider K, Ernst G, Kruger I, Kohn, MM. Paediatric fluoroscopy- results of a European-wide survey. *Pediatr Radiol* 1997; 27, 469.
141. Maubon, A.J., De Graef, M., Boncoeur-Martel M.P. and Rouanet J.P. Interventional radiology in female infertility: technique and role. *Eur Radiol* 2001 11,771-778.
142. Perisinakis, K., Damilakis, J., Grammatikakis, J., Theocharopoulos, N. and Gourtsoyiannis N. Radiogenic risks from hysterosalpingography. *Eur. Radiol* 2003 13,1522–1528.
143. Devereaux CE, Bionmoeller KF. Endoscopic retrograde cholangiopancreatography in the next millennium. *Gastrointest Endosc* 2000; 10:117-130.
144. Perissat J, Huibregste K, Keane FBV, Russel RCG, Neoptolemos JP. Management of bile duct stones in the era of laparoscopic cholecystectomy. *Br J Surg* 1994; 81:799–810.
145. Mahant S, Friedman J, MacArthur C. Renal ultrasound findings and vesicoureteral reflux in children hospitalised with urinary tract infection. *Arch Dis Child* 2002;86:419-20.
146. King S, Pitcher EM, Smail MA. Optimizing medical radiation exposures for urological procedures, with special emphasis on paediatric imaging. *BJU Int* 2002;89:510-16.
147. Singh-Grewal , Macdessi J, Craig J. Circumcision for the prevention of urinary tract infection in boys: a systemic review of randomised trials and observational studies. *Arch Dis Child* 2005 90,853-858.
148. Franchi-Abella S: Cyclic voiding cystourethrography for children with Urinary tract infection. *J Radiol* 2000; 81: 1615-18.

149. Persliden J, Helmorot E, Hjort P, Resjo M. Dose and image quality in comparison of analogue and digital techniques in paediatric urology Examinations. *Eur Radiol* 2004;14:638-44.
150. Mantovani A, Giroletti E. Evaluation of the dose to paediatric patient undergoing Micturating cystourethrography examination and optimisation of the examination. *Radiol Med* 2004;108 **3** : 283-91.
151. Schneider K, Perlmutter N, Arthur R, Cook V, Horwitz E, Thomas P, Kramer P, Montagne P, Ernst G, Kohn M, Panzer W, Wall B. Micturating cystourethrography in paediatric patients in selected children's hospitals in Europe: evaluation of fluoroscopy technique, image quality criteria and dose. *Radiat Prot Dosim* 2000; 90 1-2 ,197-01.
152. Fotakis M, Molyvda Athanasopoulou E, Psarrakos K, Economou I. Radiation doses to paediatric patients up to 5 years age undergoing micturating cystourethrography examinations and its dependence on patient age: a Monte Carlo study. *Br J Radiol* 2003;76:812-17.
153. King S, Pitcher EM, Smail MA. Optimizing medical radiation exposures for urological procedures, with special emphasis on paediatric imaging. *BJU Int* 2002;89:510-16.
154. Cleveland RH, Constantinou C, Blickman JG, Jaramillo D, Webster E. Voiding cystourethrography in children: value of digital fluoroscopy in reducing radiation dose. *Am J Roentgenol* 1992;158:137-42.
155. Chateil JF, Rouby C, Brun M, Labessan C, Diard F. Practical measurement of paediatric Radiology: use of the dose area product in digital fluoroscopy and neonatal chest radiographs. *J Radiol.* 2004;85:619-25.
156. Schultz FW, Geleijns J, Holscher HC, Weststrate J, Zonderland HM, Zoereleif J. Radiation Burden to paediatric patients due to Micturating cystourethrography examinations in a Dutch children's hospital. *Br J Radiol* 1999;72:763-72.
157. Schneider K, Ernst G, Kruger I, Kohn, MM. Paediatric fluoroscopy- results of a European-wide survey. *Pediatr Radiol* 1997; 27, 469.
158. Almen A, Mattsson S. The radiation dose to children from X-ray examinations of the pelvis and the urinary tract. *Br J Radiol* 1995; 68:604-13.
159. European Commission. Quality Criteria for Diagnostic Radiographic Images in Paediatrics. Report EUR 16261, Luxembourg: Office for Official Publications of the European Communities, 1996:1-35.
160. Vano E, Gonzalez L, Guibelalde E, Fernandez JM, Ten JJ. Radiation exposure to medical staff in interventional and cardiac radiology. *Br J Radiol* 1998; 71: 954-60.
161. Kushner, D.C., Yoder, I.C., Cleveland, R.H., Herman, T.E., and Goodsitt, M.M. Radiation dose reduction during hysterosalpingography: an application of scanning-beam digital radiography. *Radiology* 1986 16, 31-33.
162. Calcchia, A., Chiacchiararelli, L., De Felice, C., Gigliotti, T., Indovina, P.L., Mazzei, F., and Porfiri, L.M. Evaluation of effective dose in hysterosalpingography. *Radiat. Prot. Dosim.* 1998 80 ,1-3 159-61.
163. Gegan, A.C.M., Peach, D., McHugo, J.M. Patient dosimetry in hysterosalpingography: a comparative study. *Br. J. Radiol.* 1998 71:1058-1061.
164. Khoury, H.J., Maia, A., Oliveira, M., Kramer, R. and Drexler, G. Patient dosimetry in hysterosalpingography. Proceedings of the International Conference on Radiological Protection of Patients in Diagnostic, Interventional Radiology, Nuclear Medicine and Radiotherapy. Malaga 26-30 march 2001. IAEA-CSP-7/P, Vienna, IAEA-CN-85-94 2001 139-142.

165. Merkle, E., Vogel, J. and Aschoff, A.J. Radiation exposure during digital hysterosalpingography: how much is due to fluoroscopy? *Rofo* 1995 163 3 :256-258.
166. Abdullah, B.J.J., Ng, K.H., Rassiah, P. A comparison of radiation dose and image quality in hysterosalpingography using conventional and high kilovolt techniques. *J. H.K. Coll. Radiol.* 2001 4,133-136.
167. Fernandez, J.M., Vano, E. and Guibelalde, E. Patient doses in hysterosalpingography. *Br. J. Radiol.* 1996 69,751–754.
168. Perisinakis, K., Damilakis, J., Grammatikakis, J., Theocharopoulos, N. and Gourtsoyiannis N. Radiogenic risks from hysterosalpingography. *Eur. Radiol.* 2003 13,1522–1528.
169. Schultz, F., Teeuwisse, W., Broerse, J., Chandie Shaw.M. and Geleijns, J. Dosimetric consequences of implementation of digital radiology for hysterosalpingography. *AAPM manual meeting program. Med. Phys* 1998 25 7 -1,A156.
170. Buls, N. and Osteaux, M. Patient and staff dose during hysterosalpingography. *Proceedings of the International Conference on Radiological Protection of Patients in Diagnostic, Interventional Radiology, Nuclear Medicine and Radiotherapy. Malaga 26-30 march 2001. IAEA-CSP-7/P, Vienna, IAEA-CN-85-73, 2001* 135-138.
171. King, S., Pitcher, E.M. and Smail, M.A. Optimizing medical radiation exposures for urological procedures, with special emphasis on paediatric imaging. *Brit. J. Urol* 2002 89,510–516.
172. Verdun, F.R. and Schnyder, P. Reduction of radiation doses to staff during diagnostic X ray procedure. *Eur. Radiol. Syllabus* 2004 14,84-90 .
173. Haussler, M.D., Merk, J., Tomczak, R. and Schnarkowski, P. Radiation dosage during hysterosalpingography using a digital image intensifying technique. *Rofo* 1992 157 6 596-598 .
174. Murase, E., Ishiguchi, T., Ikeda, M. and Ishigaki, T. Is lower- dose digital fluorography diagnostically adequate compared with higher dose digital radiography for the diagnosis of fallopian tube stenosis. *Cardiovasc. Intervent. Radiol.* 2000 23,126-130 .
175. Broadhead, D.A., Chapple, C-L. and Faulkner, K. Reference doses during fluoroscopic procedures. *Radiat. Prot. Dosim.* 1998 80, 1-3 143-44.
176. Larkin CJ, Workman A, Wright RER, Tony Tham, CK Radiation doses to patients during ERCP. *Gastrointest Endosc* 2001 53:161–164.
177. Naidu LS, Singhal S, Preece DE, Vohrah A, Loft DE . Radiation exposure to personnel performing Endoscopic retrograde Cholangiopancreatography. *Postgrad Med J* 2005 81:660–662.
178. Buls N, Pages J, Mana F, Osteaux M. Patient and staff exposure during endoscopic retrograde cholangiopancreatography. *Br J Radiol* 2002 75, 435-443.
179. Tsalafoutas IA, Paraskeva KD, Yakoumakis EN, Vassilaki AE, Maniatis PN, Karagiannis JA, Koulentianos ED. Radiation doses to patients from endoscopic retrograde cholangiopancreatography examinations and image quality considerations. *Radiat Prot Dosim* 2003 106: 3, 241–246.
180. Chen MY, Van Swearingen FL, Mitchell R, Ott DJ. Radiation exposure during ERCP: effect of a protective shield. *Gastrointest Endosc* 1996 43:1-5.
181. Singhal A, Rowe G, Faizallah R. Pulse Fluoroscopy in ERCP: Reducing Radiation Exposure [abstract]. *Gastrointest Endosc* 2006 63:5 AB300.

182. Uradomo LT, Goldberg EM, Darwin PE Pulsed Fluoroscopy to Reduce Radiation Exposure During ERCP: A Prospective Randomized Trial. *Gastrointest Endosc* 2007 66:84-89.
183. Heyd RL, Kopecky KK, Sherman S, Lehman GA, Stockberger SM Radiation exposure to patients and personnel during interventional ERCP at a teaching institution. *Gastrointest Endosc* 1996 44:287-292.
184. Ramirez-Jimenez FJ, Lopez-Callejas R, Benitez-Read JS, Pacheco-Sotelo JO. Considerations on the measurement of practical peak voltage in diagnostic radiology. *Br J of Radiol* 2004; 77:745–750.
185. Mitchell RM, Grimm IS. ERCP radiology Basics. *Techniques in Gastrointest Endosc* 2003 5:11-16.
186. Johlin FC, Pelsang RE, Mary Greenleaf RN. Phantom Study to Determine Radiation Exposure to Medical Personnel Involved in ERCP Fluoroscopy and Its Reduction Through Equipment and Behavior Modifications. *Am J Gastroenterol* 2002 97: 4,893-897.
187. Mark S. Parker, Jiyeam K. Chung, Panos P. Fatouros, Jessica A. Hoots, Nicole M. Kelleher, Stanley H. Benedict. Reduction of Radiation Dose to the Female Breast: Preliminary Data with a Custom-Designed Tungsten-Antimony Composite Breast Shield. *The Journal of Applied Research*. Vol. 6, No. 3, 2006
188. Broggi S, Fiorino C, Calandrino R. In vivo dosimetry of midline dose maps by transit dosimetry in head and neck radiotherapy. *The british journal of radiotherapy*. 75.(2002)974-981.
189. Johansson, K.A., Horiot, J.C., Van Dam, J., Lepinoy, D., Sentenac, I., Sembo, G. Quality assurance control in the EORTC cooperative group of radiotherapy. 2. Dosimetric comparison. *Radiother. Oncol.* 1986;7(3):269-279.

Annex A.

TLD correction factors for high energy beams

A. 1. CORRECTION FACTORS (Ci) for 6 MV.

No	ID	Ci
1	A1	0.982351
2	A2	0.973523
3	A3	1.266533
4	A4	1.072304
5	A5	1.094096
6	A6	1.109254
7	A7	1.116938
8	A8	1.104492
9	A9	1.135118
10	A10	0.99791
11	B1	1.194334
12	B2	1.080733
13	B3	1.079438
14	B4	1.123132
15	B5	1.076686
16	B6	1.049839
17	B7	1.036444
18	B8	1.120789
19	B9	1.050182
20	B10	1.044839
21	C1	0.920873
22	C2	1.004425
23	C3	0.999283
24	C4	1.02691
25	C5	0.980175
26	C6	0.981853
27	C7	0.885816
28	C8	1.026137
29	C9	0.88212
30	C10	0.911712
31	D1	0.823143
32	D2	0.925832
33	D3	1.028433
34	D4	0.94328
35	D5	0.952222
36	D6	0.982859
37	D7	1.012884
38	D8	0.991935
39	D9	1.053668
40	D10	0.936612
41	E1	0.908041
42	E2	0.959
43	E3	1.030468
44	E4	0.909706
45	E5	0.99235
46	E6	1.015758
47	E7	1.036227
48	E8	0.905913
49	E9	0.984737
50	E10	0.910763
51	K1	0.99733
52	K2	0.826713
53	K3	0.922143
54	K4	0.918854
55	K5	1.00721

A. 2. CORRECTION FACTORS (Ci) for 15 MV

No	ID	Ci
1	F1	0.987592
2	F2	1.086674
3	F3	0.98446
4	F4	0.936635
5	F5	0.872165
6	F6	1.064949
7	F7	0.88336
8	F8	1.006307
9	F9	1.029334
10	F10	1.004239
11	G1	0.989231
12	G2	0.944708
13	G3	1.027077
14	G4	1.029842
15	G5	0.981853
16	G6	1.038335
17	G7	1.00679
18	G8	1.002834
19	G9	0.96446
20	G10	1.057187
21	H1	0.966962
22	H2	0.953165
23	H3	0.984212
24	H4	0.990936
25	H5	1.022938
26	H6	1.016514
27	H7	0.952046
28	H8	1.004307
29	H9	0.981844
30	H10	1.012551
31	I1	1.044413
32	I2	0.963651
33	I3	1.048985
34	I4	1.03682
35	I5	1.020876
36	I6	1.022268
37	I7	0.987638
38	I8	0.985916
39	I9	0.975716
40	I10	1.001345
41	J1	0.889184
42	J2	0.982408
43	J3	1.023789
44	J4	0.979074
45	J5	1.108179
46	J6	0.951554
47	J7	1.02903
48	J8	1.147776
49	J9	1.056889
50	J10	1.058996
51	K6	0.949968
52	K7	0.93847
53	K8	0.985351
54	K9	1.028308
55	K10	0.989968

A. 3. TLD Correction Factors: Radiology sample

No	ID	Ci
1	A1	0.995365
2	A2	0.994744
3	A3	0.985642
4	A4	0.968746
5	A5	1.034037
6	A6	0.973383
7	A7	1.039164
8	A8	0.98062
9	A9	1.053349
10	A10	1.024843
11	B1	0.950095
12	B2	0.954831
13	B3	0.975512
14	B4	1.048047
15	B5	0.980442
16	B6	1.042228
17	B7	1.053594
18	B8	0.971455
19	B9	0.983575
20	B10	0.991914
21	C1	1.019155
22	C2	1.051585
23	C3	1.038882
24	C4	1.010608
25	C5	0.967703
26	C6	0.986683
27	C7	0.958119
28	C8	1.040773
29	C9	1.022073
30	C10	0.961701
31	D1	0.964052
32	D2	0.967259
33	D3	0.97316
34	D4	0.973703
35	D5	0.961466
36	D6	0.969658
37	D7	1.046257
38	D8	1.022705
39	D9	1.032589
40	D10	0.959008
41	E1	0.994588
42	E2	0.966824
43	E3	1.014741
44	E4	0.989617
45	E5	1.02371
46	E6	1.027726
47	E7	1.059472
48	E8	1.003783
49	E9	0.997833
50	E10	1.041297
51	F1	0.963308
52	F2	1.042576
53	F3	1.054556
54	F4	0.956637
55	F5	0.960019
56	F6	0.957343
57	F7	1.012593
58	F8	1.003365
59	F9	1.023712
60	F10	1.017296

Annex B

Patient dosimetry data documents

B.1. Patient dosimetry data documents (radiotherapy)**Patient No()**

Patient name Age Date
 Clinical Diagnosis.....
 Previous History.....
 Therapy
 Anatomical Site.....

Field In : Eso (AP, RL).....

SSD.....
 Energy.....
 Field size
 X1..... Y1..... Equal Field size
 X2..... Y2.....
 Gantry/table.....
 Collimator Rot.....
 Wedge.....TrayBolus.....
 DepthTMR/PDD.....
 Dose.....MU.....

Field out: Exo (PA, LL)

SSD.....
 Energy.....
 Field size
 X1..... Y1..... Equal Field size
 X2..... Y2.....
 Gantry/table.....
 Collimator Rot.....
 Wedge.....TrayBolus.....
 DepthTMR/PDD.....
 Dose.....MU.....

Required Corrections Factors:

1.....2.....3.....4.....

SkinTLD.....comments.....

ThyroidTLD.....comments.....

Anatomical positron	TLDs	Prescribed dose	Measured dose	Sd	SEM
Thyroid					
Skin					
Field In					
Field out					

B.2 Radiation dosimetry data documents (Radiology)**Exam (HSG,MCU, ERCP)**

Date:..... No.....

Patient's data

ID: Age: (years) Height:(cm)

Weight:Kg BMI.....Kg/cm²

Clinical Indications.....

TLD Positions

Patient

1. ESD... 1.....2.....3.....

2. EXIT... 5.....6.....7.....

3. Throid.4.....

Staff doses measurements

Staff 1:TLD position

1.....2.....3.....4.....

Staff 2:.....5.....6.....7.....

Staff 3: 8.....9.....10.....11.....

Radiographic data:

Projection

1.KV: mA: time(s):

2. KV: mA: time(s):

3. KV: mA: time(s):

4. KV: mA: time(s):

5. KV: mA: time(s):

Total films.....FFD.....Focal Spot.....

Fluoroscopic Data

1. KV.....mA..... Total time

2. KV.....mA.....

3. KV.....mA.....

4. KV.....mA.....

5. KV.....mA.....

Total fluoroscopic time Total fluoroscopic Films.....

X ray Unit:

Company:..... model: year:

Focal spot size (mm): permanent filtration:

Rectification:

Comments:

.....
.....

Annex C

Staff and co-patient dose measurements program

Annex C: A program of staff dose measurements from the TLD placed outside the lead apron (Dr K.Theodorou, Medical Physics Department) [18,87]

Name	Staff dose		Estimated dose	0.14(mGy)
Tissue or organ	Wt	Ht(mSv)	E(mSv)	
Gonads*	0.2	0.014	0.0028	33.34
Bone marrow*	0.12	0.014	0.00168	26.75
Colon*	0.12	0.014	0.00168	19.18
Lung*	0.12	0.014	0.00168	9.46
Stomach*	0.12	0.014	0.00168	15.39
Bladder*	0.05	0.014	0.0007	
breast*	0.05	0.014	0.0007	
Liver*	0.05	0.014	0.0007	
Oesophagus*	0.05	0.014	0.0007	
Thyroid*	0.05	0.014	0.0007	
Bone surface*	0.005	0.014	0.00007	
Bone surface	0.005	0.14	0.0007	
Skin*	0.005	0.014	0.00007	
Skin	0.005	0.14	0.0007	
Remainder	0.05	0.14	0.007	
Total	1		0.02156	

* Under protective shield=10% of dose

Ισοδύναμη δόση ακρων: 0.14 οριο 500

Ισοδύναμη δόση φακών: 0.014 οριο 150

Name	Staff dose		Estimated dose	0.14(mGy)
Tissue or organ	Wt	Ht(mSv)	E(mSv)	
Gonads*	0.2	0.14	0.028	
Bone marrow*	0.12	0.14	0.0168	
Colon*	0.12	0.14	0.0168	
Lung*	0.12	0.14	0.0168	
Stomach*	0.12	0.14	0.0168	
Bladder*	0.05	0.14	0.007	
breast	0.05	0.14	0.007	
	0.05	0.14	0.007	
Oesophagus*	0.05	0.14	0.007	
Thyroid*	0.05	0.14	0.007	
Bone surface*	0.005	0.14	0.0007	
Bone surface	0.005	0.14	0.0007	
Skin*	0.005	0.14	0.0007	
Skin	0.005	0.14	0.0007	
Remainder	0.05	0.14	0.007	
total	1		0.14	

* under protective shield=10% of dose

Ισοδύναμη δόση ακρων: 0.14 οριο 500

Ισοδύναμη δόση φακών: 0.014 οριο 150

Annex D.

Patient dosimetry results

D.1 Head and Neck

No	Dose (cGy)	Depth	Field size	LL	RL	Expected dose (cGy)		Dose ratio	%	sd LL	RL
1	90	9	8x9	123.8	122.71	130	0.943	1.4	95.8	3.5	4.2
2	90	10	8x10	133.2	134	135	0.992	2.1	98.6	1.3	1.2
3	90	8	6x10	110	109.25	108	1.011	1.085	1.018	2.4	2.35
4	100	8	8x9	113	121	117	1.0341	96.58	0.965	3.6	3.26
5	100	7	7x7	108.23	124	105	1.180	1.02	1.030	2.1	1.03
6	125	9	6x7	170	151	155	0.974	0.982	1.096	2.5	2.36
7	100	7	8x13	140	133.5	130	1.026	1.02	1.0769	2.1	3.01
8	120	7	8x9	145	143	140	1.021	1.035	1.035	3.4	4.21
9	90	8	7x9	98	97.6	103	0.947	0.951	0.951	3.6	2.36
10	90	6.5	12x8	107	113	110	1.027	0.972	0.972	2.45	4.95
11	100	8	5x7	115	126	120	1.05	0.958	0.958	1.23	1.32
12	120	7	9x6	148	136	140	0.971	1.057	1.057	4.32	4.36
13	187	7.5	20x15	213.56	215.56	210	1.026	1.0169	1.016	1.54	2.36
14	150	8	12x9	182	172	175	0.982	1.04	1.04	4.23	3.24
15	100	7	8x9	130	112	114	0.982	1.140	1.140	3.54	4.01
16	90	8	8x7	102	103	106	0.971	0.962	0.9624	3.36	1.23

D.2 Breast

No	Dose(cGy)	Depth	Field size	F _{in}	F _{out}	Expected dose(cGy)		Dose ratio		sd _{in}	sd _{out}
1	90	2 and 7	6.5x17	87.2	108.8	91	103	0.956	1.04	1.23	2.04
2	133	3.6	5x7	182.2	165	185	160	0.984	1.031	1.23	1.67
3	133	9.5	12x19	193.5	180.6	189	176	1.023	1.026	1.23	1.06
4	133	8-May	9.15.5	159.2	180.8	153	175	1.04	1.033	2.12	1.52
5	90	6 and 8	8x16	123.26	119.25	120	120	1.03	99.32	2.31	1.83
6	133	8 6	9x16	172.54	165.4	175	170.2	98.59	1.034	3.12	2.14
7	90	3.6	4x7	95.2	104.3	100	106	0.952	0.983	4.2	2.6
8	133	4.7	5x8	99.4	166.2	105	158	0.946	1.051	3.5	6.2
9	90	4.8	6x8	104.7	116.8	100	111	1.047	1.052	2.3	5.2
10	133	3.58	6x8	137.6	167.9	142	163	0.969	1.030	5.2	5.6
11	133	5.7	4x5	156.2	154.2	152	163	1.027	0.946	3.7	2.3
12	133	5.9	6x7	157.5	159.4	151	166	1.043	0.960	2.4	3.5
13	266	8x10	d _{max}	274.6	259.2	266	266	1.032	0.974	4.2	4.6
14	266	20x20	d _{max}	276.2	277.4	266	266	1.038	1.042	4.3	3.2
15	200	7x10	d _{max}	195.2	192.5	200	200	0.976	0.9625	2.3	3.5
16	200	20x20	d _{max}	207.9	195.2	200	200	1.039	0.976	2.6	3.5
17	300	6x6	d _{max}	308.2	293.2	300	300	1.027	0.977	3.6	2.5
18	90	10x18	8.6	94.2	106.3	102	98	0.923	1.084	4.2	3.6
19	100	8x10	12	139.2	142.6	135	135	1.031	1.056	2.3	3.6
20	100	8x10	5	119.9	107.6	112	112	1.070	0.960	3.5	2.7
21	133	5x8	5	137.5	134.3	144	144	0.954	0.932	2.5	3.6
22	133	4x8	4	158.4	142.7	150	150	1.056	0.951	4.1	2.9
23	90	7x6	6	109.8	96.1	103	103	1.066	0.933	4.6	4.5
24	100	5x7	7	129.5	125.1	123	123	1.052	1.017	4.6	3.6

D. 3. Abdomen

No	Dose(cGy)	Depth	Field size	LL	RL	Expected dose(cGy)		Dose ratio	sdLL	sdRL
1	90	11	18x11	127.3	108.4	112	1.1366	0.967	2.14	3.6
2	400	d _{max}	18x6	409.5	392.8	400	1.023	0.982	3.25	4.2
3	500	d _{max}	17x6	515.2	492.5	500	1.030	0.985	4.23	5.2
4	150	5	12x5	157.4	170.2	163	0.965	1.044	3.625	5.2
5	400	d _{max}	12x11	405.2	395.7	400	1.013	0.989	4.25	3.6
6	200	6	12x7	229.2	219.3	224	1.023	0.979	4.3	4.6
7	150	11.5	14x6	193.2	19.6	193	1.001	0.101	5.21	5.9
8	100	4	10x5	104.2	109.8	105	0.992	1.045	3.4	4.3

D 4. Pelvis

No	Dose(cGy)	Depth	Field size	Angle	AP	PA	Expected dose(cGy)		Dose ratio	%	sd LL	sdRL
1	150	10	12x12	0.18	218.2	226.4	220	220	0.9918	99.2	99.2	1.02
2	90	9	9x10	90.27	202.8	198.6	205	205	0.9892	98.9	98.9	96.8
3	120	13	8x12	0.18	158	157	165	165	0.9575	0.9515	2.31	2.31
4	100	10	7x12	0.18	120	122	130	130	0.9230	0.938	3.21	2.31
5	90	11	9x10	0.18	116	114	120	120	0.9666	0.95	2.31	2.12
6	90	5	13x13	0.18	103.6	83.2	100	100	1.036	0.832	1.03	1.54
7	150	12	12x14	0.18	195	180	202	202	0.9653	0.891	1.12	3.32
8	167	12.5.8	7x8.4x3	90.27	228.3	195.3	220	220	1.036	97.5	1.2	2.1
9	211	10	4.3	83	160	160	156.2	156.2	97.610	1.01	1.02	2.01
10	200	12	9x8	0	210	208	212	212	0.9905	99.05	2.13	3.25
11	150	14	8x9	0.18	223	210	215	215	1.0372	0.976	2.14	3.45
12	200	10	7x12	0.18	263	251	257	257	1.0233	0.976	2.14	4.25
13	160	9	7x8.4x3	180.27	187	203	195	195	0.9589	1.041	3.51	2.56
14	200	14	12x10	180	218	226	222	222	0.9819	1.018	2.21	3.25
15	140	10	10x7	180	147	159	154	154	0.9545	1.032	2.32	3.25
16	180	12	12x14	27	185	201	190	190	0.9736	1.057	1.54	2.35
17	200	13	8x8	27	222	219	215	215	1.0325	1.018	1.25	3.25
18	200	13	7x10	270	213	223	210	210	1.0142	1.061	4.23	2.14
19	150	10	10x6	90	162	173	168	168	0.9642	1.029	2.31	2.32
20	150	10	10x8	90	176	179	170	170	1.0352	1.052	3.65	5.32
21	200	14	8x9	90	246	249	240	240	1.025	1.03	3.25	5.32